Aus dem Institut für Medizinische Mikrobiologie
und Krankenhaushygiene
Direktor: Prof. Dr. Michael Lohoff
des Fachbereichs Medizin der Philipps-Universität Marburg

Titel der Dissertation:

A defined bacterial community restores immunity in germ-free mice via maturation of the intestinal vascular system.

Inagural-Dissertation zur Erlangung des Doktorgrades der
Naturwissenschaften

dem Fachbereich Medizin der Philipps-Universität Marburg
vorgelegt von

Rossana Victoria Romero Pérez

aus Caracas, Venezuela

Marburg, 2021

Angenommen vom Fachbereich Medizin der Philipps-Universität Marburg
am: 13.12.2021
Gedruckt mit Genehmigung des Fachbereichs
Dekan/in: Frau Prof. Dr. D. Hilfiker-Kleiner
Referent/in: Herr Prof. Dr. U. Steinhoff
Korreferent/in: Herr Prof. Dr. L. Schulte

Table of contents

List of Figures

Abbreviations

A	
ABX	Antibiotic cocktail
ACN	Absolute cell number
A/E	Attaching and effacing
AF700	Alexa fluor 700
AHL	N-acylhomoserine lactone
A. muciniphila	*Akkermansia muciniphila*
A. muris	*Acutalibacter muris*
APC	Allophycocyanin
APCs	Antigen presenting cells
ASF	Altered Schaedler flora
B	
B. caecimuris	*Bacteroides caecimuris*
BBB	Blood-brain barrier
B. longum	*Bifidobacterium longum*
BM	Bone marrow
β-ME	Beta-mercaptoethanol
B. thetaiotaomicron	*Bacteroides thetaiotaomicron*
C	
°C	Degree celsius
CD	Cluster of differentiation
cDCs	Conventional dendritic cells
cDNA	Complementary DNA
cm	Centimeters
C. rodentium	*Citrobacter rodentium*
CFU	Colony forming units
D	
DAPI	4′,6-diamidino-2-phenylindole
DNA	Deoxyribonucleic acid
DPI	Diphenyleneiodonium chloride
E	
EAE	Experimental Autoimmune Encephalomyelitis

ECM	Extracellular matrix
E. coli	*Escherichia coli*
e.g.	For example
E. gallinarum	*Enterococcus gallinarum*
EHEC	Enterohemorrhagic *Escherichia coli*
EPEC	Enteropathogenic *Escherichia coli*
EUB 338	Eubacteria 16S RNA position 338
et al.	And others
F	
FA[3]	Three facultative anaerobes
FCS	Fecal calf serum
FELASA	Federation of European Laboratory Animal Science Association
FISH	Fluorescence-in-situ hybridization
FITC	Fluorescein isothiocyanate
FRET	Fluorescence Resonance Energy Transfer
FSC	Forward scatter
FMT	Fecal microbiota transplant
G	
g/ gr	Gramm
GALT	Gut-associated lymphoid tissue
GEO	Gene Expression Omnibus
GF	Germ-free
GO	Gene Ontology
GSEA	Gene Set Enrichment Analysis
GVB	Gut-vascular barrier
H	
HBSS	Hank's balance salt solution
HEPES	4-(2-hydroxyethyl)-1-piperazineethanesulfonic acid
HEVs	High endothelial cells
HFD	High fat diet
HIF	Hypoxia-inducible factor
I	
IBDs	Inflammatory bowel diseases

ICAM	Intercellular Adhesion Molecule
IECs	Intestinal epithelial cells
iELs	Intraepithelial lymphocytes
Ig	Immunoglobulin
IL	Interleukin
ILCs	Innate lymphoid cells
iLFs	Isolated lymphoid follicles
i.p.	Intraperitoneal
ISCs	Intestinal stem cells
i.v.	Intravenous
IVC	Individual ventilated cages
IVM	Intravital microscopy
J	
K	
Ki67	Marker of proliferation Ki-67
KO	Knockout
K. oxytoca	*Klebsiella oxytoca*
K. pneumoniae	*Klebsiella pneumoniae*
L	
LB	Lysogeny broth
LECs	Lymphatic endothelial cells
LEE	Locus of enterocyte effacement
LFA-1	Lymphocyte function-associated antigen 1
L. murinus	*Lactobacillus murinus*
LP	Lamina propria
LPS	Lipopolysaccharide
LSEC	Liver sinusoidal endothelial cell
Ly6	Lymphocyte antigen 6 complex
M	
Mac-1	Macrophage-1 antigen
MACS	Magnetic cell sorting
MadCAM-1	Mucosal vascular addressin cell adhesion molecule 1
MALDI-TOF-MS	Matrix Assisted Laser Desorption Ionization Time-Of-Flight Mass-Spectrometry

MAMPs	Microbe-associated molecular patterns
MC	Minimal consortium
min	Minutes
ml	Mililiters
MLNs	Mesenteric lymph nodes
mm	Milimeters
MMPs	Metalloproteinases
mRNA	Messenger ribonucleic acid
m/z	Mass-to-charge ratio
N	
NaCl	Sodium chloride
NaHCO3	Sodium bicarbonate
NETs	Neutrophil extracellular traps
NH4CL	Ammonium chloride
ns	Non-significant
O	
OMM[12]	Oligo-Mouse-Microbiota
O/N	Overnight culture
ORA	Over Representation Analysis
OTU	Operational taxonomic unit
P	
PAI	Pathogenicity island
PBS	Phosphate buffered saline
PCs	Paneth cells
PCR	Polymerase chain reaction
PE	R-Phycoerythrin
PECAM-1	Platelet endothelial cell adhesion molecule 1
p.i.	Post-infection
PMN	Polymorphonuclear
PP's	Peyer's patches
PRRs	Pathogen recognition receptors
PSGL-1	P-selectin glycoprotein ligand-1
Q	
qRT-PCR	Quantitative real-time polymerase chain reaction

R	
RA	Relative abundance
Rag	Recombination activating gene
Reg3γ	Regenerating islet-derived protein 3 gamma
RIN	Ribonucleic acid integrity number
RNA	Ribonucleic acid
ROS	Reactive oxygen species
rpm	Revolutions per minute
rRNA	Ribosomal ribonucleic acid
RT	Room temperature
S	
SCFAs	Short chain fatty acids
SD	Standard deviation
SDS	Sodium dodecyl sulphate
SFB	Segmented Filamentous Bacteria
SI	Small intestine
SPF	Specific-pathogen-free
SSC	Side-scatter channel
S. Typhimurium	*Salmonella enterica* serovar *Typhimurium*
T	
T3SS	Type III secretion system
TGF-β	Transforming growth factor beta
TH	T helper cell
TierSchG	Tierschutzgesetz
TLR	Toll-like receptor
TMCH	Transmissible murine colonic hyperplasia
TNF	Tumor necrosis factor
Tregs	Regulatory T cells
U	
UC	Ulcerative colitis
µl	Microliters
µm	Micrometers
V	

VCAM-1	Vascular cell adhesion protein 1
VEGF	Vascular endothelial growth factor
VLA-4	Very late antigen-4
W	
(w)	With
(w/ o)	Without
WT	Wild-type
X	
Y	
Z	

1 Introduction

1.1 Gnotobiology

Due to the complexity of the microbiota, simplified *in-vitro* studies to investigate host-microbe and microbe-microbe interactions still do not offer an adequate representation of *in-vivo* model's scenarios. Moreover, studies where the gut microbiota plays a critical role, face tremendous challenges for the investigation of the role of specific bacterial strains in allergy, disease or homeostasis. Gnotobiology offers a platform for the research of microbe's interactions in a complex environment, where the host complete microbial composition is known.

1.1.1 Germ-free mice

Germ-free (GF) animals are a suitable tool to investigate direct microbiota-host interactions. They were first successfully raised in the 1910's, but it was not until the 1940's that the first large-scale GF production was established, and with it, a new door of opportunities regarding gnotobiology research was opened (Mallapaty, 2017). Already during this time, a series of unexplained effects were seen in animals that led a germless life, such as smaller lymphatic tissue, enlarged middle bowels and the inability of the tissue to decay even after death ("Life without germs", 1949). Therefore, the early stages of GF animal model research focused on the investigation of the role of the microbiota in gut morphology, development of the immune system as well as immune responses, especially in infectious diseases. Since then, it has been widely acknowledged that GF mice are highly susceptible to different viral and bacterial pathogenic challenges (Abt et al. 2012; Fagundes et al. 2012; Collins and Carter 1978). This is mostly because GF mice lack one of the most important barriers against external pathogens, namely the microbiota; but also due to their inability to mount appropriate immune

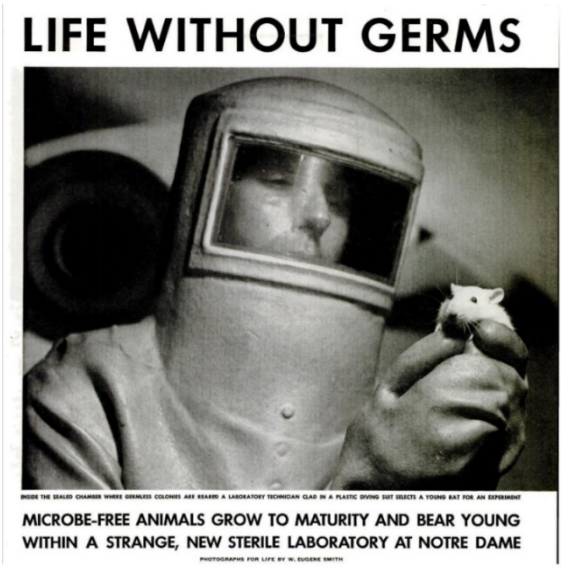

Figure 1. „Life without germs"

Life Magazine (1949)

responses (Round and Mazmanian, 2009). The immune-hyporesponsive state of GF mice can also be seen in several autoimmune models, such as Experimental Autoimmune Encephalomyelitis (EAE) and arthritis, where they show a protective phenotype with minimal symptoms (Luu et al. 2019; Wu et al. 2010). The latter observations were attributed to the fact that Segmented Filamentous Bacteria (SFB) drive autoimmunity by inducing TH17 differentiation in the gut (Castillo-Alarez and Marzo-Sola, 2017). Thus, the intestinal microbiota trains and primes the mucosal immune system by keeping it in a state of "controlled physiological inflammation" (Shanahan, 2002).

1.1.2 Minimal bacterial consortia

Along with GF mice came the first experiments involving a defined microbiota. In 1965, Russell W. Schaedler developed a minimal bacterial consortium consisting of eight bacterial strains, which he named the altered Schaedler flora (ASF) (Wymore et al. 2015). The main reasons that were used to choose the ASF consortium were the persistence of the strains to colonize in the mice through several generations and their ability to induce caecum shrinkage comparable to that of conventional mice (Schaedler et al. 1965). Even though the methodology and parameters used for the isolation and establishment of the ASF community were rather unrefined in comparison to modern techniques, the ASF consortium has been used for decades to study host-microbiota interactions. Although ASF colonizations have been shown to improve intestinal immune- and metabolic functions in ex-GF mice, one of its main limitations is the poor diversity within the eight bacterial strains (Wymore et al. 2015).

Using a genome-guided design for the identification of bacterial functions within the murine conventional microbiome, a new defined mouse microbiota was developed, the Oligo-Mouse-Microbiota (OMM^{12}). The OMM^{12} consortium consists of 12 bacterial strains that represent the five most prevalent and abundant bacterial phyla in the murine gut of laboratory mice (Brugiroux et al. 2016). In a *Salmonella* infection model, OMM^{12} bacteria enriched with three facultative anaerobes (FA^3) were able to provide full colonization resistance against the pathogen (Brugiroux et al. 2016). This effect, however, was absent in ASF mice enriched with FA^3. Consequently, it was postulated that the OMM^{12} consortium potentially allows FA^3 to occupy some crucial niche-space that *Salmonella enterica* serovar *Typhimurium* cannot longer exploit (Brugiroux et

al. 2016). Moreover, we could recently show that enriching the OMM[12] consortium with *Alistipes finegoldii*, an anti-inflammatory and cellulose-degrading bacterium, could protect mice against DSS colitis (Fischer et al. 2020). Thus, the OMM[12] is a suitable minimal consortium that can be enriched and adjusted to better fit the researcher's scientific question and possibly is a preferable model than the ASF bacterial community for microbiome intervention studies.

1.2 Intestinal physiology and immune homeostasis

The intestine is a complex organ mainly involved in the absorption of water and nutrients derived from the food into the bloodstream, but it also has a critical immunological function that together with the gut microbiota provides an efficient defence mechanism against harmful external challenges (Gasbarrini et al. 2008).

1.2.1 Structure

The intestine is divided into morphologically and functionally different regions, principally, the small and the large intestine. The small intestine (SI) is the longest part of the gastrointestinal tract measuring at around ~7 meters in length in humans and ~30 centimetres in mice; it is comprised of the duodenum, the jejunum and the ileum (Helander and Fändriks, 2014; Hugenholtz and de Vos, 2017). The main role of the SI is to absorb food-nutrients derived from the digestion process (Gasbarrini et al. 2008). Structurally, the SI is made of intestinal crypts (glands or crypts of Lieberkühn), which are invaginations of the epithelium, and of villi, hair-like projections consisting of side-by-side enterocytes equipped with microvilli protruding into the lumen (Nigam et al. 2019). This structural organization is especially adapted to increase the absorption-area of digestion products (Gasbarrini et al. 2008).

The large intestine or colon, on the other hand, consists only of colonic crypts and is significantly smaller than the SI, despite its name, which was given to it due to its increased width (Humphries and Wright, 2008). Unlike the SI, the colon houses the largest proportion of the gut microbiota and its main roles are the intake of water and the mobilization of waste material (stool) (Gasbarrini et al. 2008; Kahai et al. 2020).

In many mammals, the small and the large intestine are connected through the caecum, a small pouch in which contents from the SI are mixed and lubricated with mucus to enter the colon (Britannica, 2020). In humans, the caecum is morphologically considered the beginning of the colon and does not appear to have an important role, however, in mice, it is anatomically compartmentalized and has been shown to harbour specific bacteria and to be important for certain immune responses (Treuting and Dintzis, 2012; Brown et al. 2018).

Each intestinal compartment has a distinct microbial composition, function and morphology, which varies depending on the host age-maturity (Dehmer et al. 2011). During postnatal development, the intestine undergoes several morphological changes where its surface area greatly increases via a process called *crypt fission* also known as *crypt bifurcation* (Dehmer et al. 2011). During the boost of crypt fission, the crypts appear bifurcated (Bruens et al. 2017). This is due to the intestinal crypts undergoing multiple rounds of replication, where out of one individual crypt two progenitor crypts arise (Bruens et al. 2017). This process is critical for intestinal development and elongation, and correspondingly, it becomes less frequent in adulthood (Langlands et al. 2016).

1.2.2 The intestinal barriers

In addition to the digestion and absorption of dietary nutrients, the intestine is constantly exposed to a myriad of commensal bacteria and harmless food antigens (Kagnoff, 1993). Therefore, it must remain in a non-belligerent state towards benign environmental factors, but still be able to quickly react and maintain a barrier against harmful agents and pathogens in order to ensure homeostasis (Faria et al. 2017).

1.2.2.1 The gut-associated lymphoid tissue (GALT)

The gut is by far the largest immune organ, with the GALT containing over 40% of the lymphoid cells in the body (Gasbarrini et al. 2008). The GALT consists of aggregated lymphoid follicles as well as isolated lymphocytes dispersed throughout the small and the large intestine (Mörbe et al. 2021). Its main role is to keep both commensal and pathogenic microorganisms at bay by maintaining immune tolerance or inducing an inflammatory response, respectively (Faria et al. 2017). Lymphoid follicles can be divided into Peyer's patches (PP's) found solely in the SI as well as numerous isolated lymphoid follicles (iLFs), present

both in the SI and in the colon (Buettner and Lochner, 2016). Moreover, the murine caecum harbours the *caecal patch*, which consists of a single lymphoid cluster, morphologically and cellularly similar to PP's (Mizoguchi et al. 1996). The distribution of these immune-compartments seems to correlate with the density of luminal commensal bacteria, since the SI harbours higher numbers of intraepithelial lymphocytes (iELs) as well as the PP's, which are absent in the colon. This most likely is the case in order to warrant immune-tolerance towards the much denser colonic microbiota (Miron and Cristea, 2012). It is within the lymphoid follicles that antigen presenting cells (APCs) prime adaptive immune cells to undergo differentiation and subsequently localize either in the lamina propria (LP) or in the epithelium to become iELs in order to maintain barrier integrity and provide protective immunity (Mörbe et al. 2021). The most prominent cell type within the GALT are B cells, in particular IgA-producing plasma cells (Buettner and Lochner, 2016). The secretory IgA neutralizes toxic antigens and prevents bacterial adhesion to the intestinal epithelium (Gasbarrini et al. 2008). Moreover, another particular cell type found almost exclusively in the mucosal tissue and considered the innate counterparts of T-cells, are the innate lymphoid cells (ILCs) (Panda and Colonna, 2019). ILCs are tissue resident cells that secrete specific cytokines and have been shown to mediate crucial innate immune responses against enteric pathogens (Satoh-Takayama et al. 2008). Thus, the immune cells that reside in the GALT produce immunomodulatory molecules that keep the gut under an active immunosurveillance, hence constituting one of the three "intestinal barriers" (Gasbarrini et al. 2008).

1.2.2.2 The mucosal barrier

Apart from the GALT, the intestine houses specialized absorptive and secretory enterocytes that together with the mucus play a fundamental role in the mucosal barrier mechanism all the while preserving the intestine's ability to absorb nutrients (Noah et al. 2011). The intestinal epithelial cells (IECs) are absorptive cells that form the luminal single-cell-layer lining of the gut (Sansonetti, 2004). The apical side of IECs is equipped with microvilli that create the so-called *brush border*, which allows mucus mobilization and the absorption of end-products from the ingested food (Holmes and Lobley, 1989). For many years, they were thought to only play a role in nutrient absorption and in being the physical division between the LP and the commensal microbiota (Gasbarrini et al. 2008).

However, several studies could demonstrate the capability of enterocytes to sense harmless and pathogenic environmental factors and act accordingly by secreting cytokines/ chemokines for leukocyte recruitment as well as expressing adhesion molecules to aid in leukocyte transmigration (Miron and Cristea, 2012). For instance, IECs express pathogen recognition receptors (PRRs), such as toll-like receptor 4 (TLR-4), however, only in the Golgi apparatus, which stands in contrast to innate immune cells which express TLR-4 on their surface (Espevik et al. 2003). This allows IECs to react to bacterial lipopolysaccharide (LPS) only once it penetrates into their cytoplasm. Furthermore, IECs facilitate the trafficking of immunoglobulins produced in the LP to the lumen and can mount efficient innate immune responses upon pathogen invasion (Miron and Cristea, 2012). IECs are constantly undergoing differentiation, maturation and renewal every 3-7 days. Their renewal relies on cell division of intestinal stem cells (ISCs) located at the bottom of the intestinal crypts, which migrate to the top where they eventually reach full maturity and undergo apoptosis (Miron and Cristea, 2012).

Other cells from the intestinal epithelium, such as Paneth cells (PCs), also originate from ISCs, but remain at the bottom of the crypts and are phagocytized by neighbouring cells approximately every 20 days (Porter et al. 2002). PCs are granular secretory enterocytes that actively modulate the microbial flora by producing lysozyme and antimicrobial peptides (Gassler, 2017). Unlike IECs, PCs are solely found in the small intestine, particularly in the ileum, and their differentiation differs within different mammalian species (Falk et al 1998). While PCs appear during the embryonic stage in humans, they emerge and start their differentiation during the postnatal stage in mice (Lueschow and McElroy, 2020). PC numbers in both human- and rodent newborns are low, but increase drastically during the postnatal phase, a time-point that coincides with the start of microbial colonization (Lueschow and McElroy, 2020). Concordantly, histological analyses of jejunal PCs showed decreased numbers as well as decreased expression of the antimicrobial protein, Regenerating islet-derived protein 3 gamma (Reg3γ), in GF mice in comparison to conventional mice (Schoenborn et al. 2019). Moreover, PCs have been shown to directly control crypt fission in a Wnt-signalling-dependent manner and conversely, the Wnt-signalling pathway has been linked to directly mediate PC differentiation (Gassler, 2017; van Es et al. 2005). While most studies on PCs were performed

using histological approaches, PCs are beginning to being characterized using flow cytometry. Flow cytometry analysis revealed that PCs expressed the CD24 marker and can be distinguished from enteroendocrine cells by using the side-scatter channel (SSC) to assess the granularity (Sato et al. 2011). Thus, $CD24^{+}SSc^{hi}$ cells were shown to be PCs that contained lysozyme granules and $CD24^{+}SSC^{low}$ cells were enteroendocrine cells which produced chromogranin A (Sato et al. 2011). Further characterization of PCs beyond the small intestine revealed that the colon is equipped with Paneth-like cells that express the CD24 marker but were also positive for goblet-cell markers such as Muc2 (Rothenberg et al. 2012). Therefore, antimicrobial peptide production and control of morphological changes like crypt fission might be supported by Paneth-like cells in the colon (Langlands et al. 2016).

Lastly, the mucosal barrier is further comprised of more secretory cells, such as enteroendocrine, tuft and mucus-producing goblet cells as well as the mucus (Noah et al. 2011). Enteroendocrine cells make up approximately 1% of the intestinal epithelium and produce hormones like serotonin (Noah et al. 2011). Tuft cells are even rarer than enteroendocrine cells and its function has been debated for many years, nevertheless, they have been shown to be involved in chemical sensation (Kokrashvili et al. 2009). Conversely, goblet cells are the most abundant of all the secretory enterocytes and their main role is the production of mucus (Noah et al. 2011). Together with the cells that form the intestinal epithelium, the mucus is a potent weapon against microorganisms but it also functions as a lubricant of luminal contents (Herath et al. 2020). It is within the mucus that secretory IgA and many antibacterial mediators produced by PCs accumulate (Herath et al. 2020). This allows the mucus to repel most of the commensal bacteria; however, some bacterial strains have adapted to the harsh mucus-environment and can use it as a nutrient source (Shin et al. 2019). Moreover, experiments on GF mice demonstrated that commensal bacteria positively regulate mucus production, since GF mice have a thinner mucus layer than specific-pathogen-free (SPF) mice (Petersson et al. 2011).

1.2.2.3 Gut microbiota

The last intestinal barrier, which is considered by some an organ in itself, is the commensal microbiota (O'Hara and Shanahan, 2006). The gut microbiota profoundly guides the development, education and function of the intestine, but

it also exerts powerful effects on the host physiology and has been shown to even influence mood and behaviour (Knight, 2019). The intestinal microbiota consists of different microorganisms and the most studied are the bacterial species, while the knowledge on viral, protozoan and fungal microbes is still quite scarce (Tlaskalova-Hogenova et al. 2015). This is because the gut microbiota harbours an incredibly high number of bacterial communities that substantially exceed the amount of host eukaryotic cells (Al Nabhani et al. 2019). Their distribution, however, is not homogenous. The microbiota is largely absent at the beginning of the small intestine, probably due to the enzymes and acidic conditions needed for digestion (Saavedra and Moore, 2005). It gradually increases in diversity and numbers of bacterial species along the gastrointestinal tract, until it reaches the highest concentration at the most densely colonized compartment, the colon (Knight, 2019).

Straight after birth, a direct symbiotic relationship between the microbiota and all mammals begins (Tlaskalova-Hogenova et al. 2015). This relationship, however, may even start indirectly during the prenatal stage. Recent studies could show that the foetus senses microbial metabolites; hence, the maternal microbial colonization may play a role in our metabolic phenotype and innate immune development long before we are born (Kimura et al. 2020; Gomez de Agüero et al. 2016). Nevertheless, it is widely acknowledged that all mammals are born GF, which is how the first GF animals came to be: through aseptic caesarean sections (Mallapaty, 2017). It is during the postnatal period, after the GF newborn babies emerge from the sterile environment of the mother's uterus, when the body is most sensitive to the effects of microbial colonization (Tlaskalova-Hogenova et al. 2015). At the same time, the colonizing microbiota is shaped by environmental factors such as the delivery method (vaginal or caesarean), the dietary and immunological components of the milk and the introduction of solid foods (Dominguez-Bello et al. 2010; Gomez de Agüero et al. 2016; Al Nabhani et al. 2019). It is not until around three years of age in humans and 5-6 weeks of age in mice that the gut microbiota fully matures and resembles that of an adult individual (Yatsunenko et al. 2012; Al Nabhani and Eberl, 2020). Early microbiota in mice is characterized by γ-Proteobacteria and Lactobacillales, the latter being the best adapted to the milk environment (Al Nabhani et al. 2019). At weaning the microbiota induces a strong immune response, which was named a

weaning reaction, associated with a marked expansion of Clostridia and Bacteroidia (Al Nabhani et al. 2019). Indeed, Clostridia colonization in neonatal mice increases the chances of survival from *S. Typhimurium* and *Citrobacter rodentium* infections (Kim et al. 2017). Moreover, Clostridia can better colonize neonatal mice which were preinoculated with *Lactobacillus murinus* or *Escherichia coli*, two bacterial strains from the order/ class Lactobacillales and γ-Proteobacteria, respectively (Kim et al. 2017). This is a typical example of microbes engaging in cooperative behaviours (Figueiredo and Kramer, 2020). After the weaning period, the microbiota slowly starts to acquire an adult-type complex microbiome with predominant bacterial communities from Bacteroidetes, Firmicutes and Proteobacteria at the phylum level both in humans and in mice (Tanaka and Nakayama, 2017; Xiao et al. 2015).

The interactions between the microbiota and the development and function of the immune system were made evident thanks to experiments on GF mice; these animals, as previously mentioned, have a severely underdeveloped intestinal immune system (Round and Mazmanian, 2009). Moreover, associations of GF mice with selected bacterial strains could elucidate the dramatic effects of specific members of the microbiota on the host immune system. Therefore, several commensals were categorized as "Inflammatory commensals", "Immunoregulatory commensals" or "Pathobionts" (Palm et al. 2015). Inflammatory commensals, such as SFB, intimately bind to IECs, which leads to the induction of TH17 differentiation and IgA production in the gut (Hedblom et al. 2018). On the other hand, immunoregulatory commensals like *B. fragilis* induce intestinal regulatory T cells (Tregs), which aid in the maintenance of immunological tolerance (Palm et al. 2015). Lastly, pathobionts are commensal bacteria that under certain circumstances can become opportunistic pathogens or cause inflammation (Jochum and Stecher, 2020). For example, *A. muciniphila*, a normal occurring-commensal known to produce mucin-degrading enzymes, has been shown to mitigate the progression of several metabolic diseases (Xu et al. 2020). However, its presence exacerbates *S. typhimurium*-induced inflammation in gnotobiotic mice (Ganesh et al. 2013). Thus, in a complex microbial environment, a dysregulated expansion of certain commensals (e.g. antibiotic treatment) can lead to dysbiosis and be detrimental to the intestinal homeostasis.

Finally, the gut microbiota also provides strong colonization resistance against pathogens, is involved in the synthesis of vitamins and short chain fatty acids (SCFAs) derived from dietary fibres as well as in the metabolism of bile acids, hormones, lipids and several drugs (Gasbarrini et al. 2008). Colonization resistance is mediated through commensal competition for nutrients, adhesion and colonization of spatial intestinal niches that potential pathogens cannot longer use and exploit (Kamada et al. 2012). But colonization resistance is also important for the maintenance of microbial homeostasis and prevention of dysbiosis (Spees et al. 2013). Moreover, it is closely supported by SCFAs. The production of SCFAs carefully ensures that members of the phylum Proteobacteria do not overgrow in order to maintain an optimal microbial balance. To this end, bacteria from the phyla Bacteroides and Firmicutes ferment complex polysaccharides into SCFAs, such as acetate, butyrate and propionate, which evoke a metabolic exclusion of members of the phylum Proteobacteria (Spees et al. 2013). SCFAs, in turn, reduce inflammation by inducing Tregs, and can be utilized by enterocytes as an energy source (Spees et al. 2013; Donohoe et al. 2012). Microbiota-derived SCFAs, in addition, inhibit virulence-gene expression of enteric pathogens and may help resolve intestinal inflammation after infection by suppressing neutrophil-induced tissue damage (Gantois et al. 2006; Maslowski et al. 2009). Ergo, their anti-inflammatory properties work both on eukaryotic and prokaryotic cells (Spees et al. 2013).

1.2.3 The intestinal vascular system

The intestine is a highly vascularized organ, due to its main role: the absorption of nutrients and water into the bloodstream (Granger et al. 2015). The intramural blood supply of the intestine can be divided into blood vessels in the submucosa (or muscularis) and the mucosa (Kvietys, 2014). The submucosal arterial plexus, located in the submucosa, arterially supplies both the mucosa and the submucosa (Geboes, 2001). It branches into capillary networks in the mucosa, where, in the SI crypt and villus, microcirculations form (Figure 2) (Kvietys, 2014). In the colon, the submucosa arterioles form capillary networks that surround the crypts and resemble a honeycomb appearance, when viewed from above (Figure 2) (Araki et al. 1996).

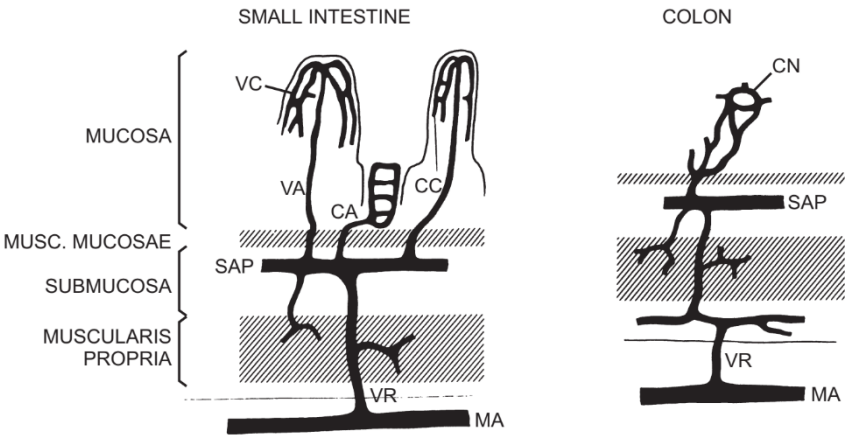

Figure 2: Vascular organization of the small intestine and colon.

Image abbreviations: CA: cryptal arteriole, CC: capillaries, CN: capillary network, MA: marginal artery, SA: supplying artery, SAP: submucosal arterial plexus, VA: villous arteriole, VC: villous capillaries, VR: vasa recta. (Source: Geboes, 2001)

Within the small intestine LP and surrounded by the villi capillaries, blind-ended capillaries (also known as lacteals), are found (Bernier-Latmani et al. 2015). Lacteals are a part of the intestinal lymphatic vessels and drain into a submucosal lymphatic vascular network (Bernier-Latmani and Petrova, 2017). They are formed by a single cell-layer of lymphatic endothelial cells (LECs) connected through cell-cell "button-like" junctions (Bernier-Latmani and Petrova, 2017). Lacteals help support the role of the GALT by constituting a one-way drainage system for interstitial fluids and immune cells. Moreover, lacteals are in a permanent regenerative and proliferative state, indicating an ongoing lymphangiogenesis (Bernier-Latmani et al. 2015). Concordantly, villus capillaries show an unusual dependence on vascular endothelial growth factor (VEGF) signalling in contrast to quiescent endothelial cells in other tissues (Yang et al. 2013; Kamba et al. 2006). This constant regeneration mode of intestinal lymphatic- and blood vessels may be due to the continuous exposure to dietary and microbial products as well as the mechanical strain that the intestine is subjected to (Bernier-Latmani et al. 2015). However, the microbiota might play a direct role in controlling this constant renewal. Gut microbiota depletion led to lacteal regression and villus capillary network reduction in antibiotic-cocktail (ABX)-treated mice (Suh et al. 2019). Studies on GF mice could show that the microvascular density of the villous capillary network in the sterile gut was lower than in conventionally raised mice (Stappenbeck et al. 2002). Mono-association of GF mice with *B. thetaiotaomicron* induced angiogenesis in the villous

capillaries and this observation directly correlated with the presence of PCs (Stappenbeck et al. 2002). In accordance, depletion of PCs in SPF mice resulted in a reduction of the villous microvascular density in addition to a decreased expression of angiogenic genes in the small intestine (Hassan et al. 2020). Additional bacteria have been shown to elicit angiogenic effects in the small and large intestine of GF mice. Transient colonization of GF mice with *E. coli* induced an increase in the villous capillary network, which persisted once the mice returned to the GF status (Uchimura et al. 2018). Another study could show that monocolonization of GF mice with *S. boulardii* promoted an increase in the blood vessel diameter and upregulation of genes involved in angiogenesis in the colon (Hoffmann et al. 2016). These studies suggest that specific bacterial strains regulate intestinal angiogenesis through a PCs-mediated mechanism.

Due to the close symbiotic relationship between the intestine and the commensal microbiota, the intestinal vascular system meticulously checks the passage of antigens from the gut into the bloodstream (Thomas, 2015). It was shown that similarly to the endothelial cells from the blood-brain barrier (BBB), intestinal endothelial cells constitute another line of defence by generating the gut-vascular barrier (GVB) (Spadoni et al. 2015). The GVB is impermeable to 70 kDa particles, and enteric pathogens like *S. Typhimurium* can change this permeability by down-regulation of the Wnt-signalling (Spadoni et al. 2015). The permeability of the GVB can also be modulated by the host. For instance, during pathogen invasion, the host's tissue-resident leukocytes and IECs secrete cytokines, reactive oxygen species (ROS) and lipid mediators that activate intestinal endothelial cells to express chemokine receptors and adhesion molecules to facilitate immune cell extravasation into the LP (Gentile and King, 2018).

1.3 Leukocyte migration

During infection, inflammation or tissue injury, leukocytes are required to migrate through activated venular walls and reach the inflamed-site in question. Innate and adaptive effector cells such as neutrophils and T cells, directly interact with activated endothelial cells to abandon the bloodstream and enter the tissue (Nourshargh and Alon, 2014).

1.3.1 Neutrophils

Neutrophils are polymorphonuclear (PMN) leukocytes that belong to the innate immune system (Scher et al. 2013). Around 60% of the hematopoietic capacity of the bone marrow (BM) is dedicated to neutrophil-production, making them, once released into the bloodstream, the most abundant white-blood cell type in the human blood (Scher et al. 2013). In contrast, murine neutrophils make up around 10-25% of the cells in the peripheral blood (Hidalgo et al. 2019). Neutrophil development, also known as granulopoiesis, starts in the BM, where hematopoietic stem cells take about 14 days to differentiate into either eosinophils, basophils or neutrophils (Scher et al. 2013). Mature neutrophils can either reside in certain tissues, such as the liver, lung, spleen, and BM, or circulate in the bloodstream (Summers et al. 2010). Circulating mature neutrophils are short-lived cells, with a half-life of approximately 6-8 hours (Hidalgo et al. 2019). The reason for their extremely short half-life is largely uncertain, however, some studies suggest that this reduced life cycle ensures less neutrophil-induced collateral damage to the host's tissues during inflammation (Wang, 2018). This is because neutrophils can contribute to tissue injury by amplifying the inflammatory response through degranulation of antimicrobial products like serine proteases and the release of neutrophil extracellular traps (NETs) (Kruger et al. 2015).

Neutrophils are highly motile cells and can infiltrate tissues that other migrating cells cannot, making them first-responders to inflammatory stimuli. Neutrophilic tissue-recruitment, also known as extravasation, is a multi-step process involving neutrophil response to inflammatory cytokines, chemokines and microbe-associated molecular patterns (MAMPs) (Filippi, 2019). Circulating neutrophils first begin to roll on endothelial cells with weak (low-affinity) interactions mediated by selectins like PSGL-1 and L-selectin (Granger and Senchenkova, 2010). Subsequently, the selectin-signalling, accompanied by chemokines presented on the luminal site of endothelial cells, triggers the activation of neutrophil integrins, such as LFA-1, Mac-1 and VLA-4, evoking firm adhesion and arrest on the endothelium (Nourshargh and Alon, 2014). Once neutrophils are firmly attached, they begin transmigration across the endothelial barrier, a step known as diapedesis (Filippi, 2019). Diapedesis can occur transcellularly, through endothelial cells, or paracellularly, in between them.

Neutrophils seem to prefer paracellular transmigration, probably due to their highly malleable and multi-lobular nucleus, which allows them to better squeeze in between the endothelial tight-junctions (Nourshargh et al. 2010; Olins et al. 2008). While the majority of leukocytes (~70%-90%) also actively engage in paracellular migration, some vascular beds, like the BBB which possess specialized tight junctional structures, favour transcellular migration (Nourshargh and Alon, 2014).

Once transmigration is complete and neutrophils are at the inflamed site, different antibacterial effector functions are activated depending on the inflammation type and location. For instance, the presence of serum inhibits NETs formation, while the complement system and IgG antibodies enhance the phagocytic activity (Hakkim et al. 2010; Kruger et al. 2015). Upon pathogen encounter, neutrophils can multitask by showing strong phagocytosis and NETosis (Yipp et al. 2012). NETosis or NET formation is a mechanism in which neutrophils release DNA traps composed of decondensed chromatin and antimicrobial proteins (Brinkmann et al. 2004). Since NETs are fatal to neutrophils, they are considered a form of cell death which should not be mistaken with programmed-cellular apoptosis (Kruger et al. 2015).

Granulopoiesis, neutrophil effector activity and leukocyte migration might be regulated by mucosal commensals. Prolonged ABX-treatment of neonatal mice was shown to reduce neutrophil numbers in the blood and BM, while GF rats also suffered from severe neutropenia (Deshmukh et al. 2014; Ohkubo et al. 1990). Moreover, the phagocytic activity of BM neutrophils from GF mice and ABX-treated mice is diminished (Zarzycka, 2017; Clarke et al .2010). This regulation of neutrophil function was attributed to the translocation of peptidoglycan from the gut to BM-neutrophils (Clarke et al .2010). Lastly, neutrophil recruitment into the lung during *K. pneumoniae* infection was severely impaired in GF mice, which led to a higher mortality rate due to pathogen dissemination (Fagundes et al. 2012). Also, intraperitoneal injection of zymosan led to a decreased neutrophil extravasation into the peritoneum in GF and ABX-treated mice (Karmarkar and Rock, 2013). In line with the last two studies, GF mice also showed impaired mast-cells gut-homing and B-cell recruitment in models of food-allergy and autoimmunity, respectively (Schwarzer et al. 2019; Berer et al. 2011).

1.3.2 Endothelial cells

Endothelial cells constitute the single-cell layer that line blood vessels and capillaries. They are the body's crucial life-support system in which cell migration and passage of materials into almost every region takes place (Alberts et al. 2002). Endothelial cells adapt to their environment and show significant heterogeneity among organs and tissues. For instance, endothelial cells from arterioles, capillaries and venules have different phenotypes when it comes to adhesion molecule expression (Ley, 2008). Moreover, sinusoidal-, BBB-, GVB- and lymph vessel endothelial cells have further specialized to exert different pro- or anti-inflammatory functions (Ley, 2008).

In order for leukocytes to reach inflamed tissues, they must interact with activated endothelial cells (Granger and Senchenkova, 2010). Thus, endothelial activation represents a crucial step in the inflammatory response. Many factors have been shown to activate the endothelium, most importantly the complement system, cytokines, chemokines and MAMPs (Ley, 2008). TLR ligands like LPS and cytokines, such as IL-1β and TNF-α, strongly induce the expression of ICAM-1 and VCAM-1 on endothelial cells (Ley, 2008). Both adhesion molecules are known to interact with LFA-1 and VLA-4 on leukocytes to facilitate arrest and transmigration (Granger and Senchenkova, 2010). The complement C5a induces endothelial degranulation of Weibel-Palade bodies and subsequent P-selectin expression on the surface (Fischetti and Tedesco, 2006). The regulation of additional cell adhesion molecules that are functionally involved in paracellular migration, such as CD31 (PECAM-1), remains to be determined (Woodfin et al. 2007). PECAM-1 is expressed on both endothelial cells and leukocytes and engages a homophilic interaction with neighbouring PECAM-1 proteins on adjacent cells (Sun et al. 1996; Dejana, 2004). Nevertheless, at least in endothelial cells, PECAM-1 is a major constituent of the endothelial intercellular junctions and is therefore crucial for the maintenance of the vascular barrier. Additionally, it also plays a prominent role during angiogenesis (Privratsky and Newman, 2014). Another cell adhesion molecule involved in the organization of intercellular junctions between endothelial cells is CD146 (LSEC) (Leroyer at al. 2019). CD146 is expressed on endothelial cells and pericytes and has been shown to play an important role in the development of the BBB by controlling vessel integrity and permeability (Chen et al. 2017). In mucosal tissues, endothelial cells

express specific adhesion molecules that are not found elsewhere in the body and gut microbes have been linked to influence cell adhesion molecules' expression (Komatsu et al. 2000; Formes and Reinhardt, 2019). MadCAM-1 is an adhesion molecule expressed on high endothelial venules (HEVs) in the mesenteric lymph nodes (MLNs) and PPs (Ley, 2008). MadCAM-1 has been shown to have a central role in the formation of the gut lymphoid tissue during the postnatal stage in addition to the recruitment of leukocytes into the LP (Schippers et al. 2009; Clahsen et al. 2015).

Endothelial proliferation via angiogenesis, sprouting of existing blood vessels, can occur in response to injury or hypoxic conditions during tissue development/ growth and cancer (Alberts et al. 2002). In normal physiological conditions, endothelial cells are usually in a quiescent state and their turnover is very slow (Krüger-Genge et al. 2019). As previously mentioned, however, intestinal endothelial cells undergo constant regeneration during homeostasis, as seen by their dependency on and expression of VEGF, an important angiogenesis marker (Yang et al. 2013). VEGF is a crucial growth factor involved in the initiation of angiogenesis, and its expression can be stimulated by HIF-proteins like HIF-1α that activate the HIF-pathway (Al-Soudi et al. 2017). Regulation of angiogenesis has been shown to be triggered by similar mechanisms that induce endothelial activation. For example, cytokines such as TNF-α, IL-1, TGF-β and IL-17 can enhance angiogenesis usually via VEGF-signalling. Activation of different TLRs also induces angiogenesis by increasing VEGFs as well as metalloproteinases (MMPs) (Bhagwani et al. 2020). MMPs degrade the extracellular matrix (ECM), which facilitates endothelial migration to form new vascular tubes (Sun et al. 2017). Lastly, SCFAs may also play a role in regulating angiogenesis, as administration of sodium butyrate was shown to increase the capillary density in the myocardium of high fat diet (HFD)-mice (Zhang et al. 2018).

1.4 *Citrobacter rodentium*

The murine gastrointestinal pathogen *C. rodentium*, previously known as *C. freundii* 4280, belongs to a family of extracellular enteric pathogens, related to human enteropathogenic- (EPEC) and enterohemorrhagic (EHEC) *E. coli* infections (Barthold, 1980; Mundy et al. 2005; Luperchio and Schauer 2001). Genome analyses of *C. rodentium* confirm its evolutional relationship with EPEC

and EHEC bacteria, namely the sharing of ~67% of its genes with both bacterial strains (Petty et al. 2010). Thus, mouse experiments with *C. rodentium* represent an ideal *in-vivo* model for the investigation of EPEC and EHEC infections.

1.4.1 Course of infection

Similar to most enteric pathogenic bacteria, *C. rodentium* is transmitted via the fecal-oral route (Collins et al. 2014). In the wild, *C. rodentium* infection involves infected mice in close proximity with naïve mice and transmission via coprophagy (Bouladoux et al. 2017). This infection cycle can be reproduced in a laboratory setting by cohousing infected and naïve mice (Crepin et al. 2016). However, in order to establish reproducibility, most *C. rodentium*-infection studies are done by inoculation of mice via oral gavage (Bouladoux et al. 2017). Laboratory-cultured *C. rodentium* is usually grown in LB-media, which has been shown to downregulate the virulence genes of enteric pathogens (Abe et al. 2002; Mullineaux-Sanders et al. 2017). Cultivation of *C. rodentium* in DMEM upregulates its virulence genes due to the presence of NaHCO3 (Abe et al. 2002). Therefore, it is believed that *C. rodentium* has evolved to upregulate the virulence genes needed for colonization when it reaches the bicarbonate-rich host environment of the gastrointestinal tract (Yang et al. 2008; Yang et al. 2010). Once in the intestine, few *C. rodentium* bacteria begin to establish and expand in the caecum, more specifically in the caecal patch (Wiles et al. 2004). The caecal patch is a place that is thought to provide essential signals for the triggering of virulence factors, thus allowing *C. rodentium* to adapt to the intestinal environment (Wiles et al. 2004). Nevertheless, caecum removal did not impair *C. rodentium*'s ability to colonize its host (Brown et al. 2018). Colonization then expands to the colon, where *C. rodentium* predominately stays and bacterial loads reach a peak at day 10 post-infection (p.i.) (Wiles et al. 2004). Yet, *C. rodentium* colonization dynamics can vary greatly due to the different microbiota composition between animal facilities (Osbelt et al. 2020). During the peak of infection, *C. rodentium* is able to comprise 1-3% of the total intestinal microbiota, leading to acute dysbiosis in SPF mice (Lupp et al. 2007). Colonic pathogen burden starts to decrease on day 14 p.i., simultaneously with a decrease in the colonization of the caecal patch (Wiles et al. 2004). This finding pointed to the caecal patch as a bacterial reservoir, thus, continuously releasing new bacteria into the colon and subsequently representing an important starting point for

pathogen elimination (Wiles et al. 2004). Cecectomized mice, however, showed no difference in densities of *C. rodentium* shed in the feces to mice that received sham surgeries (Brown et al. 2018).

The mechanisms by which *C. rodentium* infects its host include the use of attaching and effacing (A/E) lesions that in turn consist of the induction of pedestal-like structures on the apical site of enterocytes by intimate bacterial attachment, resulting in the damage of the *brush-border* and cytoskeletal rearrangements in the underlying cytoplasm (Schauer and Falkow 1993; Luperchio and Schauer 2001). *C. rodentium*'s ability to form A/E lesions is encoded, as seen in EPEC and EHEC bacteria, by the presence of a pathogenicity island (PAI), known as the locus of enterocyte effacement (LEE) (Nataro and Kaper, 1998; Collins et al. 2014). LEE encodes a type III secretion system (T3SS) composed of approximately 20 proteins and known as an injectisome, which allows the translocation of different effector proteins into the cytoplasm of enterocytes (Collins et al. 2014; Cornelis, 2006). These virulent proteins provoke structural changes in enterocytes, which lead to transmissible murine colonic hyperplasia (TMCH) (Luperchio and Schauer 2001). TMCH development and disease severity correlate with mice age and strain. Adult in-bred mice develop a milder disease progression, less morbidity and mortality than suckling mice or susceptible mice strains, who have a higher probability to develop rectal prolapse, acute diarrhea and severe colonic inflammation (Papapietro et al. 2013; Barthold et al. 1978). The intestinal lesions as a result of TMCH in mice resemble lesions found in humans suffering from inflammatory bowel diseases (IBDs) (Luperchio and Schauer 2001). Therefore, the research of *C. rodentium* can also be used to study IBDs and colon carcinogenesis, since the infection is known to cause elongation of colonic crypts, decrease of goblet cells and an increase of the mitotic activity in enterocytes (Collins et al. 2014). The subsequent epithelial hyper-proliferation can create a perfect environment for colon tumorigenesis, as seen in patients suffering from ulcerative colitis (UC) (Luperchio and Schauer 2001).

1.4.2 Immune response

C. rodentium infections promote several host immune responses, some of which are essential for pathogen clearance. Even though *C. rodentium* is a strictly extracellular pathogen and does not invaded the LP or become systemic in wild-type (WT) mice, Neutrophil-, Rag1- and c-rel knockout (KO) mice have been

shown to succumb to the infection due to systemic bacteremia (Kamada et al. 2015; Luu et al. 2020). Thus, the first line of defence against *C. rodentium* constitutes the cells of the innate immune system, particularly neutrophils. Neutrophils are crucial to reduce the bacterial load of *C. rodentium* in the gut by migrating into the intestinal lumen and phagocytizing IgG-opsonized virulent bacteria (Spehlmann et al. 2009; Kamada et al. 2015). They work closely together with IgG-plasma cells, which are absent both in Rag1- and c-rel KO mice, to keep pathogenic-attaching *C. rodentium* at bay, while avirulent *C. rodentium* is outcompeted by the intestinal microbiota in the colonic lumen (Kamada et al. 2015; Luu et al. 2020). Further important immune mediators, such IL-17, elicit a key role in neutrophilic migration during infection (de Oliveira et al. 2016). Indeed, due to *C. rodentium*'s close contact with and adherence to epithelial cells, as seen in SFB, a strong IL-17 is induced (Atarashi et al. 2015). This IL-17 production is triggered and produced by cells of both the innate and adaptive immune systems, namely ILC3, TH17 and a subset of conventional dendritic cells (cDCs) (Collins et al. 2014; Schreiber et al. 2013). IL-17 A/F KO mice show impaired neutrophilic recruitment into the gut throughout *C. rodentium* infections; however, clearance was achieved due to infiltrating macrophages, which, in the absence of neutrophils, control and clear the pathogen (Zarzycka, 2017). This finding implies that the immune response against *C. rodentium* can vary depending on the mouse strain as well as their immunological status. For instance, in WT mice, macrophage immunity is dispensable during *C. rodentium* infection (Zarzycka, 2017). IL-22, produced mainly by ILC3, is another important soluble mediator in the defense against *C. rodentium* infection (Collins et al. 2014). Apart from inducing the production of antimicrobial peptides, IL-22 further represents a crucial promoter of intestinal epithelial barrier integrity during *C. rodentium* infection (Zheng et al. 2008). Lastly, infections with *C. rodentium* provide immunity to immunocompetent mice against re-infection, although, it appears to wane over time, thus making the animals newly susceptible to *C. rodentium* infection (Barthold 1980).

1.4.3 Role of the microbiota

Under physiological conditions, the murine gut flora is devoid of *C. rodentium*, meaning that there is no known carrier-state in wild or SPF WT mice (Baker, 1998). A study on the impact of antibiotic treatment towards host response to

different bacterial challenges revealed that *C. rodentium* can act as an opportunistic pathogen, as antibiotic treatment caused its overgrowth in the murine gut (van Ogtrop et al. 1991). Moreover, metrodinazole-antibiotic treatment prior to an infection with *C. rodentium* led to increased susceptibility, whereas streptomycin treatment did not affect disease severity (Wlodarska et al. 2011). This observation indicates that specific bacteria or bacterial communities confer resistance against *C. rodentium*. A study in genetically identical mouse lines from different animal facilities, revealed that microbiota composition predetermines whether the mice present a resistant or susceptible colonization phenotype (Osbelt et al. 2020). The resistant microbiota harboured multiple Enterobacteriaceae such as *C. amalonaticus*, *E. coli* and *K. oxytoca* as well as elevated levels of the SCFA butyrate (Osbelt et al. 2020).

The importance of the microbiota during *C. rodentium* infections is further emphasized in experiments involving GF mice. While SPF mice eradicate the infection in around 3 weeks, *C. rodentium* persists lifelong in GF mice and behaves as a commensal by downregulating its virulence factors (Kamada et al. 2012; Zarzycka, 2017). A similar scenario has been observed in asymptomatic EPEC human carriers, however the circumstances that incline certain individuals to become carriers remain unclear (Nataro and Kaper 1998; Hu and Torres, 2015). Despite the asymptomatic infection, monocolonization of GF mice with *C. rodentium* quickly leads to high bacterial numbers ($\geq 10^9$ CFU/ g), which remain unchanged even after 1 year p.i. (Zarzycka, 2017). Monocolonization of GF mice with selected bacterial strains like *E. coli* was shown to exert a reduction of the *C. rodentium* bacterial burden in the intestine (Kamada et al. 2012). As both *E. coli* and *C. rodentium* are Enterobacteriaceae, it was hypothesized that bacterial competition for certain nutrients as well as intestinal niches plays a role in the colonization dynamics of *C. rodentium* (Kamada et al. 2012). Consistently, mice with ASF bacteria are unable to eliminate *C. rodentium*, probably due to the lack of competing bacteria, as the ASF community lacks Enterobacteriaceae (An et al. 2021; Wymore et al. 2015). Even though the competition provided by the microbiota plays a crucial role in *C. rodentium* elimination, a functional immune system is also essential. B-cell deficient SPF mice are unable to eliminate *C. rodentium* and show no mortality after 40 p.i. (Maaser et al. 2004). But the presence of the microbiota may actually regulate whether *C. rodentium*

downregulates its virulence genes or not through a quorum sensing system (Coulthurst et al. 2007). C-rel KO SPF mice remain *C. rodentium* carriers for at least 3 months, but show decreased survival and bacteria septicaemia at later time-points (Luu et al. 2020). Thus, *C. rodentium* elimination involves a careful interplay between the gut microbiota and the immune system.

1.5 Aim of the work

This study's main goal is to understand how specific commensal bacterial strains shape the maturation of a previously sterile and immature intestine to effectively fight and eliminate an enteric infection.

2 Material and methods

2.1 Material

2.1.1 Mice

Strain	Hygiene status	Origin	Maintenance
C57BL/6	SFP	Charles River Laboratories	Institute for Medical Microbiology and Hospital Hygiene, University Marburg
C57BL/6	OMM[12]	Institute for Laboratory Animal Science and Central Animal Facility, Hannover Medical School	Institute for Medical Microbiology and Hospital Hygiene, University Marburg
C57BL/6	germ-free	Institute for Laboratory Animal Science and Central Animal Facility, Hannover Medical School	Institute for Medical Microbiology and Hospital Hygiene, University Marburg

2.1.2 Consumables and equipment

Consumables, equipment	Type	Company
Anaerobic culture system	Anaerocult® A anaerobic jar	Merck, Millipore, Darmstadt
	GasPak™ EZ anaerobe container system	BD, Heidelberg
Bioanalyzer	2100	Agilent, USA
	Experion™ Automated Electrophoresis System	Biorad, USA
Cell counter	Cell counting slides	BioRad, Hercules, USA

	TC20™ Automated Cell Counter	BioRad, Hercules, USA
Cell homogenisators and dissociaters	gentleMACS Octo dissociator	Miltenyi Biotec, Bergisch Gladbach
	Ultra-Turrax	IKA, Staufen im Breisgau
Cell strainers	Easystrainer, 100 µm	Greiner, Kremsmünster, Österreich
	Pre-separation cell strainer, 30 µm	Miltenyi Biotec, Bergisch Gladbach
Centrifuges	Megafuge	Heraeus, Hanau
	Microstar 17R, Ministar	Avantor, VWR, Pennsylvania, USA
Flow cytometer	Attune™ NxT	Thermo Fisher Scientific, Waltham, USA
	BD FACSCanto™	BD, New Jersey, USA
	CytoFLEX	Beckman Coulter, California, USA
Gel documentation system	Herolab	Herolab, Wiesloch
	omniDOC	Cleaver Scientific, UK
Heater and shaker	IKA KS260	IKA, Staufen
	Thermomixer comfort	Eppendorf, Hamburg
	Unitexer 1	LCG Labware, Meckenheim
Incubator	HERAcell240i	Heraeus, Hanau
Inoculation loop	10 µl	Sarstedt, Nümbrecht
Microplate reader	FLUOstar omega	BMG Labtech, Ortenberg
Microscope	Leica DM 5500 wide field microscope	Leica Mikrosysteme, Wetzlar
NanoDrop system	1000	Thermo Fisher Scientific, Waltham,

		USA
Digital pH meter	inoLab pH Level 2	Xylem, WTW, Weilheim
Pipettes	Eppendorf Research® plus	Eppendorf, Hamburg
	TipOne® filter tips	Starlab, Hamburg
Power supply		Biometra, Göttingen
(RT-) PCR systems	LightCycler® 480 Instrument II	Roche Molecular Systems, Basel, Switzerland
	Personal cycler	Biometra, Göttingen
	StepOnePlus Real-time PCR System	Thermo Fisher Scientific, Applied Biosystems, Waltham, USA
Scales	Adventurer® Analytical AV812M, Explorer® Analytical EP114CM	Ohaus, Nänikon, Switzerland
Sequencing system	MiSeq sequencing system	Illumina, San Diego, USA
	NovaSeq 6000	Illumina, San Diego, USA
	HiSeq2500	Illumina, San Diego, USA
Sterile filters	Fitropur BT50 filters, 0.22 µm	Sarstedt, Nümbrecht
	Syringe filters, 0.2 µm	Thermo Fisher Scientific, Waltham, USA
Syringes and needles	Syringe, 1.0 ml	B. Braun, Melsungen
	Gavage needle	Thermo Fisher Scientific, Waltham, USA
Tubes and dishes	Biosphere® plus SafeSeal tube, 1.5 ml,	Sarstedt, Nümbrecht

	2.0 ml	
	Centrifuge tube, 15 ml, 50 ml	Sarstedt, Nümbrecht
	Cell culture dishes, 24 wells	Sarstedt, Nümbrecht
	C tubes	Miltenyi Biotec, Bergisch Gladbach
	DNA LoBind tubes, 1.5 ml	Eppendorf, Hamburg
	Microplates, polystyrene	Greiner, Kremsmünster, Österreich
	Microplates, polypropylene	Greiner, Kremsmünster, Österreich
	Reaction tubes, 0.5 ml, 1.5 ml, 2.0 ml	Eppendorf, Hamburg
	Petri dishes	Greiner, Kremsmünster, Österreich
Water purification system	Milli-Q Integral	Bruker Daltonics, Billerica, USA

2.1.3 Bacteria

Strain	**Origin**
Citrobacter rodentium	Kindly provided by Till Strowig, Department Microbial Immune Regulation, HZI, Braunschweig
Escherichia coli	Institute of Medical Microbiology and Hygiene, Marburg
Citrobacter amalonaticus	Institute of Medical Microbiology and Hygiene, Marburg
Lactobacillus murinus	Institute of Medical Microbiology and Hygiene, Marburg
Enterococcus gallinarum	Institute of Medical Microbiology and

	Hygiene, Marburg
Peanibacillus sp.	Institute of Medical Microbiology and Hygiene, Marburg
Escherichia coli DH5α	Institute of Medical Microbiology and Hygiene, Marburg

2.1.4 Enzymes

Enzyme	Origin
Lysozyme, chicken egg white	Merck, Sigma-Aldrich, Darmstadt
HindIII	Fermentas, Vilnius, Litauen
NcoII	Fermentas, Vilnius, Litauen
NotI	Fermentas, Vilnius, Litauen

2.1.5 Antibodies

2.1.5.1 Antibodies for FACS

Antibody	Conjugate	Clone	Working concentration	Company/ cat #
human α-mouse CD146 (LSEC)	FITC	REA1064	1:100 (0,5x10^6 cells)	Miltenyi/ 130-118-252
human α-mouse CD11a/ CD18 (LFA-1)	FITC	REA880	1:100 (0,5x10^6 cells)	Miltenyi/ 130-114-423
human α-mouse CD326 (EpCAM)	FITC	REA977	1:100 (0,5x10^6 cells)	Miltenyi/ 130-117-863
human α-mouse CD24	APC	REA743	1:100 (0,5x10^6 cells)	Miltenyi/ 130-110-824
hamster α-mouse ICAM-1	APC	3E2	1:400 (0,5x10^6 cells)	BD/ 561605
rat α-mouse MadCAM-1	BB700	MECA-367	1:300 (0,5x10^6 cells)	BD/ 746132
rat α-mouse Ly6G	PE	1A8	1:300 (0,5x10^6 cells)	Biolegend/ 127608
rat α-mouse Ly6C	AF700	HK1.4	1:300 (0,5x10^6 cells)	Biolegend/ 128024

2.1.5.2 Antibodies for histology

Antibody	Conjugate	Clone	Working concentration	Company/ cat #
α-mouse VEGFA	none	VG-1	1:200	abcam/ ab1316
rat α-mouse CD31	AlexaFluor® 594	390	1:400	Biolegend/ 102432

2.1.6 Primers and probes

2.1.6.1 Primers and probe for OMM[12] qPCR

Primer	Sequence (5'-3')	Source
Isol46_Exonucl.2_fwd	CGG ATC GTA AAG CTC TGT TGT AAG	Brugiroux et al. 2016, biomers
Isol46_Exonucl.3_rev	GCT ACC GTC ACT CCC ATA GCA	
Probe3_Isol46	FAM-AAG AAC GGC TCA TAG AGG-BHQ1	
sol49_Exonucl._fwd	GCA CTG GCT CAA CTG ATT GAT G	Brugiroux et al. 2016, biomers
Isol49_Exonucl._rev	CCG CCA CTC ACT GGT GAT C	
Probe_Isol49	HEX-CTT GCA CCT GAT TGA CGA-BHQ1	
YL58_Exonucl._fwd	GAAGAGCAAGTCTGATG TGAAAGG	Brugiroux et al. 2016, biomers
YL58_Exonucl._rev	CGG CAC TCT AGA AAA ACA GTT TCC	
Probe_YL58	FAM-TAA CCC CAG GAC TGC ATB-HQ1	
YL27_Exonucl.2_fwd	TCA AGTCAG CGG TAA AAA TTC G	Brugiroux et al. 2016, biomers
YL27_Exonucl.2_rev	CCC ACT CAA GAA CAT CAG TTT CAA	
Probe2_YL27	HEX-CAA CCC CGT CGT GCC-BHQ1	
YL31_Exonucl.2_fwd	AGG CGG GAT TGC AAG TCA	Brugiroux et al. 2016, biomers
YL31_Exonucl.3_rev	CCA GCA CTC AAG AAC TAC AGT TTC A	
Probe2_YL31	FAM-CAA CCT CCA GCC TGC-BHQ1	

Primer	Sequence (5'-3')	Source
YL32_Exonucl.2_fwd	AAT ACC GCA TAA GCG CAC AGT	Brugiroux et al.
YL32_Exonucl.2_rev	CCA TCT CAC ACC ACC AAA GTT TT	2016, biomers
Probe2_YL32	HEX-CGC ATG GCA GTG TGT-BHQ1	
KB1_Exonucl._fwd	CTT CTT TCC TCC CGA GTG CTT	Brugiroux et al.
KB1_Exonucl._rev	CCC CTC TGA TGG GTA GGT TAC C	2016, biomers
Probe_KB1	FAM-CAC TCA ATT GGA AAG AGG AG-BHQ1	
YL2_Exonucl._fwd	GGG TGA GTA ATG CGT GAC CAA	Brugiroux et al. 2016, biomers
YL2_Exonucl._rev	CGG AGC ATC CGG TAT TAC CA	
Probe_YL2	HEX-CGG AAT AGC TCC TGG AAA-BHQ1	
KB18_Exonucl.2_fwd	TGG CAA GTC AGT AGT GAA ATC CA	Brugiroux et al. 2016, biomers
KB18_Exonucl.2_rev	TCA CTC AAG CTC GAC AGT TTC AA	
Probe2_KB18	FAM-CTT AAC CCA TGA ACT GCB-HQ1	
YL44_Exonucl._fwd	CGG GAT AGC CCT GGG AAA	Brugiroux et al.
YL44_Exonucl._rev	GCG CAT TGC TGC TTT AAT CTT T	2016, biomers
Probe_YL44	HEX-TGG GAT TAA TAC CGC ATA GTA-BHQ1	
YL45_Exonucl._fwd	AGA CGG CCT TCG GGT TGT A	Brugiroux et al.
YL45_Exonucl._rev	CGT CAT CGT CTA TCG GTA TTA TCA A	2016, biomers
Probe_YL45	FAM-ACC ACT TTT GTA GAG AAC GA-BHQ1	
Isol48_Exonucl._fwd	GGC AGC ATG GGA GTT TGC T	Brugiroux et al.
Isol48_Exonucl._rev	TTA TCG GCA GGT TGG ATA CGT	2016, biomers
Probe_Isol48	HEX-CAA ACT TCC GAT GGC GAC-BHQ1	

2.1.6.2 Probe for fluorescence in situ hybridisation (FISH)

Probe	Sequence (5'-3')	Source
Eub338	FITC-GCT GCC TCC CGT AGG AGT	Amann et al. 1990, biomers

2.1.7 Plasmids

Plasmid	Backbone	Insert	Restrictions site	Source
pSAB7	pJET 1.2	*'B. caecimuris'* I48	HindIII	Brugiroux et al. 2016
pSAB3	pJET 1.2	*'M. intestinale'* YL27	NotI	Brugiroux et al. 2016
pSAB9	pJET 1.2	*E. faecalis* KB1	NotI	Brugiroux et al. 2016
pSAB12	pJET 1.2	*'A. muris'* KB18	HindIII	Brugiroux et al. 2016
pSAB4	pJET 1.2	*B. coccoides* YL58	HindIII	Brugiroux et al. 2016
pSAB8	pJET 1.2	*L. reuteri* I49	HindIII	Brugiroux et al. 2016
pSAB6	pJET 1.2	*C. innocuum* I46	NotI	Brugiroux et al. 2016
pM1459-1	pCR® 2.1-TOPO®	*A. muciniphila* YL44	HindIII	Brugiroux et al. 2016
pM1460-1	pCR® 2.1-TOPO®	*'T. muris'* YL45	NcoII	Brugiroux et al. 2016
pM1452	pCR® 2.1-TOPO®	*B. longum* YL2*	HindIII	Brugiroux et al. 2016
pM1457-1	pCR® 2.1-TOPO®	*C. clostridioforme* YL32	HindIII	Brugiroux et al. 2016
pM1456-1	pCR® 2.1-TOPO®	*F. plautii* YL31	HindIII	Brugiroux et al. 2016

2.1.8 Kits

Kit	Company
AllPrep DNA/ RNA/ Protein Mini Kit	Qiagen, Hilden, Germany
eBioscience™ Foxp3/ Transcription Factor fixation/ permeabilization	Thermo Fisher Scientific, Waltham, Massachusetts, USA

concentrate and diluent	
QIAmp DNA stool mini kit	Qiagen, Hilden, Germany
Lamina Propria Dissociation Kit, mouse	Miltenyi Biotec Germany, Bergisch Gladbach, Germany
LightCycler® 480 Probes Master	Roche Molecular Systems, Baser, Switzerland
RNeasy Plus Micro Kit	Qiagen, Hilden, Germany
RNeasy Plus Mini Kit	Qiagen, Hilden, Germany

2.1.9 Software and databases

Software/Database	Source
Adobe Illustrator 2021	Adobe Inc.
AmiGO	GO Consortium
Fiji	National Institutes of Health
FlowJo 10	Becton Dickinson GmbH
GraphPad Prism 9	Graphpad Software, Inc.
ImageJ	National Institutes of Health
Imaris	Bitplane
Imaris File Converter	Bitplane
Imaris Stitcher	Bitplane
Imaris Viewer	Bitplane
MC Office 2016	Microsoft
PANTHER	University of Southern California
QuantAnalysis 2.2	Bruker Daltonics GmbH
R, RStudio	RStudio Inc.
STRING	Academic Consortium

2.2 Methods

2.2.1 Ethic statement

All animal experiments have been performed in agreement with the guidelines of the national animal protection law (Tierschutzgesetz (TierSchG) and animal experiment regulations (Tierschutz-Versuchstierverordnung (TierSchVersV)), and the recommendations of the Federation of European Laboratory Animal

Science Association (FELASA). The study was approved by the Regierungspräsidium Gießen, (Germany) under project numbers EX7-2015, Ex9-2019, Ex22-2020, Mr 40/2015 and G49/2020.

2.2.2 Mice maintenance and breeding

All mice were kept in the animal facility of the Biomedical Research Centre of Philipps-University Marburg. WT mice (C57B/6 background) were purchased from Charles River Laboratory and bred under SPF conditions in individual ventilated cages (IVC), with 12 h light cycle, standard rodent pellet diet (LasQCdiet Rod18, HiHyg (Altromin)) and water *ad libitum*. For transcriptome and metabolomics analyses, SPF mice were bred with the same condition as GF mice. GF and mice harboring the OMM^{12} minimal consortium (C57B/6 background) were kindly provided by Dr. M. Basic (Hannover). GF and gnotobiotic mice were bred in sterile isolators with positive pressure differential and filter-top cages (Tecniplast) with autoclaved bedding, food (Altromin 1324 P Forti) and water *ad libitum*. Sterility in GF mice was checked monthly by culturing feces in thioglycollate medium under aerobic and anaerobic conditions for at least 10 days as well as fecal gram-staining. Contamination in gnotobiotic mice was checked by culturing the feces on blood agar plates under aerobic conditions. All handling procedures for GF and gnotobiotic mice were conducted under a laminar flow hood under sterile conditions.

2.2.3 Experiments with *C. rodentium*

2.2.3.1 Nalidixic acid preparation

Nalidixic acid (powder) was weighted using gloves, face mask and protective clothing due to its mutagenic properties. Using a precision scale, 500mg Nalidixic acid powder was weighed and transferred into a 15ml Falcon tube containing 5ml 1xPBS. Since Nalidixic acid is soluble at a basic pH, therefore, 1M NaOH was added dropwise until the solution turned clear. Subsequently, 1xPBS was added to the solution to reach 10ml and a final concentration of 50µg/ml. Under a sterile hood, the solution was filtered through a 0, 22µm filter and freeze in aliquots of 600µl at -20°C.

2.2.3.2 Preparation of LB-agar plates supplemented with nalidixic acid

For Lysogeny Broth (LB) medium preparation, 20 gr LB-powder was diluted in 1 Liter distilled water and autoclaved. 7,5 gr Agar powder was added to 500ml

autoclaved LB-medium and the solution was newly autoclaved. Autoclaved LB-agar was allowed to cool down in a water bath at ca. 50°C and supplemented with 0,1% Nalidixic acid (50µg/ml) solution. Under a sterile hood, LB-agar supplemented with nalidixic acid was distributed onto sterile petri dishes (2-5ml per dish) and allowed to solidify at room temperature. The petri dishes were then stored in sealed plastic bags at 4°C.

2.2.3.3 Overnight culture of C. rodentium for oral gavage

Under a sterile hood, 100ml autoclaved LB-medium were transferred into a sterile Erlenmeyer flask and supplemented with 100µl nalidixic acid (50µg/ml). A single colony from a nalidixic acid plate containing single colonies of *C. odentium* was added to the liquid media. The flask was then placed on a shaker at 150 rpm at 37°C overnight (~16-18hrs).

2.2.3.4 Oral gavage preparation and CFUs quantification

Overnight culture of *C. rodentium* was transferred into two 50ml falcon tubes and centrifuged at 4000 rpm for 20 minutes at 4°C. Supernatant was discarded and the pellet resuspended in 10ml sterile PBS. Mice received an oral gavage (200µl) containing the bacterial solution. For titer quantification, 1 ml was put aside and used later for serial dilution (1:10) with 1xPBS. 10µl of each dilution was placed on a LB-agar plate supplemented with nalidixic acid (50µg/ml). Plates were incubated overnight at 37°C and colony forming units were counted the next day.

2.2.3.5 Stool sample collection and serial dilution for titer quantification of infected mice

Fecal samples were collected by manually restraining the mice and waiting until spontaneous defecation. Samples were collected on 2ml Eppendorf tubes and weighed using a precision scale. 100µl sterile PBS was added per 10mg of stool sample. With the help of an inoculation loop each sample was homogenized till all visible lumps were gone. The serial dilution was performed on a 96-well plate with each well previously filled with 90µl PBS. Undiluted samples were vortexed, 10µl of each sample was transferred to the first wells to make a 10-fold dilution. Subsequently each sample was serially diluted by 10-fold. After dilution, two 10µl drops of each dilution were placed on LB-agar plates supplemented with Nalidixic acid (50µg/ml). Plates were incubated over night at 37°C and colony forming units were counted for quantification the next day.

$$CFU/ml = \frac{Counted\ colonies\ per\ dilution}{2\ (drops\ per\ dilution)}\ x\ 10^{\text{dilution factor}}\ x\ 10^{3}\ (ml)$$

2.2.4 Microbiological experiments

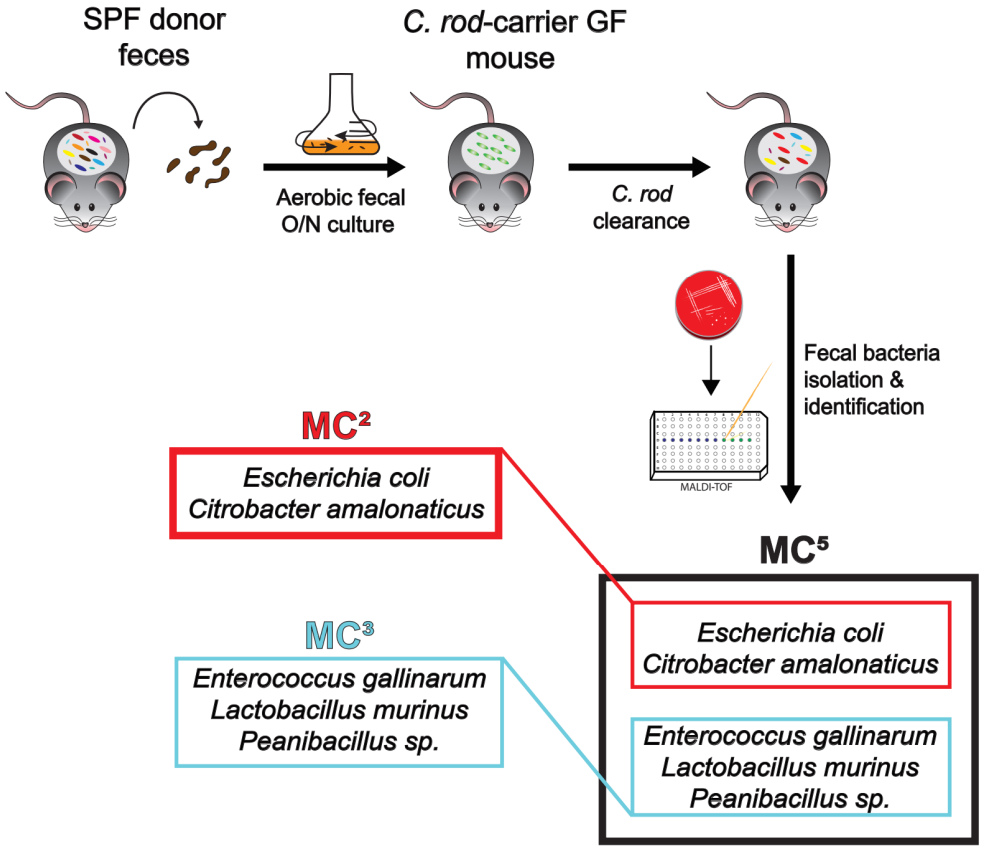

Figure 3: Mining the gut microbiota of SPF mice for facultative anaerobic bacteria.

Outlining of the bacterial isolation process. O/N: Overnight culture, MC: Minimal consortium.

2.2.4.1 Preparation of an aerobic bacteria suspension from SPF stool samples

SPF mice from Charles River laboratory were euthanized by cervical dislocation and stool contents from ceacum and colon were transferred to an Erlenmeyer flask containing 100 ml LB-medium. The suspension was incubated overnight (~16-18hrs) at 37°C on a shaker at 150rpm. 200µl of the suspension was given to GF mice infected with *C. rodentium* (day 22 pi).

2.2.4.2 Isolation of commensal bacteria from ex-GF mice colonized with aerobic bacteria suspension

Stool samples from mice that received the aerobic bacteria suspension (2.1.4.1) were weighted and 100µl PBS was added per 10mg stool. After homogenization, the samples were streaked onto different agar plates (Columbia-blood agar, chocolate-, clostridium difficile-, müller-hinton- and schaedler- agar) and incubated under different conditions (aerobic, anaerobic and CO_2) at 37°C overnight or until colonies were formed. Colonies with different morphologies were isolated and streaked onto new plates. The identification of the different isolated bacterial strains was done using Matrix Assisted Laser Desorption Ionization Time-Of-Flight Mass-Spectrometry (MALDI TOF-MS).

2.2.4.3 Association of mice with commensal bacteria

Facultative anaerobes: A single colony from the isolated bacterial strains was inoculated in 50ml LB- medium and allowed to incubate at 150 rpm at 37°C overnight. The overnight culture was then centrifuge for 20 minutes at 4000 rpm at 4°C. The pellets were resuspended in 5ml PBS and mix together.

MC^5: *L. murinus* (1:4), *E. gallinarum* (1:4), *Paenibacillus sp* (1:4), *E. coli* (1:8) and *C. amalonaticus* (1:8)

MC^3: *L. murinus* (1:3), *E. gallinarum* (1:3) and *Paenibacillus sp* (1:3)

MC^2: *E. coli* (1:1) and *C. amalonaticus* (1:1)

Mice were manually restrained and received an oral gavage (200µl) of bacteria suspension.

2.2.4.4 DNA isolation from faecal and caecal samples

Fecal samples were collected and transferred into 2-ml Eppis containing InhibitEX (Qiagen) buffer and store at -20°C until further processing. Genomic DNA was isolated using the QIAamp DNA Stool mini Kit (Qiagen) following the manufacturer's instructions for DNA isolation for pathogen detection. In brief, faecal samples were homogenized using an inoculation loop and vortexed vigorously for 1 min. The suspension was heated (70°C, 5 min) and vortexed again for 15 sec. Samples were centrifuged (13,000 x g, RT, 1 min) and 200 µl of the supernatant was transferred into a fresh 1.5 ml tube containing 15 µl proteinase K, 200 µl Buffer AL was added and samples were vortexed for 15 sec and incubated at 70°C for 10 min. Afterwards, 200 µl ethanol (96-100%) was added

and the lysate was transferred onto a QIAamp spin column and centrifuged (13,000 x g, RT, 1 min). The column was washed twice with 500 µl Buffer AW1 and subsequently 500 µl Buffer AW2, each wash step followed by centrifugation (13,000 x g, RT, 1 min). Finally, the column was dried by one more centrifugation step (13,000 x g, RT, 3 min). The column was transferred into a fresh 1.5 ml microcentrifuge tube and 100 µl 70°C-prewarmed Buffer ATE was added on the column. The DNA was eluted by centrifugation (13,000 x g, RT, 1 min). The concentration and purity of the DNA were measured with the NanoDrop system (Thermo Fisher Scientific). DNA samples were stored at -20°C.

2.2.4.5 Quantitative PCR for OMM[12] consortium

Quantification of the OMM12 consortium bacterial distribution within stool samples, was made using hydrolysis probe-based RT-qPCR assays (Brugiroux et al. 2016). Here, the probe contains a fluorophore reporter at the 5'-end and a quencher at the 3'-end, which allow FRET (Fluorescence Resonance Energy Transfer). The quencher quenches the fluorescence emitted by the fluorophore and only during amplification, the polymerase hydrolyses the probe leading to the release of the fluorophore and the quencher resulting in the emission of a detectable signal. The amount of specific DNA sequences in the sample correlates with the amount of fluorophores being release and the intensity of the fluorescent signal. Using this method, one can detect several templates per reaction by using probes with different fluorophores.

Genomic bacterial DNA was isolated from faecal and caecal samples as mentioned above.

Duplex RT-qPCRs were run using the LightCycler® 480 Probes Master (Roche) with the following features:

Component	**Volume**
2 x Probes Master	10 µl
forward primer 1 (30 µM)	0.2 µl
forward primer 1 (30 µM)	0.2 µl
probe 1 (25 µM), FAM-labelled	0.2 µl
forward primer 2 (30 µM)	0.2 µl
forward primer 2 (30 µM)	0.2 µl

probe 2 (25 µM), HEX-labelled	0.2 µl
template/ standard DNA (4 ng/ µl)	2.5 µl
PCR grade water	ad 20 µl

Cycling Conditions	**Temperature and time**
1. polymerase activation	95°C, 2 min
2. denaturation	95°C, 2 min
3. annealing	43°C, 10 sec
4. extension	70°C, 10 sec
Repeats of steps 2-4	40 cycles

For quantification, a standard curve with known DNA concentrations was used (2.1.4.6). Beginning with the calculation for the concentration of sequence copy numbers, ten-fold serial dilutions (10^8-10^2 copies/ µl) were prepared in water supplemented with 100 ng/ µl yeast t-RNA. Standard curves measured once can be used for absolute quantification of the copy number in template DNA, for example DNA isolated from faecal samples. Just one single standard in every further run is needed to reproduce the standard curves by the software of the LightCycler® 480 Instrument (Roche). Establishment of the OMM^{12} qPCR quantification was made by Dr. Florence Fischer.

2.2.4.6 Plasmids for OMM^{12} qPCR-standard curve

The absolute quantification of a DNA template via quantitative RT-qPCR requires a standard with known concentration of the copy number. Therefore, plasmids harbouring a sequence of the bacterial 16S rRNA gene were prepared to serve as standard for RT-qPCR assays. Plasmids containing the 16S rRNA gene of OMM^{12} bacteria were kindly provided by Prof. B Stecher (Max von Pettenkofer-Institute Munich). The dried plasmids were solved in 10 µl water and transformed into *E. coli* DH5α via heat shock (42°C, 30 sec).Bacteria were cultured on LB-Agar plates containing ampicillin (100 µg/ ml) at 37°C overnight. Several clones of the overnight culture were picked and cultured in 30 ml LB Medium containing ampicillin (100 µg/ ml) at 37°C overnight. The overnight cultures were centrifuged (3,000 x g, 4°C, 10 min). Plasmid DNA was isolated using the NucleoSpin Plasmid Kit (Macherey-Nagel) according to manufacturer's

instructions. In short, bacterial cells were resuspended and lysed, following centrifugation (11,000 x g, RT, 10 min) to remove cell debris. The supernatant was loaded on a DNA-binding column. After a washing procedure and drying of the membrane the DNA was eluted by addition of elution buffer and centrifugation (11,000 x g, RT, 1min). The yielded plasmids were linearized by cleaving once by restriction enzymes (NotI, NcoI, HindIII). The DNA concentration was measured by NanoDrop system (Thermo Fisher Scientific) and the sequence was controlled by sequencing (Seqlab). Establishment of the Plasmids for OMM[12] qPCR-standard curve was made by Dr. Florence Fischer.

2.2.4.7 In vitro bacterial competition assay

Bacterial competition assay was performed as previously described with a few modifications (Speare et al. 2019). A single colony from *C. rodentium* was incubated in 100-LB medium with a single colony of another commensal bacterial strain overnight at 37°C (150 rpm). Bacterial suspension was centrifuged and the CFU/ ml of *C. rodentium* was quantified using serial dilutions. Growth inhibition was measured as normalized fold changes to *C. rodentium* normal growth in LB-medium.

2.2.4.8 Ultra-High Performance Liquid Chromatography Mass Spectrometry Analysis of Short Chain Fatty Acids

SCFAs isolation was performed in collaboration with Dr. Alesia Walker (Helmholtz Center Munich).

Caecum content (~20mg) were weighed in sterile ceramic bead tubes (NucleoSpin® Bead Tubes, Macherey-Nagel, Dueren, Germany) and extracted with 1 mL chilled methanol (–20°C; LiChrosolv, Supelco, Merck, Darmstadt, Germany) containing 10 parts per million (ppm) of butyric acid-4,4,4-d3 (98 atom% D, Sigma Aldrich, St Louis, MO, USA) as internal standard.

Homogenization and extraction were performed with Precellys® Evolution Homogenizer (Bertin Corp., Rockville, Maryland, USA; 4,500 rpm, 40×3 s, 2 s pause time). Then, samples were centrifuged for 10 min at 21,000 × g and 4°C. SCFA standards including acetic, propionic, and butyric acid were all purchased from Sigma Aldrich (St Louis, MO, USA). They were prepared in methanol as stock solutions at a concentration of concentration of 1,000 ppm. SCFA stock

solutions were diluted 1:10 with methanol to a SCFA working solution of 100 ppm. We prepared a 100 ppm stock solution of butyric acid-4,4,4-d3 in methanol.

Derivatization of SCFAs was performed with 3-nitrophenylhydrazone. Stock solutions of 200 mM 3-nitrophenylhydrazine hydrochloride (3-NPH) and 120 mM of N-(3-dimethylaminopropyl)-N0-ethylcarbodiimide hydrochloride (EDC) were prepared in MilliQ Water (milliQH2O, Milli-Q Integral Water Purification System, Billerica, MA, USA). In total, 3 µL of fecal extract, 3 µL 100 ppm SCFA Mix, 3 µL butyric acid-4,4,4-d3, 20 µL of 3-NPH and 20 µL of EDC were mixed and incubated for 30 min at 40 °C and 1000 rpm in a Thermomixer. A volume of 257 µL MilliQ H2O was added to the derivatized mixture to stop the reaction and was used for LC-MS analysis. DerivatizedSFCAs were prepared at different concentrations (0.4ppm – 0.02 ppm) in MilliQ H2O for calibration spiked with 0.1 ppm 3-NPH-butyric acid-4,4,4-d3.

UHPLC (Acquity UPLC, Waters, Milford, MA, USA) coupled to MS. A reversed-phase separation was applied using a C8 column (C8: 1.7 µm, 2.1 mm × 150 mm, Acquity UPLC BEH, Waters, Milford, MA, USA). Elution of 3-NPH-SCFAs was ensured by the following solvent system of ammonium acetate (NH4Ac, 5 mM, Sigma Aldrich, St Louis, MO, USA) in 0.1% (v/v) acetic acid (Ac, A) (Acetic acid glacial ULC/MS, Biosolve, Valkenswaard, Netherlands) and acetonitrile (B) (ACN, LiChrosolv®, Supelco®, Merck, Darmstadt, Germany). Samples were injected via partial-loop-injection (5 µL). The flow rate was set to 0.3 mL/min, and column temperature to 45°C. A gradient profile was applied by starting at 15% B for 1 min, increasing to 55% B until 10 min, following an increase to 99% B within 4 min. The 99% B was maintained for 2 min, resulting in a total run time of 16 min. A pre-run time of 5 min ensured equilibration of the column applying the starting condition of 15% B.

The MS analysis (amaZon ETD IonTrap, Bruker Daltonics GmbH, Bremen, Germany) was performed in negative electrospray ionization mode with the following parameters: nebulizer gas pressure of 2.0 bar, dry gas flow of 8.0 L/min, dry heater of 250°C, capillary voltage of 4,500 V, and end plate offset of 500 V.

Theoretical m/z values and corresponding retention times of the 3-NPH-SCFAs were the following: acetic acid ([M-H]-: 194.06, 4.1 min), propionic acid ([M-H]-

: 208.08, 5.2 min), butyric acid ([M-H]-: 222.09, 6.5 min), and butyric acid-4,4,4-d3 ([M-H]-: 225.11, 6.5 min). The MS analysis was time-segmented, and mass signals were recorded in multiple reaction monitoring mode with an isolation window on (5 Dalton).

Targeted peak picking and calibration was performed in QuantAnalysis 2.2 (Bruker Daltonics GmbH, Bremen, Germany) with following settings: retention time window 0.1–0.2 min, m/z window ± 0.5 Dalton, Gaussian smoothing window of 0.3 and 6 cycles. Data was exported to comma-separated values files for further analysis. Picked data was normalized to wet caecal weight with a final concentration unit of µmol/g.

2.2.4.9 Non-targeted metabolomics using HILIC UHPLC-MS/MS

Metabolomics was performed in collaboration with Dr. Alesia Walker (Helmholtz Center Munich).

An aliquot of methanol extract (50µL) was evaporated (40°C, SpeedVac Concentrator, Savant SPD121P, ThermoFisher Scientific, Waltham, MA, United States) and reconstituted in an aqueous solution containing 75% ACN. Samples were analyzed by using an UHPLC system (ExionLC, Sciex LLC, Framingham, MA, USA) coupled to a quadrupole time-of-flight mass spectrometer (X500 QTOF MS, Sciex LLC, Framingham, MA, USA).

Mass calibration of the MS was performed prior the analysis of the study by using the calibrant delivery system pump of the X500 QTOF MS (ESI Negative Calibration Solution). Additionally, after every fifth injection an automatic mass calibration of the X500 QTOF MS was conducted for the TOF MS and TOF MS/MS mode. The MS method was set to IDA (Information Dependent Acquisition). The parameters are summarized in Table 1 for negative ionization IDA mode.

Hydrophilic interaction liquid chromatography was conducted by using an iHILIC® - Fusion UHPLC column SS (100 × 2.1 mm, 1.8 µm, 100 Å, HILICON AB, Umea, Sweden). Chromatographic conditions are as follows: Eluent A consisted of 5 mmol/L NH4Ac (pH 4.6) in 95% ACN (pH 4.6) and eluent B of 25 mmol/L NH4Ac (pH 4.6) in 30% ACN.

The LC-run started with 0.1% B and kept for 2 minutes, following by the increase of B to 99.9% over 7.5 minutes. The starting condition of 99.9% B was kept for 2 minutes and reversed to 0.1% B within 0.1 minutes and equilibrated for 4 minutes prior next injection. The run was finished after 12.1 minutes. The flow rate was set to 0.5 mL/min, column temperature was set to 40°C and 5 µL of sample was injected on the column and sample manager was set to 4°C. Weak and strong wash consisted of 95% ACN and 10% ACN.

2.2.4.9.1 Data processing and analysis

Raw LC-MS (.wiff2) data were post-processed using GeneData Expressionist Refiner MS 13.5 (GeneData GmbH, Basel, Switzerland) including chemical noise subtraction, intensity cutoff filter, chromatographic peak picking, deisotoping and library MS search on MS1 level (precursor mass tolerance 0.005 Dalton). Data processing resulted in a data matrix containing clusters (m/z and retention time values) and observed maximum intensity values for each sample. Maximum intensity values were normalized to the wet caecal weight.

Metabolite identification was done by matching experimental tandem MS spectra against spectral libraries, downloaded from MassBank of North America by using MS PepSearch (0.01 Dalton mass tolerance for Precursor and Fragment Search) or by running authentic standards within the study batch. Matches with dot product over 500 were kept for further analysis. Multiple matches were filtered for the best match. For identification levels, level 1 identification was included matching against the set of authentic standards, level 2 included metabolites that were identified by spectral libraries search and level 3 was set for metabolites solely based on MS1 annotation within a precursor mass tolerance of 0.005 Dalton.

2.2.5 Histology

2.2.5.1 Fixation and embedding in paraffin

Around 1 cm of piece of intestine was fixated either with the water-free methacarn (methanol-Carnoy's) fixation to preserve the intestinal mucus layer (Puchtler et al. 1970) or 4% PFA. Following steps were done prior to embedding in paraffin:

Solution	Time
Dry methanol	2 x 30 min

Ethanol, 100%	2 x 15 min
Ethanol/ xylene (1:1, [v/ v])	1 x 15 min
Xylene	2 x 15 min

For PFA fixation, the tissue was transferred into 5 ml PFA solution and fixed over night at 4°C. Following steps were done prior to embedding in paraffin:

Solution	**Time**
Running water	3 h
Ethanol, 70%	2 h-O/ N
Ethanol, 80%	2h
Ethanol, 100%	2h
Isopropanol I	1,5-2h
Isopropanol II	1,5-2h

2.2.5.2 Periodic acid–Schiff (PAS) staining of Paraffin-Embedded Tissue

After sectioning in 3-5 µm thin sections dewaxing was accomplished by an initial incubation at 60°C for 10 min and subsequent incubation in xylene prewarmed at 60°C for 10 min and ethanol for 5 min. The sections were stained with periodic-acid-Schiff (PAS):

Solution	**Time**
Periodic acid, 0,5% [w/ v]	10 min
Running water	5-10 min
Schiff's reagent	20-30 min
Running water	20 min
Mayer's Hämalaun	1-5 min
Running water	5 min

2.2.5.3 Immunohistochemistry Staining of Paraffin-Embedded Tissue

For immunohistochemistry, heat-induced epitope retrieval was performed with EDTA. Staining was performed on a DAKO autostainer plus. After blocking endogene peroxidase, sections were incubated for 45 minutes with mouse monoclonal anti-VEGFa antibody (1:200; abcam #ab1316, clone VG-1). Sections were washed and incubated with Dako REAL EnVision HRP Rabbit/ Mouse

polymer, which reacts with DAB-Chromogen, according to the manufacturer´s protocol.

2.2.5.4 Fluorescence in situ hybridisation (FISH)

Colonic intestinal tissues containing fecal pellets were fixed over night with methacarn as described in 2.1.5.1. For FISH analysis, 3–5 µm thin tissue sections were dewaxed by incubating the slides for 10min at 68°C. The following incubation steps were done:

Solution	**Time**
ROTI® histol, 60°C prewarmed	1 x 5 min
ROTI® histol	2 x 5 min
Ethanol, 100 %	2 x 3 min
Ethanol, 80 %	1 x 3 min
Ethanol, 60 %	1 x 3 min
Aqua dest.	1 x 30 sec

Slides were then treated with 50 µl 4% lysozyme solution (45 min, 37°C) for nucleic acids demasking. After washing, 50 µl hybridization solution containing the primer-probe EUB338 (Amann et al. 1990) was added and incubated for 3 hours at 50°C. Slides were washed several times at 37°C and were dried at RT before mounted with ProLong™ Gold Antifade Mountant with DAPI (Thermo Fisher Scientific) following manufacturer's instructions. The samples were documented at a Leica DM 5500 wide field microscope (Leica) and analyzed with Imaris Software (Bitplane).

2.2.5.5 Tissue preparation for whole-mount staining and ECi clearing

Mice were euthanized with isoflurane and perfused with ice-cold PBS containing heparin. Colon was cut longitudinally and faeces washed out. The tissues were placed in a 12-well plate containing paraformaldehyde (PFA) solution as fixative reagent. After 2 h at 4 °C the samples were washed 3 times (30 min at 4°C) with PBS with 0,3 % Triton-X. Tissues incubated for two hours at RT in 10% normal goat serum (NGS) containing 0,2 % Triton-X. Vessels were stained with Alexa Fluor® 594 anti-mouse CD31 Antibody (Biolegend) in 2% NGS and incubated for ca. 60 h at 4 °C. After antibody incubation the immunolabeled samples were washed in PBS overnight and transferred into the bracket of the autostainer. The

first vial contained a 50% EtOH solution with Aqua ad iniectabilia. For adjusting the pH value, 0.1M NaOH and 0.1M HCl was used. The samples were placed into an ascending ethanol order, starting from 50% to 70% and two times 100% EtOH, to slowly dehydrate the tissue. Each dehydration step was performed for 4 h. After dehydration, the sample was played into a glass vessel and incubated with Ethyl cinnamate (ECi) (Sigma). After at least 2 h incubation in refractive index (RI) matching agent the translucent sample was put into a modified view chamber containing ECi and was analyzed using a 2-photon microscope (Olympus FVMPE-RS) fitted with a 25X water immersion objective (NA = 1,05) with a correction collar set to 0,17 to adjust the RI to the microscopy chambers. Autofluorescence was stimulated using a laser (Spectra Physics) with an excitation wavelength of 780 nm (MaiTai). The Alexa Fluor 594 conjugated CD31 Antibody was excited using the DeepSee laser with an excitation wavelength of 810 nm. Pictures recorded by 2-photon microscopy covered 509 µm2 in total. For quantification, up to 200 crypts per individual image were examined. Using Imaris surface modules for marking crypts partially surrounded by vascular vessels, the vascularization of crypts was quantified.

2.2.5.6 Intravital microscopy (ITM)

Mice were anesthetized by intraperitoneally injection of Ketamine (0,1g/ Kg BW) and 0.01 g Xylazin (0,01g/ KG BW) (Injection solution: 10µl/ g BW). Mice were placed on a preheated plate at 37°C and the depth of anesthesia was monitored by checking withdrawal reflexes and using the MouseSTAT® Jr (Kent Scientific) heart monitor. A small piece of the Ileum (~1 cm) was taken, longitudinally open, feaces were flushed out and the tissue was fixed on a preheated metal plate using agarose gel and tissue glue. After preparation of the ileum, mice were injected intravenously with Qtracker™ 655 Vascular Labels (Invitrogen) to provide real-time vascular contrast. Afterwards mice were euthanized. Quantification was made using Imaris Stitcher and Imaris Software (Bitplane) to manually construct surface modules from the fluorescence intensity. The surface area was measure within a surface bounding box area.

2.2.6 Cell isolation techniques

2.2.6.1 Collecting leukocytes from murine whole blood using Histopaque 119

Mice were euthanized with isoflurane and blood was drawn through cardiac puncture. Blood was collected in 2-ml Eppi tubes with 1 ml HBSS prep

supplemented with 80µl of heparin solution (25.ooo I. E/5ml). Blood was then carefully pipetted on top of 3 ml Histopaque 119 in a 15-ml falcon tube to obtain a density gradient. Samples were centrifuged at room temperature for 5 min at 300 g followed by 20 min at 800 g without break. Interphase containing white blood cells was pipetted into a new 15 falcon tube and wash with FACS buffer. Pellets were treated for erythrocyte lysis with 5ml NH4CL solution for 5 min at room temperature.

2.2.6.2 Isolation of intraepithelial and lamina propria lymphocytes from the murine gut

Before starting, the lab ambient temperature was lowered, all consumables were stored at 4°C and buffers were supplemented with DPI (referred in materials) to reduce intraepithelial neutrophils NETosis (Brinkmann et al. 2004). Mice were euthanized by cervical dislocation. For small intestine preparation, Peyer's patches were removed. Intestines were longitudinally dissected and feces were removed by washing with HBSS WO solution on a petri dish. Intestines were cut into 0,5 cm pieces and transferred into 50-ml falcon tubes with 20ml predigestion solution. Samples were incubated for 20 min at 37°C under constant rotation. Tubes were vortexed for 10 seconds and filtered through a 100 µm strainer, the flow-through containing intraepithelial lymphocytes was stored on ice. The incubation procedure with predigestion solution and vortexing was repeated one more time.

Intraepithelial lymphocytes isolation: Working fast, intraepithelial cells were centrifuged and cell number was quantified as described in 2.1.6.5. Intraepithelial cells were transferred into a 15 ml tube and washed with ice-cold MACS buffer. CD45 magnetic beads were added to the pellets (10µl/10^7 cells) and samples were incubated for 15 min at 4°C. Cells were washed and resuspended in 500µl ice-cold MACS buffer. Cell suspensions were applied onto cold-LS columns holding 70 µm and 30 µm filters (to avoid obstruction of the column) on a MACS separator. Columns were wash 3 times with 500 µl ice-cold MACS buffer, removed from the separator, placed on new 15 ml tubes and labeled cells were flushed out with 5 ml ice-cold MACS buffer. The CD45-negative flow-through cell suspension was used for epithelial cells isolation (2.1.6.4). Cells numbers were quantified as previously described and stained for FACS analysis.

Lamina propia lymphocytes isolation: After the second incubation with predigestion solution, samples were incubated with HBSS WO solution for 20 min at 37°C under constant rotation, vortexed for 10 seconds and filtered through a 100 µm strainer (flow-through was discarded). The intestinal pieces were then transferred into a C tube and incubated with digestion solution containing enzyme D, R and A on the gentleMACS Dissociator with heaters (Program: 37C_m_LPDK_1). Samples were shortly centrifuged and lamina propria cells were resuspended several times with 5 ml MACS buffer. Samples were then filtered through a 100 µm strainer and the filter was washed with 10 ml MACS buffer. Samples were centrifuged and cell number was quantified as described in 2.1.6.5. Samples were centrifuged and pellets were resuspended in the remaining buffer. CD45 magnetic beads were added to the cell suspension (10µl/ 10^7 cells) and samples were incubated for 15 min at 4°C. Cells were washed and resuspended in 500µl MACS buffer. Cell suspensions were applied onto LS columns holding 30 µm filters (to avoid obstruction of the column) on a MACS separator. Columns were wash 3 times with 500 µl MACS buffer, removed from the separator, placed on new 15 ml tubes and labeled cells were flushed out with 5 ml MACS buffer. The CD45-negative flow-through cell suspension was used for endothelial cells isolation (2.1.6.3) Cells numbers were quantified as described in 2.1.6.5 and stained for FACS analysis.

2.2.6.3 Isolation of lamina propria endothelial cells from the murine gut

The $cd45^-$ flow-through cell suspension after lamina propria isolation from 2.1.6.5 was washed with MACS buffer. Pellets were resuspended in the remaining buffer and CD45 magnetic beads were added to the cell suspension (10µl/ 10^7 cells). Samples were incubated for 15 min at 4°C. Cells were washed and resuspended in 500µl MACS buffer. Cell suspensions were applied onto LS columns on a MACS separator. Columns were wash 3 times with 500 µl MACS buffer, removed from the separator, placed on new 15 ml tubes and labeled cells were flushed out with 5 ml MACS buffer. Cells numbers were quantified as described in 2.1.6.5 and stained for FACS analysis.

2.2.6.4 Isolation of epithelial cells from the murine gut

The $cd45^-$ flow-through cell suspension after intraepithelial lymphocytes isolation from 2.1.6.5 was washed with MACS buffer. Cells numbers were quantified as described in 2.1.6.5 and stained for FACS analysis.

2.2.6.5 Cell counting

Cell number was quantified using trypan blue, an azo dye that selectively dyes dead cells blue. Cells suspension was mixed together with trypan blue (1:1) and the mixture was pipetted into dual-chambered slides (Biorad). Cell number was analyzed by the TC20 automated cell counter (gating setup: 6 µm – 15 µm).

2.2.7 Flow cytometry analysis (FACS)

This technology uses laser light to classify and count cells upon their morphologic characteristics and or the presence of biomarkers. With the help of the forward scatter channel (FSC), information on the cell size and the side scatter channel (SSC), information on the granularity of the cells can be gathered. Using both channels, living cells were selected, different cells population identified and cell debris discarded from the analysis. Moreover, fluorochromes bounded to specific antibodies were used to recognize cell markers. Upon encounter with the laser, these fluorochromes become excited and emit light of a certain wavelength, which allows classification of the cells according to the labeled feature.

2.2.7.1 Cell surface staining

Isolated cells were transferred into FACS tubes and washed with FACS buffer before staining. Cells were incubated with FcR blocking reagent for 10 min on ice. After washing, cells were incubated with antibodies for 15 min at 4°C. Cells were washed with 1 x PBS and fixed with 2% Formaldehyde for 20 min at 4°C. After one more washing step, cells were analyzed in a flow cytometer or stained for intracellular markers.

2.2.7.2 Intracellular staining of transcription factors

After surface staining, 100µl fixed cell suspension was permeabilized with 100µl fixation/ permeabilization buffer at RT for 20 min. Cells were washed with 1 x permeabilization buffer and incubated for 15 min at RT in 100µl 1 x permeabilization buffer. After washing with 1 x permeabilization buffer, cells were staining with antibodies diluted in 1 x permeabilization buffer for 30 min at RT. Cells were washed one last time and analyzed in a flow cytometer.

2.2.7.3 Gating for FACS analysis

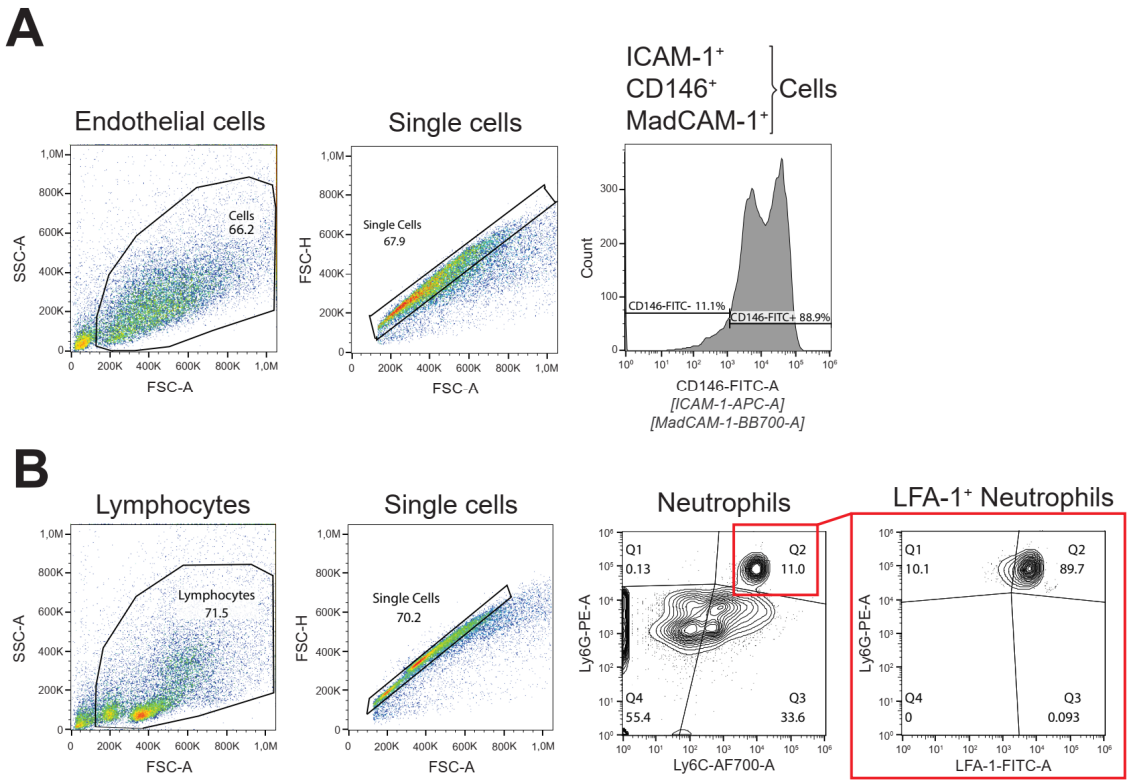

Figure 4: Gating strategy for FACS

(A) Endothelial cells were gated on single ICAM-1+, CD146+ and MadCAM-1+ cells. (B) Neutrophils were gated for single Ly6G+Ly6C+ cells. LFA-1 expression was measured on Ly6G+Ly6C+ cells.

2.2.8 Transcriptional profiling methods

2.2.8.1 RNA sequencing of sorted endothelial cells

The RNA sequencing of endothelial cells was performed in collaboration with Dr. Matthias Klein (Immunology Department, Mainz). Sorted endothelial cells were resuspended in RLT-Buffer containing b-mercaptoethanol. RNA was purified using the RNeasy Plus Micro Kit (Qiagen) according to the manufacturer's instructions. RNA was quantified with a Qubit 2.0 fluorometer (Invitrogen) and the quality was assessed on a Bioanalyzer 2100 (Agilent) using a RNA 6000 Pico chip (Agilent). Samples with an RNA integrity number (RIN) of > 8 were used for library preparation. Barcoded mRNA-seq cDNA libraries were prepared from 20ng of total RNA using NEBNext® Poly(A) mRNA Magnetic Isolation Module and NEBNext® Ultra™ II RNA Library Prep Kit for Illumina® according to the manual with a final amplification of 15 PCR cycles. Quantity was assessed using Invitrogen's Qubit HS assay kit and library size was determined using Agilent's 2100 Bioanalyzer HS DNA assay. Barcoded RNA-Seq libraries were onboard

clustered using HiSeq® Rapid SR Cluster Kit v2 using 8pM and 59bps were sequenced on the Illumina HiSeq2500 using HiSeq® Rapid SBS Kit v2 (59 Cycle). The raw output data of the HiSeq was preprocessed according to the Illumina standard protocol. Sequence reads were trimmed for adapter sequences and further processed using Qiagen's software CLC Ge-nomics Workbench (v20 with CLC's default settings for RNA-Seq analysis). Reads were aligned to GRCm38 genome. Total read counts were further processed in R using the DeSeq2 package to compute differential gene expression and adjusted P values. Gene ontology (GO) analysis and pathway enrichment were performed using PANTHER and AmiGO. Known and predicted interactions for differentially regulated genes (log2fold change higher than 1 and adjusted p value lower than 0.05) were derived using the STRING database. The RNA-Seq data were deposited in the Gene Expression Omnibus (GEO) of the National Center for Biotechnology Information and can be accessed with the GEO accession number GSE 180156 (https://www.ncbi.nlm.nih.gov/geo/query/acc.cgi?acc=GSE180156).

2.2.8.2 Microarray of isolated endothelial cells

Microarrays were done in collaboration with Dr. Hans-Joachim Mollenkopf (MPI, Berlin). MACS-isolated endothelial cells were resuspended in RLT-Buffer containing b-mercaptoethanol. RNA was purified using the RNeasy Plus Mini Kit (Qiagen) according to the manufacturer's instructions. RNA quantity and quality was assessed with an Experion StdSens Chip on an Experion™ Automated Electrophoresis System (Biorad). Microarray experiments were performed as dual-color dye-reversal color-swap hybridizations. Total RNA was labeled with the Low Input Quick-Amp Labeling Kit (Agilent Technologies). In brief, 100 ng total RNA was reverse transcribed and amplified using an oligo-dT-T7 promoter primer and labeled with cyanine 3-CTP and/or cyanine 5-CTP by T7 in-vitro transcription. After precipitation, purification and quantification, 500 ng labeled cRNA of each ratio sample was mixed, fragmented and hybridized to SurePrint G3 Mouse GE v2 8x60K multipack microarrays (Agilent-074809) according to the supplier's protocol (Agilent Technologies). Scanning of microarrays was performed with 3 µm resolution and 20-bit image depth using a G2565CA high-resolution laser microarray scanner (Agilent Technologies). Microarray image data were processed with the Image Analysis/Feature Extraction software

G2567AA v. A.12.1.1.1 (Agilent Technologies) using default settings and the GE2_1200_Dec17 extraction protocol.The extracted MAGE-ML files were analyzed with Rosetta Resolver, Build 7.2.2 SP1.31 (Rosetta Biosoftware). Color-swap Ratio profiles comprising single hybridizations were combined in an error-weighted fashion to create ratio experiments. A 0.5 log2 fold change expression cut-off for ratio experiments was applied together with anti-correlation of ratio profiles, rendering the microarray analysis highly significant ($p < 0.05$). In addition, microarray data was analyzed using the R package limma [Ritchie ME, Phipson B, Wu D, et al. limma powers differential expression analyses for RNA-sequencing and microarray studies. Nucleic Acids Res. 2015;43(7):e47. doi:10.1093/nar/gkv007]. The microarray readout txt files were background corrected, normalized and controlled for quality [Smyth, G. K., and Speed, T. P. (2003). Normalization of cDNA microarray data. Methods 31, 265{273.] (version 3.40.6). Within-array normalization was done by locally estimated scatterplot smoothing (Loess) and between-array normalization was done using the Aquantile method. The hybridization control samples were removed and the gene expression values were averaged for each probe over all replicates of that probe on the microarray, using the avereps function. Microarray data were deposited in the Gene Expression Omnibus (GEO) of the National Center for Biotechnology Information and can be accessed with the GEO accession number GSE 180907 (https://www.ncbi.nlm.nih.gov/geo/query/acc.cgi?acc=GSE180907).

2.2.8.3 RNA sequencing of whole colon

RNA sequencing of whole colon was done in collaboration with MedGenome.Inc (California, USA). Colon tissues were preserved directly after dissection in Allprotect Tissue Reagent (Qiagen). Total RNA was isolated using AllPrep DNA/RNA/Protein Mini Kit (Qiagen) according to the manufacturer's instructions. The RNA was then treated with RNase-Free DNase Set (Qiagen cat#: 79254) and converted to cDNA synthesis technology and generates Illumina-compatible libraries via PCR amplification (Takara cat#: 634444). The directionality of the template-switching reaction preserves the strand orientation of the original RNA according to the manufacturer's protocol. Libraries were sequenced for PE100 cycles to a depth of 30 million paired reads using Illumina NovaSeq 6000. Over Representation Analysis (ORA) and Gene Set Enrichment Analysis (GSEA) was performed for significant differentially expressed protein

coding up and down regulated genes from RNA-Seq data. Gene Ontology ORA was done using enrichGO method from clusterProfiler. Known and predicted interactions for differentially regulated genes (log2fold change higher than 1 and adjusted p value lower than 0.05) were derived using the STRING database. Correlation analysis were performed for normalized counts of all the protein coding genes from all the samples. The RNA-Seq data were deposited in the Gene Expression Omnibus (GEO) of the National Center for Biotechnology Information and can be accessed with the GEO accession number GSE 181502 (https://www.ncbi.nlm.nih.gov/geo/query/acc.cgi?acc=GSE181502).

2.2.9 Statistics

Statistical analyses were done using GraphPad Prism 9. The data are presented as mean ± standard deviation (SD). Multiple group comparisons were done using One-way ANOVA. Multiple group comparisons with kinetics were done using Two-way ANOVA. *In-vivo* data was corrected by controlling the False Discovery Rate using Two-stage step-up method for Benjamin, Krieger and Yakutieli. *In-vitro* data was corrected using statistical hypothesis testing (Tukey). Data with a p-value under 0,05 were considered statistically significant.

3 Results

3.1 14 commensal bacteria from SPF mice induce *C. rodentium* clearance in gnotobiotic mice.

Ever since the unexpected discovery that GF mice become carriers of *C. rodentium* all the while remaining healthy, the question arose as to whether a complex microbiota is needed to eliminate the pathogen (Kamada et al. 2012; Collins et al. 2014). To this date, a defined microbiota capable of inducing the elimination of the widely used enteric pathogen *C. rodentium* has not been described.

The OMM^{12} consortium was used to investigate *C. rodentium* colonization dynamics in the presence of a minimal consortium that previously showed colonization resistance against *S. Thypimurium* infection (Brugiroux et al. 2016). Mice harboring OMM^{12} bacteria were quickly colonized with *C. rodentium* as shown on the pathogen's CFUs in the shed feces on day 2 p.i. (Figure 5A). From day 10 p.i. on, there was a 200-fold reduction in the pathogen burden (Figure 5 A). The titer then remained constant until the end of the experiment on day 40 p.i. (Figure 5A). Despite harboring less pathogen CFUs than GF mice, OMM^{12} mice also became carriers of *C. rodentium*. As the OMM^{12} consortium can be enriched with different bacterial strains and facultative anaerobes, especially the Enterobactericeae, are underrepresented, we sought to find bacterial strains from

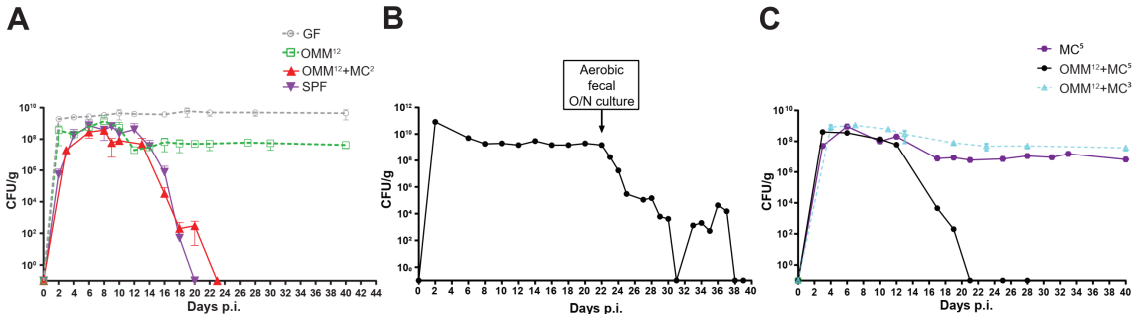

Figure 5: 14 commensal bacteria are sufficient to induce *C. rodentium* clearance in ex-GF mice.

(**A**) *C. rodentium*-carrier GF mouse was gavaged with an overnight (O/N) culture of SPF feces on day 22 p.i. (**B**, **C**) Fecal CFUs in indicated mice after infection with *C. rodentium*.

For *C. rodentium* infection: animals were orally infected with (10^9 CFU/ml) *C. rodentium*. Data shown are mean ±SD of 2-3 independent experiments (A and C).

the microbiota of SPF mice to add to the OMM^{12} consortium. In order to isolate the bacterial strains, fecal samples from the caecum and colon of SPF mice were taken. The samples were incubated under aerobic conditions to potentiate the growth of facultative anaerobic bacteria. Prolong *C. rodentium*-carrier GF mice received the fecal microbiota transfer (FMT) and the *C. rodentium* titer was monitored until pathogen elimination (Figure 5B). Once a FMT culture capable of inducing *C. rodentium* elimination in carrier mice was found, bacterial strains still present in the mice after pathogen elimination were isolated (outline in Figure 3). Five facultative anaerobic bacterial strains were successfully isolated: *E. coli*, *C. amalonaticus*, *L. murinus*, *E. gallinarum* and *Paenibacillus sp.* The five strains were named minimal consortium 5 (MC^{5}) in this study. While MC^{5} bacteria in the absence of OMM^{12} bacteria did not induce pathogen elimination (Figure 5C), OMM^{12}+MC^{5} mice eliminate the pathogen in 3 weeks as seen in SPF mice (Figures 5A and 5C). This finding prompted further selection within the MC^{5} bacteria. Both *E. coli* and *C. amalonaticus* are Enterobactericeae that have previously shown colonization resistance against *C. rodentium* (Kamada et al. 2012; Osbelt et al. 2020). Thus, MC^{5} bacteria was divided into *E. coli* and *C. amalonaticus* (MC^{2}), and *L. murinus*, *E. gallinarum* and *Paenibacills sp.* (MC^{3}). OMM^{12}+MC^{2} mice also eliminated the infection as comparable to SPF mice, while OMM^{12}+MC^{3} mice show similar pathogen titers as OMM^{12} mice (Figures 5A and 5C). Based on this finding, it was concluded that the mediated clearance observed in OMM^{12}+MC^{5} mice was promoted by MC^{2} bacteria. A breakdown of the individual contributions of the different bacteria will be provided later.

3.2 Gut microbes drive neutrophil recruitment into the gut intraepithelial compartment during *C. rodentium* infection.

Neutrophils have a crucial role in the survival and clearance of *C. rodentium* infections (Kamada et al. 2015). Transient depletion of neutrophils with neutralizing antibodies led to a high *C. rodentium* bacterial burden during the duration of the treatment followed by a markedly delayed pathogen clearance in SPF mice (Zarzycka, 2017). Previously, it was shown that GF mice show a normal LP neutrophil infiltration during the infection (Kamada et al. 2012). On the other hand, whole colon kinetic analysis of neutrophil migration showed decrease neutrophil numbers in GF mice in comparison to conventional mice during *C. rodentium* infections (Zarzycka, 2017). Moreover, neutrophil migration peaked on day 8 p.i. in GF and on day 10 p.i. in SPF mice (Zarzycka, 2017).

Analyses of the absolute cell number (ACN) of infiltrating neutrophils in the colon of GF, gnotobiotic and SPF mice showed increased neutrophils numbers in

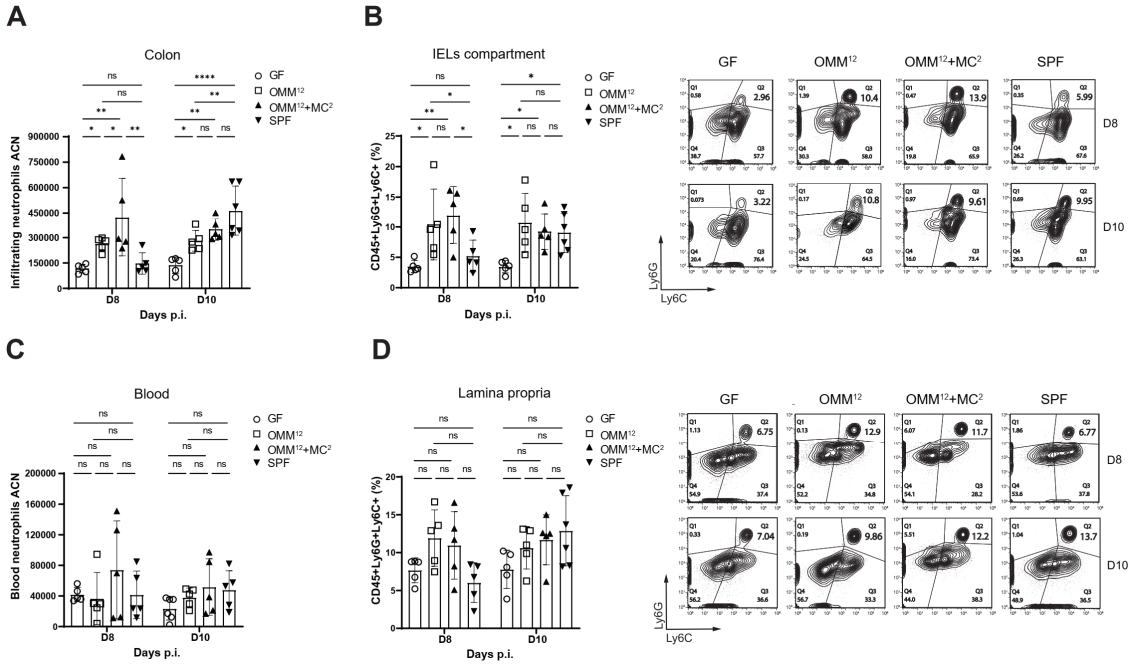

Figure 6: Neutrophil recruitment during *C. rodentium* infection into the intestinal lumen is impaired in GF mice.

(**A**, **C**) Absolute cell number (ACN) of infiltrating neutrophils in the colon (A) and blood (C) of indicated mice at day 8 and 10 p.i. (**B**, **D**) Neutrophil frequencies in the colonic iEL compartment (B) and LP (D) of indicated mice at day 8 and 10 p.i.

For *C. rodentium* infection: animals were orally infected with (10^9 CFUs/ ml) *C. rodentium*. Data shown are mean ±SD of 2-3 independent experiments, each symbol represents the individual value for one mouse. Two-way ANOVA was used: ****$p < 0.0001$; ** $p \leq 0.01$; * $p \leq 0.05$; ns, non-significant.

OMM^{12} and OMM^{12}+MC^{2} mice on day 8 p.i. in comparison to both GF and SPF mice (Figure 6A). On day 10 p.i., SPF mice showed a strong neutrophilic migration as seen in the neutrophil numbers in the whole colon tissue (Figure 6A). OMM^{12}+MC^{2}, but not OMM^{12}, mice showed similar neutrophil numbers as SPF on day 10 p.i. (Figure 6A). Notably, OMM^{12}+MC^{2} mice showed an increased neutrophil infiltration into the gut than OMM^{12}, both on day 8 and 10 p.i. (Figure 6A). As neutrophils migrate from the blood into the luminal site, they first extravasate into the LP, followed by the iEL compartment. Therefore, neutrophil frequencies in the LP and in the iEL compartment were examined. Similar to previous reports (Kamada et al. 2012), no significant differences were observed in the neutrophil frequencies in the LP of GF, gnotobiotic and SPF mice, neither on day 8 nor on day 10 p.i. (Figure 6D). The neutrophil percentages in the iEL compartment, however, showed a different outcome. Again, on day 8 p.i., OMM^{12} and OMM^{12}+MC^{2} mice had higher neutrophil percentages than GF and SPF mice (Figure 6B). On day 10.pi., the neutrophilic frequencies in the iEL compartment were significantly decreased only in GF mice. In contrast, OMM^{12}, OMM^{12}+MC^{2} and SPF mice showed similar higher percentages (Figure 6B). Analyses of neutrophil numbers present in the blood excluded a possible granulopoiesis defect in GF or OMM^{12} mice during the infection, as all mice displayed similar neutrophil amounts (Figure 6C). These data point to a microbiota-mediated mechanism that favors neutrophil recruitment into the intestinal iEL compartment during an enteric infection.

3.3 LFA-1 expression on neutrophils is not regulated by the gut microbiota.

Neutrophil function has been shown to be partially modulated by the microbiota, as neutrophils from the BM of GF mice display a reduced phagocytic activity than BM neutrophils from SPF mice (Clarke et al .2010). Due to the impaired neutrophil recruitment observed in GF mice during *C. rodentium* infection, the expression of LFA-1 on neutrophils from GF, gnotobiotic and SPF was investigated.

Circulating neutrophils and those infiltrating into the colon expressed high levels of LFA-1 on the surface independently of the host's microbial status (Figure 7). Thus, cell adhesion molecule expression on neutrophils, important for transmigration, might not be regulated by the intestinal microbiota.

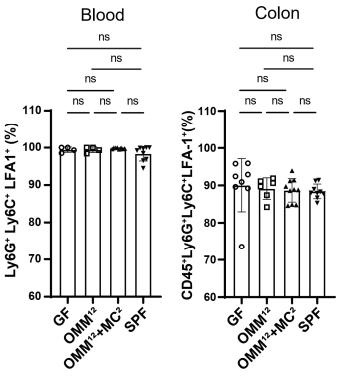

Figure 7: Neutrophils express high levels of LFA-1 regardless of the host microbial colonization.

Frequencies of LFA-1$^+$ neutrophils in the blood and colon of *C. rodentium* infected mice.

Animals were orally infected with (10^9 CFUs/ ml) *C. rodentium*. Data shown are means ±SD and representative of at least two independent experiments, each symbol represents the individual value for one mouse. One-way ANOVA was used: ns, non-significant.

3.4 Colonic endothelial cell gene expression and activation is modulated by the intestinal microbiota.

Leukocyte transmigration requires the activation of the endothelium. In particular, the presence of the gut microbiota was found to facilitate vascular leukocyte adhesion under challenge conditions (Karbach et al. 2016).

Gene expression of endothelial cells from GF and SPF mice during steady state conditions was analysed. Volcano plotting of the upregulated genes in both mice showed that endothelial cells from conventional mice had a far more active cellular transcriptome than their GF counterparts (Figure 8A). STRING analysis

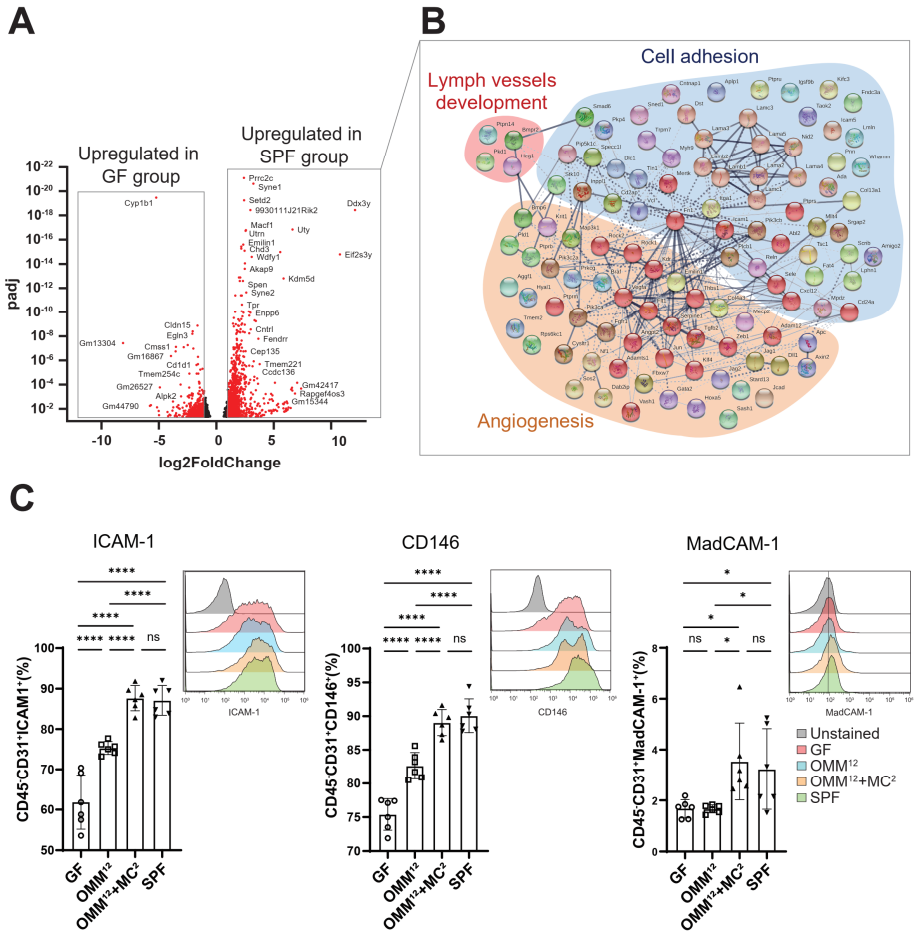

Figure 8: Gut microbes influence the transcriptome and adhesion-molecule expression of colonic endothelial cells.

(**A**) Volcano plot showing fold-change of gene expression in colonic endothelial cells of GF and SPF mice. Genes with significantly upregulated expression between the two groups are (log2-fold change ≥ 1; p-adj < 0.05) are marked in red. (**B**) STRING analysis for significantly upregulated transcripts of colonic endothelial cells from SPF mice. (**C**) Expression of ICAM1⁺, CD146⁺ and MadCAM1⁺ on colonic endothelial cells in indicated mice.

Data shown are representative of at least two independent experiments with means ±SD, each symbol represents the individual value for one mouse (C). One-way ANOVA was used: ****p < 0.0001; ** p ≤ 0.01; * p ≤ 0.05; ns, non-significant.

of the upregulated genes in SPF mice revealed gene networks for cell adhesion, lymph vessel development and angiogenesis (Figure 8B). Isolated colonic endothelial cells from GF, gnotobiotic and SPF mice were further analysed via FACS. The percentages of ICAM-1, CD146 and MadCAM-1 positive endothelial cells were similarly in OMM^{12}+MC^{2} and SPF mice, and significantly much higher than in GF and OMM^{12} mice (Figure 8C). The OMM^{12} bacteria could partially induce ICAM-1 and CD146 expression in comparison to GF mice, which had the lowest expression of all three cell adhesion molecules (Figure 8C). Interestingly, OMM^{12} bacteria did not promote MadCAM-1 expression, meaning that MC^{2} bacteria was specifically able to induce its expression in the presence of OMM^{12} (Figure 8C).

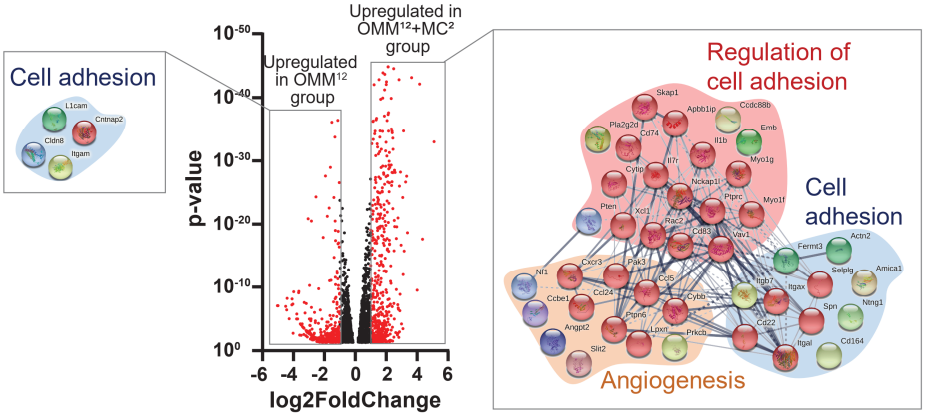

Figure 9: MC^{2} bacteria promotes expression of angiogenesis-genes in colonic endothelial cells.

Volcano plot showing fold-change of gene expression in colonic endothelial cells of OMM^{12} and OMM^{12} +MC^{2} (log2-fold change≥1; p-adj < 0.05). STRING analysis for significantly upregulated transcripts in colonic endothelial cells of OMM^{12} (left) and OMM^{12} + MC^{2} (right) mice.

As addition of MC^{2} bacteria induced endothelial activation, endothelial cells from OMM^{12} and OMM^{12}+MC^{2} mice were analysed using microarray technology. Similar to SPF mice, OMM^{12}+MC^{2} mice displayed more upregulated genes than OMM^{12} mice as shown in the volcano plot (Figure 9). Moreover, STRING analysis showed significantly upregulated gene networks for cell adhesion in both mice, however, only in OMM^{12}+MC^{2} mice gene networks for angiogenesis were detected (Figure 9).

Collectively, these data indicate that members of the commensal microbiota regulate the transcriptome and activation of colonic endothelial cells, thus, possibly making them more permissive to leukocyte transmigration.

3.5 Microbial colonization reduces crypt bifurcation thereby increasing colonic vascular connections.

Crypts undergoing fission is a typical sign of the developing and, therefore, immature intestine. Contrarily, adult GF rats have been shown to have significantly more bifurcated crypts than conventional rats (McCullough et al. 1998).

As the endothelial proliferation marker, CD146, and gene networks for angiogenesis were upregulated/induced in colonic endothelial cells from OMM^{12}+MC^{2} and SPF mice, colonic vessels were examined using whole-mount staining. Histological analyses of the medial colon revealed significantly more bifurcated crypts in GF mice than in all the other groups (Figure 10B). Crypt bifurcations were also accompanied by a reduced crypt vascularization, as seen in the missing vascular cross connections using CD31 staining (Figure 10A). Quantification of bifurcated crypts disclosed that OMM^{12} colonization led to a significant reduction in branched crypts in comparison to GF mice (Figure 10B). Importantly, only once OMM^{12} mice received MC^{2} bacteria, the crypt bifurcations were comparable to SPF mice (Figure 10B). Concordantly, the relative abundance of colonic endothelial cells was similarly reduced in GF and OMM^{12} mice and only increased in OMM^{12}+MC^{2} and SPF mice (Figure 10C).

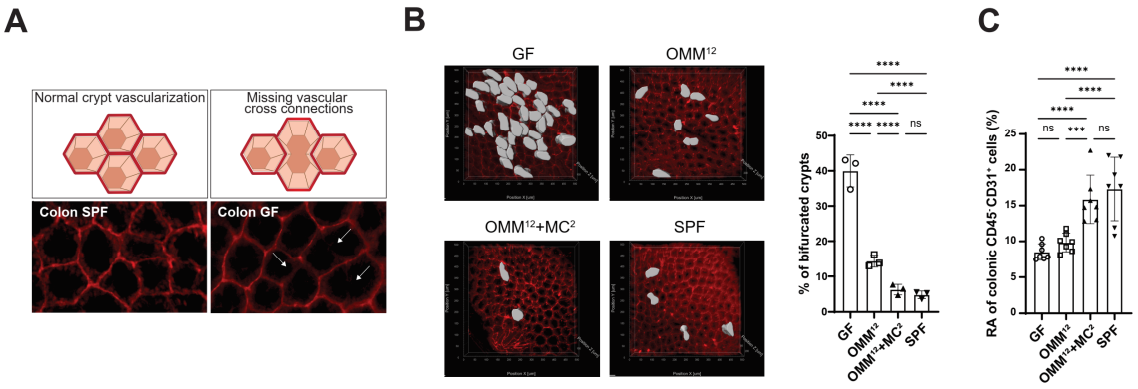

Figure 10: Strong reduction of crypt bifurcations leads to more vascular cross-connections and higher abundance of colonic endothelial cells.

(**A**) Schematic and microscopic representation of vascular cross-connections (missing: arrows) in the colon (Red staining, CD31^{+} blood vessels). (**B**) Representative images and quantification of whole-mount-staining in indicated mice. Partial vascularized crypts were quantified by insertion of contour surface modules (grey areas) (Red staining, CD31^{+} blood vessels). (**C**) Relative abundance (RA) of colonic endothelial cells in the LP of indicated mice.

Shown are representative data of at least two independent experiments with means ±SD, each symbol represents the individual value for one mouse (B and C). One-way ANOVA was used: ****p < 0.0001; ** p ≤ 0.01; * p ≤ 0.05; ns, non-significant.

3.6 Small intestinal endothelial activation is not regulated by the intestinal microbiota.

Previous studies showed that GF mice have a decreased ICAM-1 expression not only in the ileum but also in other distant organs (Komatsu et al. 2000).

Intrigued by the commensal-induced endothelial activation in the colon, the cell adhesion molecules expression in the whole SI was investigated. In contrast to the results obtained from the colon, ICAM-1, CD146 and MadCAM-1 expression was unaffected by the commensal colonization in endothelial cells of the whole SI (Figure 11). Hence, as the commensal burden in the SI is significantly less diverse and dense than in the colon, non-microbial factors might specifically regulate small intestinal endothelial activation in the duodenum and jejunum.

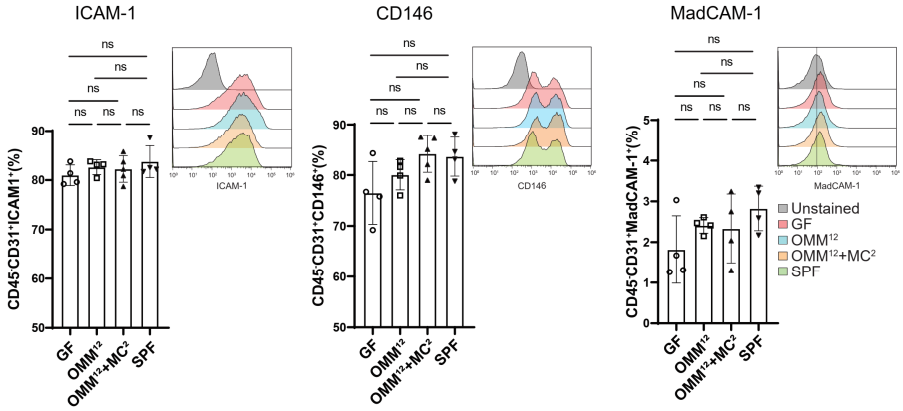

Figure 11: Cell adhesion molecule expression in endothelial cells from the whole SI is not influenced by the gut microbiota.

Expression of ICAM1+, CD146+ and MadCAM1+ on endothelial cells of the SI in indicated mice.

Data shown are representative of at least two independent experiments with means ±SD, each symbol represents the individual value for one mouse. One-way ANOVA was used: ****p < 0.0001; ** p ≤ 0.01; * p ≤ 0.05; ns, non-significant.

3.7 Small intestinal angiogenesis and VEGF expression are induced by specific bacteria.

The presence of the gut microbiota ensures the upholding of the intricate villus capillary network by inducing VEGF expression, as the SI microvascular density is substantially reduced in GF and ABX-treated mice (Suh et al. 2019; Stappenbeck et al. 2002).

In a complementary approach, the SI vascularity was examined using intravital microscopy (IVM). As previously reported (Stappenbeck et al. 2002), GF mice had a lower villus capillary network than SPF mice (Figure 12A), but also in comparison to OMM^{12} and OMM^{12}+MC^{2} mice (Figure 12A). While OMM^{12} colonization triggered partial ileal angiogenesis, the addition of MC^{2} resulted in a similar villus vascularity as SPF mice (Figure 12A). More importantly, the observed angiogenesis correlated with strong VEGFa induction in OMM^{12}+MC^{2} mice, which was almost comparable to SPF (Figure 12B). On the other hand, GF and OMM^{12} mice were found to express marginal levels of VEGFa in the ileum (Figure 12B). These data suggest that small intestinal angiogenesis and VEGFa induction are specifically modulated by MC^{2} bacteria and only partially by members of the OMM^{12} consortium.

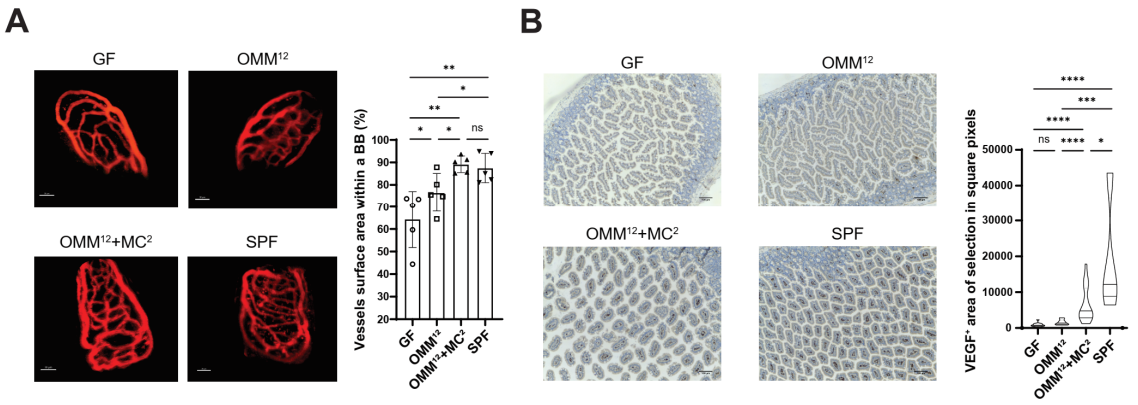

Figure 12: The microvascular density and VEGFa expression in the ileal villi positively correlate with the host microbial status.

(**A**) Representative images and quantification of IVM, multi-photon microscopy of small intestinal blood capillaries after i.v. injection of Qtracker™ 655. Vessel areas were quantified with trace image processing to make morphometric measurements within a bounding box (BB). Results are representative of 4-5 experiments. (**B**) Representative immuno-staining and violin-plot quantification of VEGFa expression (brown staining) in the ileum of indicated mice.

Shown are representative data with means ±SD, each symbol represents the individual value for one mouse (A). One-way ANOVA was used: ****p < 0.0001; ** p ≤ 0.01; * p ≤ 0.05; ns, non-significant.

3.8 MC² bacteria drive PC differentiation in the adult SI of gnotobiotic mice.

PCs play a crucial role in regulating small intestinal angiogenesis by secreting pro-angiogenic signalling molecules in response to microbial signals (Stappenbeck et al. 2002; Hassan et al. 2020).

PC frequencies were examined using FACS analyses. Total PCs were identified as EpCAM⁺CD24⁺ cells, and lysozyme producing PCs as CD24⁺SSC^{hi} cells (Figures 13A-D). The frequencies of total PCs were only elevated in OMM^{12}+MC², while GF, OMM^{12} and even SPF mice had similar quantities of total PCs (Figure 13A). A similar outcome was found when lysozyme PCs were analysed, as only OMM^{12}+MC² showed elevated levels of this cell type (Figure 13B). Since natural microbial colonization happens during the postnatal stage in SPF mice, total PCs

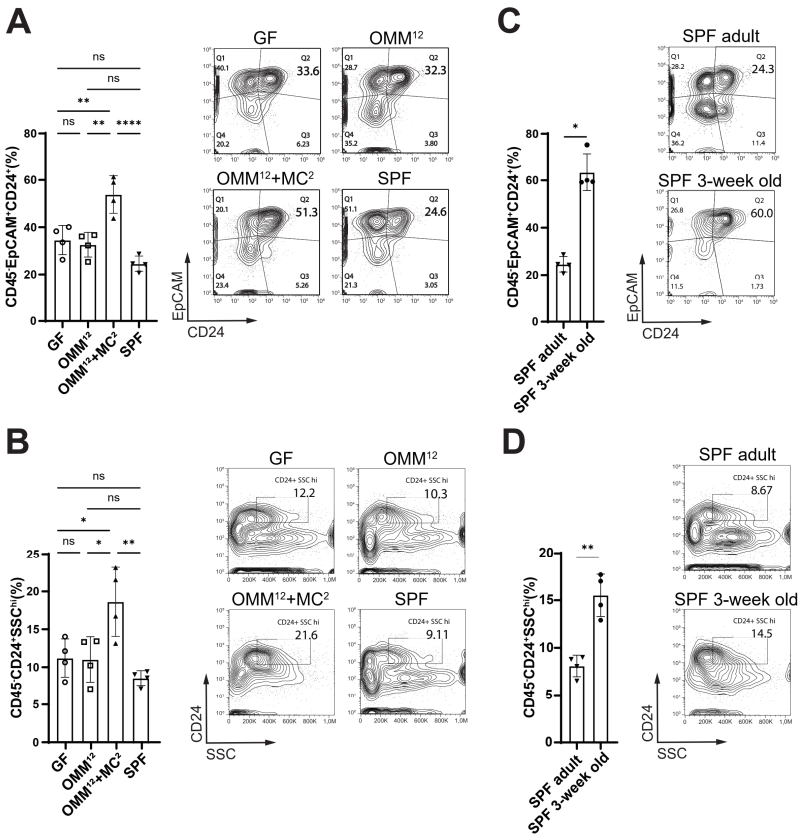

Figure 13: PCs differentiation can be triggered in the adult SI by specific bacteria.

(**A**, **B**) Quantification and representative flow cytometry plots of CD45⁻EpCAM⁺CD24⁺ and CD45⁻CD24⁺SSC^{hi} paneth cells in GF, gnotobiotic and SPF mice. (**C**, **D**) Quantification and representative flow cytometry plots of CD45⁻EpCAM⁺CD24⁺ and CD45⁻CD24⁺SSC^{hi} paneth cells in adult and 3-week old SPF mice.

Data shown are representative at least two independent experiments with means ±SD, each symbol represents the individual value for one mouse. One-way ANOVA was used: ****p < 0.0001; ** p ≤ 0.01; * p ≤ 0.05; ns, non-significant.

and lysozyme producing PCs percentages were analysed in SPF mice before weaning. 3-week old SPF mice showed significantly elevated levels of both PCs (Figures 13C and 13D). Thus, PC differentiation might possibly be a direct response towards initial microbial colonization of specific bacterial strains.

3.9 Commensals do not modulate colonic Paneth-like cell differentiation and epithelial Ki67 expression.

Even though PCs are absent in the colon, CD24$^+$ cells with analogous PC-phenotypes have been described to reside there (Sato et al. 2011). These colonic Paneth-like cells could be implicated in driving colonic crypt fission and angiogenesis (Langlands et al. 2016)

In contrast to the SI, Paneth-like cells in the colon were not affected by the microbial status of their host (Figures 14A and 14B). Further, the proliferation of colonic epithelial cells was investigated using the proliferation marker Ki67. Interestingly, despite the decreased crypt bifurcation, colonic epithelial cells did not change their proliferative properties after microbiota introduction or in SPF mice (Figure 14C). Ki67 expression was only elevated, as expected, in young SPF mice (data not shown). These data challenge the assumption that Paneth-like cells drive angiogenesis in the colon. Furthermore, as Ki67 expression remained unchanged, the question arises as to whether the GF colon is constantly undergoing crypt fission or whether the crypts are simply branched.

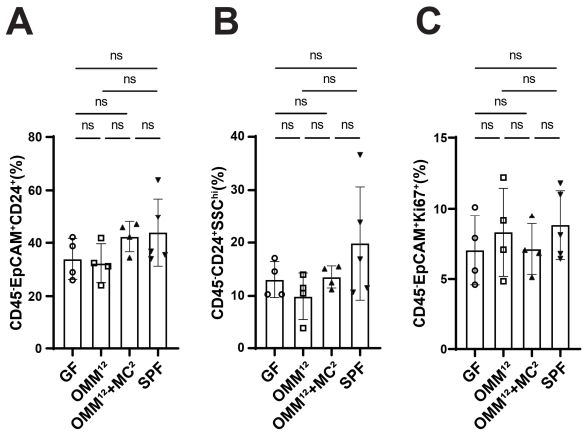

Figure 14: Paneth-like cells differentiation and ki67+ expression on epithelial cells is not mediated by the microbiota in the colon.

(**A**, **B**) Quantification of CD45$^-$EpCAM$^+$CD24$^+$ and CD45$^-$CD24$^+$SSC^{hi} Paneth-like cells, (**C**) and CD45$^-$EpCAM$^+$Ki67$^+$ epithelial cells in the colon of indicated mice.

Data shown are representative of at least two independent experiments with means ±SD, each symbol represents the individual value for one mouse. One-way ANOVA was used: ns, non-significant.

3.10 Gut microbiota promotes colon shortening and colonic crypt lengthening.

Experiments on GF mice revealed that conventionalization, as well as colonization with certain bacterial strains, induced “normalization” of the cecal size (Stecher, 2021; Koopman et al. 1984). Microscopically, colonic crypts of SPF and GF pups have a similar length, however, only in SPF mice, between days 14-20 of age, do the crypts undergo rapid elongation until reaching around 200 µm in length (Hill and Cowley, 1990).

The colon lengths of age-matched adult C57BL/6 mice were measured and analysed. GF mice had longer colons and caecums than all the other groups (Figure 15A). Interestingly, OMM^{12} colonization significantly reduced the length of the colon as comparable to SPF mice (Figure 15A). The addition of MC^{2} bacteria did not macroscopically alter the colon morphology further (Figure 15A). However, colons from OMM^{12}+MC^{2} and SPF mice did harbour higher numbers of fecal pellets than the ones from GF and OMM^{12} mice (Figure 15A). Analyses of the crypt length indicated that GF mice bear significantly shorter crypts as well (Figure 15B). Both OMM^{12} and OMM^{12}+MC^{2} bacteria could marginally increase the length of the crypts, but SPF mice still harboured the longest crypts of all groups (Figure 15B).

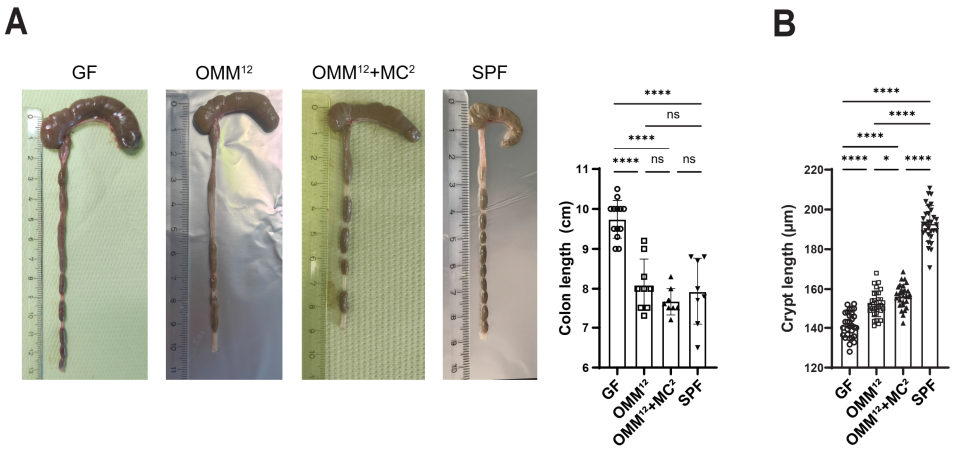

Figure 15: Morphological changes in the colon of gnotobiotic and SPF mice.

(**A**) Macroscopic alterations and colon length in response to the microbiota. Each symbol represents the individual value for one mouse (**B**) Quantification of colonic crypt length in indicated mice, each symbol represents one crypt (n=3).

Data shown are means ±SD; at least two independent experiments were performed. One-way ANOVA was used: ****p < 0.0001; ** p ≤ 0.01; * p ≤ 0.05; ns, non-significant.

Collectively, these data revealed that OMM^{12} bacteria induce colon shortening and together with MC^{2} bacteria, only partial crypt lengthening.

3.11 MC^{2} changes the bacterial distribution within the OMM^{12} consortium, increases adherent mucus, and remains in the gut lumen.

Although the OMM^{12} microbiota normally allows the addition of other bacterial strains, there are some exceptions: Mice that have been previously associated with OMM^{12} cannot be colonized with SFB bacteria (Bolsega et al. 2019). However, when mice are first monocolonized with SFB and then introduced to OMM^{12} bacteria, SFB stably remain in the intestine (Bolsega et al. 2019).

In order to determine if MC^{2} bacteria outcompetes members of the OMM^{12} consortium, four GF mice were colonized with OMM^{12} and the distribution of OMM^{12} members was examined. The presence of 10 bacterial strains was confirmed by qPCR (Figure 16A). OMM^{12} member's *B. longum* and *A. muris* were not detected in the shed feces, as seen in previous studies, where both strains either do not colonize or are below the detection limit (Brugiroux et al. 2016; Bolsega et al. 2019). The same mice were then given MC^{2} bacteria and the distribution of OMM^{12} bacteria was again investigated. MC^{2} colonization led to the significant reduction of *A. muniphila*, while *B. caecimuris* increased (Figure 16B). Next, adherent mucus was analysed using PAS-staining. SPF mice harboured the most abundance of adherent mucus, followed by OMM^{12}+MC^{2}, OMM^{12} and, finally, GF mice (Figure 16C). As OMM^{12} and MC^{2} bacteria are able to profoundly change the morphology and cellular expression of the murine intestine, FISH staining was done in order to discard possible invasive properties coming from the bacterial members of the consortia. Staining of the medial colon using FISH revealed that OMM^{12}+MC^{2} bacteria were restricted to the gut lumen and the mucus (Figure 16D). Concordantly, no bacteria were found in close proximity to the epithelium as well as no epithelial lesions were observed (Figures 16C and 16D).

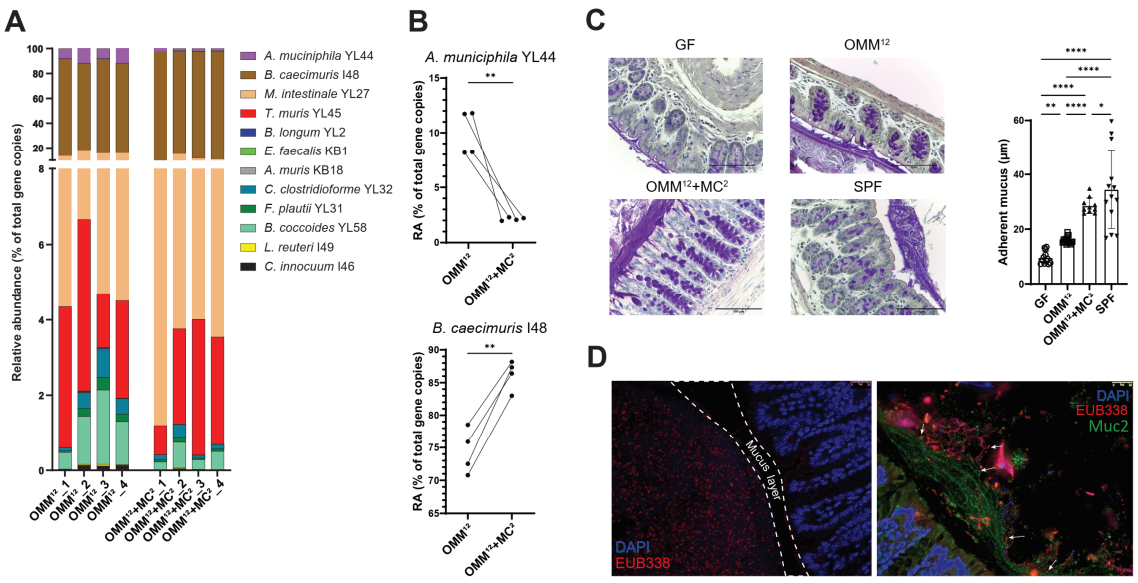

Figure 16: Mc² bacteria induce changes in the distribution of the OMM ¹² consortium and colonic adherent mucus.

(**A**) Representative OMM[12] composition (relative abundance) determined by strain-specific qPCR assay in indicated mice after co-housing with OMM[12] donor mice for 10 days followed by MC[2] colonization for 14 days. (**B**) Relative abundance (RA) of *A. muciniphila* YL44 and *B. caecimuris* I48 in OMM[12] and OMM[12]+MC[2] mice. (**C**) Representative PAS staining and quantification of adherent mucus (violet staining) in the medial colon of indicated mice. (**D**) OMM[12]+MC[2] bacteria were visualized by FISH in medial colon (red, bacteria (arrows in the right image); blue, DAPI; green, mucus (right image)).

Data shown are means ±SD and representative of at least two independent experiments, each symbol represents the individual value for one mouse (B, C). One-way ANOVA was used: ****p < 0.0001; ** p ≤ 0.01; * p ≤ 0.05; ns, non-significant.

3.12 OMM[12]+MC[2] profoundly influences the transcriptome of the murine colon by boosting the immune system.

Transcriptomics of monocolonized mice could show that certain microorganisms can have a specific impact on the host (Hoffmann et al. 2015; Uchimura et al. 2018). Some bacterial strains, e.g. *B. thetaiotaomicron*, almost recapitulate the effects of a complex conventional microbiota in terms of the immune-system's pathway activation (Hoffmann et al. 2015).

Based on the previous results on intestinal angiogenesis, endothelial activation and tissue morphology changes, the whole colon transcriptome of GF mice, mice after colonization with the minimal consortia and SPF mice was analysed. A two-group comparison from differentially expressed transcripts in a kinetic order beginning with GF mice vs OMM[12] mice was performed (Figures 17A-C). The genetic and protein interactions included up-regulated gene networks for

chemokines, cytokines, immune response/ development, B- and T- cell activation, antimicrobial response, as well as cell adhesion, epithelial proliferation and circadian rhythm after OMM^{12} colonization (Figure 17C). Contrarily, GF mice showed upregulated homeostatic gene networks for the mitotic cell cycle and response to abiotic stimuli (Figure 17A). Next, we investigated the gene networks that were distinctly upregulated after OMM^{12} mice received MC^{2} bacteria in a time dependent manner (Figure 17D). MC^{2} bacteria, similar to OMM^{12} bacteria were able to further induce gene networks for cytokines/ response to cytokines, chemotaxis, antimicrobial response, innate/ adaptive immune responses, cell adhesion and tissue development (Figure 17D). Furthermore, colonization of MC^{2} bacteria, specifically induced gene networks for angiogenesis and complement responses (Figure 17D). Principal component analysis revealed that gut colonization with OMM^{12} and OMM^{12}+MC^{2} bacteria induced a similar expression profile to that of SPF mice, while GF mice had a completely distinct profile from the other groups (Figure 17E). Lastly, a two group comparison of SPF and OMM^{12}+MC^{2} mice revealed multiple upregulated pathways involved in immune activation in OMM^{12}+MC^{2} mice, while SPF mice showed normal homeostatic pathways as seen in GF mice (data not shown).

These data show the extensive reprogramming that the adult murine colon undergoes after introduction of commensal bacteria. Particularly, colonization of GF mice with OMM^{12} and MC^{2} bacteria seems to promote intestinal immune system and vascular system maturation as well as tissue development.

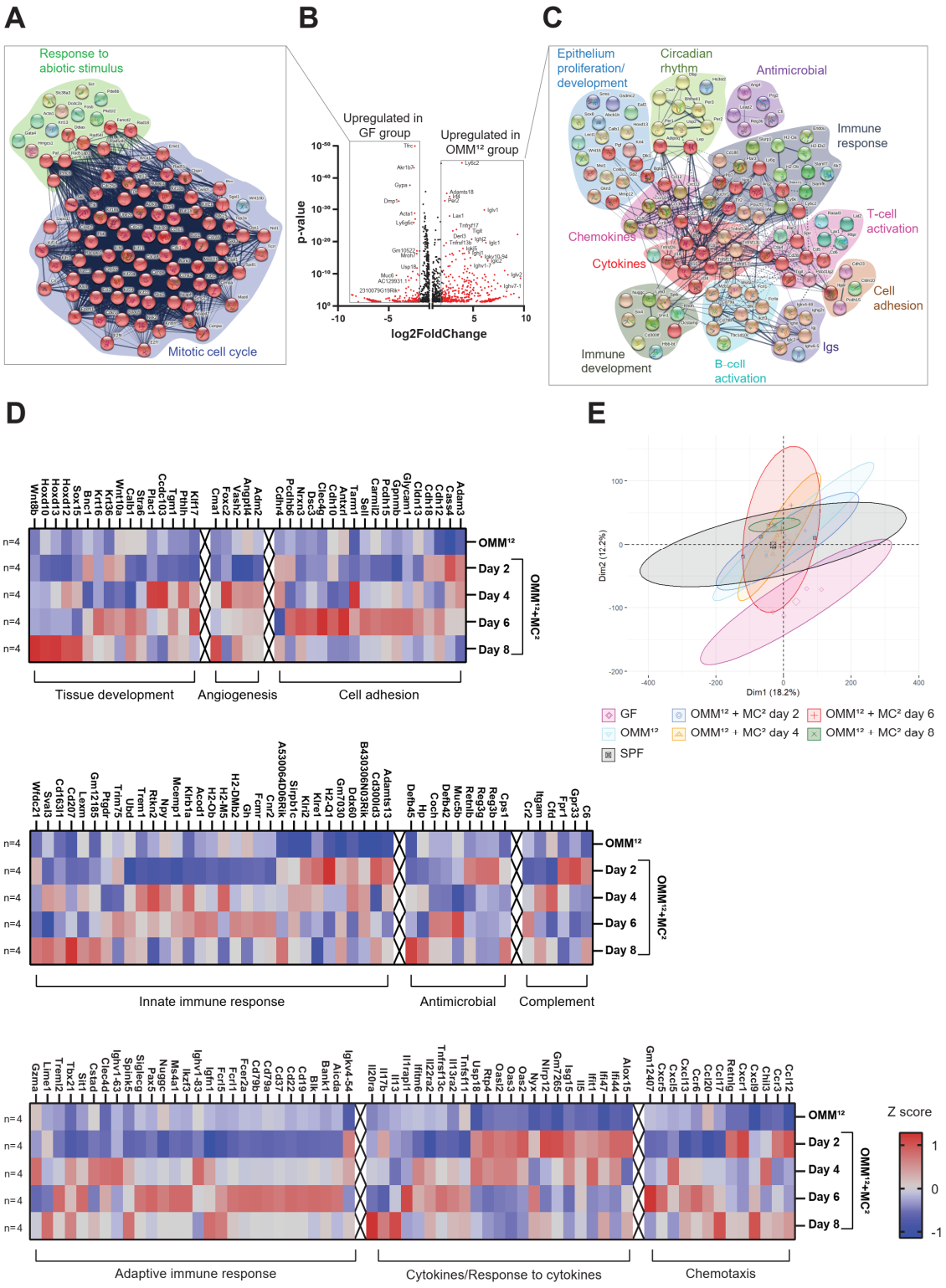

Figure 17: Commensal bacteria colonization induces intestinal reprogramming.

(**A**-**C**) Volcano plot (B) and STRING analysis showing fold-change of gene expression in whole colon of GF (A) and OMM^{12} mice (C). (**D**) Heat map of differentially expressed gene-clusters in OMM^{12} and OMM^{12}+MC^{2} at indicated time points after MC^{2} addition, log2-fold change ≥ 1; p-adj < 0.05. n = 4 biological replicates per group. (**E**) Principal component analysis of colonic gene expression in differently colonized mice. The axes correspond to principal component 1 (x axis) and 2 (y axis). The OMM^{12}+MC^{2} groups were divided in days after receiving MC^{2} bacteria.

3.13 OMM[12] and OMM[12]+MC[2] bacteria have similar metabolomics profiles.

Hundreds of bacteria-derived metabolites are known to pass the GVB, enter the bloodstream and penetrate different tissues of the host to induce host metabolic and immunological responses (Clarke et al. 2010; Uchimura et al. 2018).

Metabolomics' analysis was done to cecal fecal samples from GF, gnotobiotic and SPF mice. Metabolites that were detected and identified in at least 5 mice were used for cluster identification. 99 cluster-IDs were identified, of which 54 were unique metabolite-clusters without homologous isomers (Figure 18A). OMM[12]

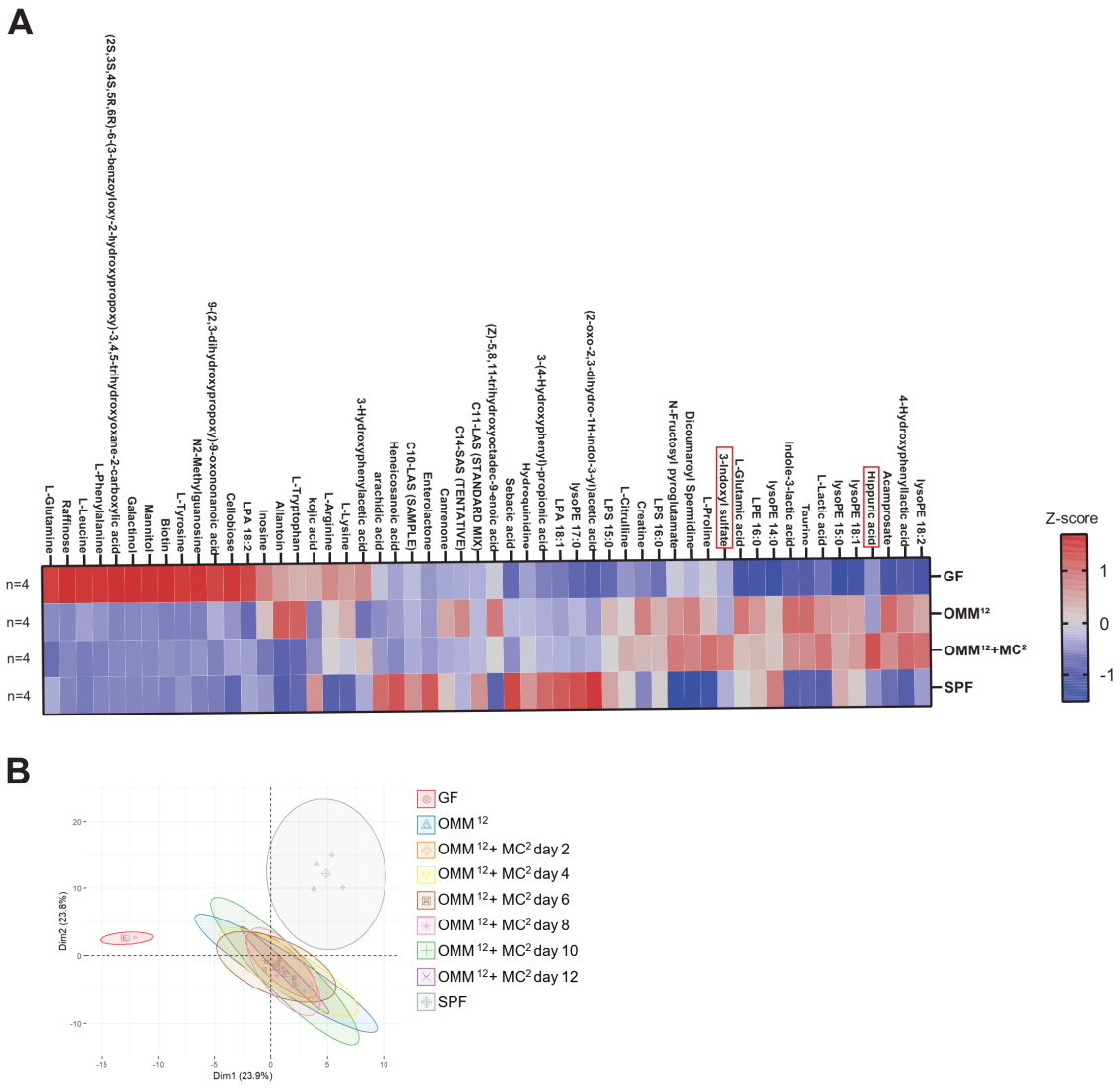

Figure 18: Metabolomics of GF, gnotobiotic and SPF mice.

(**A**) Cluster analysis heatmap of small polar metabolites (m/z<520) detected and identified in all cecal stool samples from GF, OMM[12], OMM[12]+MC[2] and SPF mice. (**B**) Principal component analysis of metabolites from cecal stool samples in indicated mice. The OMM[12]+MC[2] groups were divided in days after receiving MC[2] bacteria. The axes correspond to principal component 1 (x axis) and 2 (y axis).

and OMM^{12}+MC^{2} bacteria shared the production of around 20 metabolites, of which 8 metabolites were also shared with SPF mice. Moreover, OMM^{12}+MC^{2} bacteria exclusively produced the metabolites hippuric acid and 3-indoxyl sulfate (highlighted in Figure 18A). Principal component analysis revealed that only OMM^{12} and OMM^{12}+MC^{2} mice shared similar metabolite-contribution profiles, which differed greatly from the ones of SPF and GF mice (Figure 18B).

These data suggest that MC^{2} bacteria do not strongly impact the metabolite production already provided by OMM^{12} bacteria. Moreover, conventional microbiota have a distinct metabolomics' profile from OMM^{12} and OMM^{12}+MC^{2} bacteria

3.14 SCFAs appear after microbial colonization.

SCFAs have been linked to the regulation of gut epithelial cells, the immune system, endothelial activation and even angiogenesis (Parada Venegas et al. 2019; Miller et al. 2005; Zhang et al. 2018).

Concordantly with previous reports, GF mice showed no SCFAs production, as the presence of SCFAs directly correlates with microbial colonization (Figure 19) (Kespohl et al. 2017). SPF mice exhibited high luminal levels of acetate, propionate, and butyrate in the ceacum, whereas only the levels of acetate were comparable to OMM^{12} and OMM^{12}+MC^{2} mice (Figure 19). Despite the fact that OMM^{12} and OMM^{12}+MC^{2} mice harboured levels of butyrate and propionate, they were considerably lower than the ones in SPF mice (Figure 19). OMM^{12}+MC^{2} bacteria might slightly increase the production of propionate as seen in the significant differences between SPF vs OMM^{12} mice, and SPF vs OMM^{12}+MC^{2} mice (Figure 19). Moreover, analysis of acetate, butyrate and propionate levels in

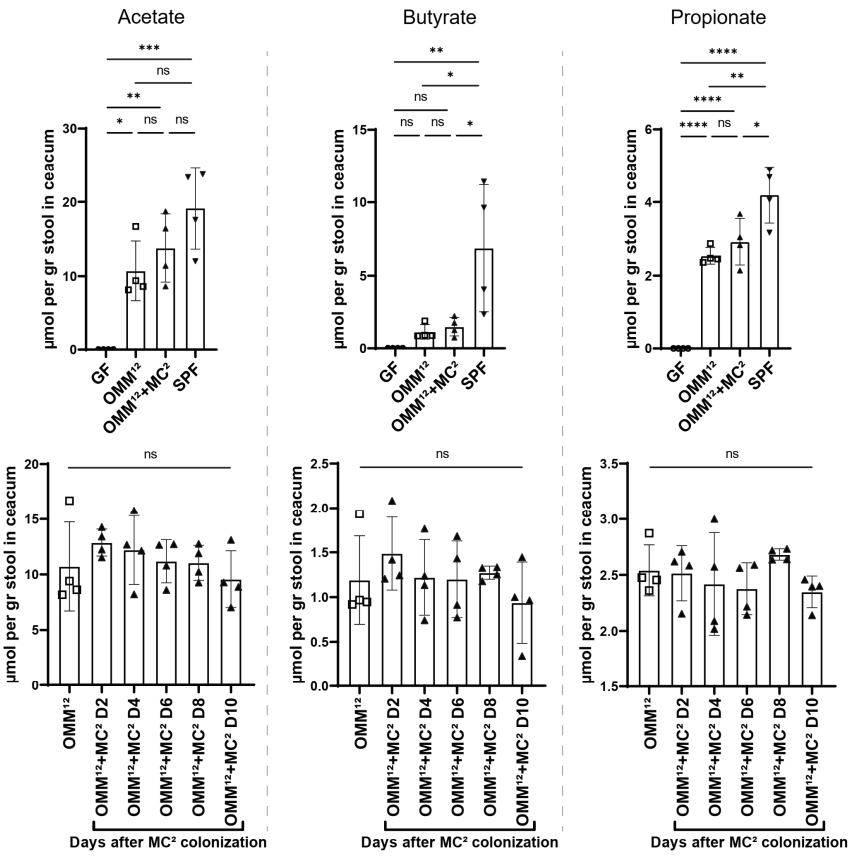

Figure 19: OMM^{12} and OMM^{12}+MC^{2} bacteria produce similar quantities of the SCFAs acetate, butyrate and propionate.

Short-chain fatty acid concentrations in cecal luminal content of GF, gnotobiotic and SPF mice measured with ultra-high performance liquid chromatography–mass spectrometry.

OMM^{12} mice after receiving MC^{2} bacteria in a time dependent manner revealed no changes in their production levels (Figure 19).

Collectively, these results could show that OMM^{12} bacteria induce SCFA production, in particular acetate, which are all completely absent in GF mice.

3.15 MC^{2} bacteria cooperate with OMM^{12} to induce pathogen elimination.

Bacteria are "social" microorganisms that frequently engage in interactions with clonemates or other microbes of the same or different species (Figueiredo and Kramer, 2020).

In order to investigate the role of OMM^{12} and MC^{2} bacteria, together or individually, in providing colonization resistance and pathogen elimination, different microbial combinations were tested. First, OMM^{12} mice were given either *E. coli* or *C. amalonaticus* and consequently challenged to a *C. rodentium* infection. OMM^{12}+*E. coli* mice showed a slightly lower pathogen burden than OMM^{12} mice at later time-points during the infection; however, these mice were unable to eradicate the pathogen (Figure 20A). OMM^{12}+*C. amalonaticus* mice, on the other hand, eventually eliminated the pathogen at around 6 weeks p.i. (Figure 20A), which stands in stark contrast to the 3 weeks that OMM^{12}+MC^{2} and

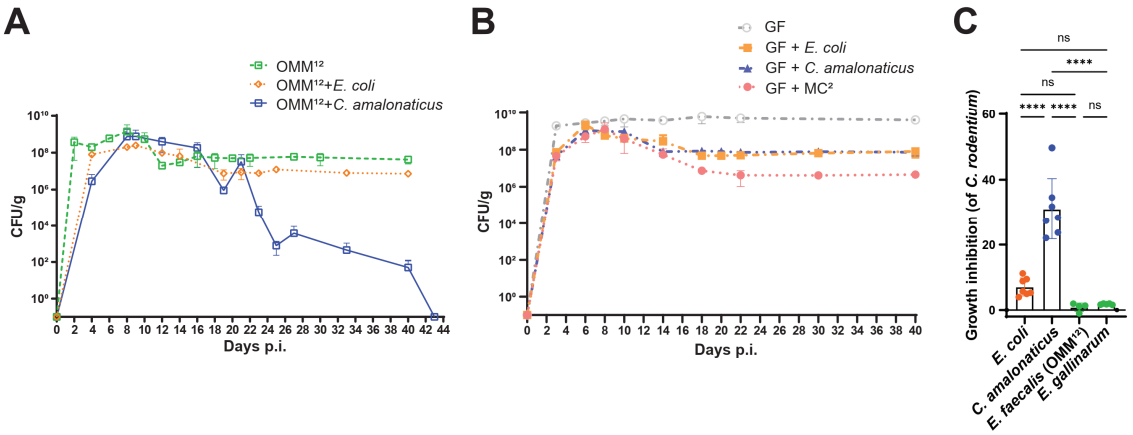

Figure 20: *C. amalonaticus* provides stronger bacterial competition against *C. rodentium* than *E. coli*.

(**A**, **B**) Course of *C. rodentium* infection in mice harbouring OMM^{12} (A), in mono- and bicolonized (B) mice. (**C**) *In-vitro* growth inhibition of *C. rodentium* in the presence of indicated bacteria. Data are shown as fold change compared to *C. rodentium* O/N culture control.

For *C. rodentium* infection: animals were orally infected with (10^{9} CFUs/ml) *C. rodentium*. Data shown are mean ± SD of 2-3 independent experiments, each symbol represents the value for one assay (C). One-way ANOVA was used: ****p < 0.0001; ** p ≤ 0.01; * p ≤ 0.05; ns, not significant.

SPF mice need to achieve same results (Figure 5A). In the absence of OMM^{12} bacteria, monocolonized mice with *E. coli* or *C. amalonaticus* and bicolonized mice with MC^{2} bacteria were unable to eradicate *C. rodentium* (Figure 20B). Monocolonized mice, nevertheless, showed a similar pathogen burden as OMM^{12} mice (Figures 20A and 20B), while in GF+MC^{2} mice it was significantly lower (Figure 20B). An *in-vitro* bacterial competition assay disclosed the strong growth inhibition that *C. amalonaticus* provides against *C. rodentium* (Figure 20C). Interestingly, neither *E. coli*, *E. faecalis* from the OMM^{12} consortium, nor *E. gallinarum* from MC^{3} provided substantial *C. rodentium*-growth inhibition *in-vitro* (Figure 20C).

To conclude, MC^{2} bacteria seem to engage in complex interactions with OMM^{12} bacteria to provide colonization resistance against *C. rodentium*. In addition, bacterial competition greatly differs *in-vitro* vs *in-vivo.*

3.16 *E. coli* and *C. amalonaticus* individually or in combination with OMM^{12} bacteria induce ICAM-1 and CD146 expression in colonic endothelial cells.

Having observed that OMM^{12}+MC^{2} bacteria strongly induced endothelial activation in the colon, the cell adhesion molecules of colonic endothelial cells in mice with *E. coli* or *C. amalonaticus* in the presence or absence of OMM^{12} bacteria were examined.

OMM^{12}+*E. coli* and OMM^{12}+*C. amalonaticus* mice showed upregulation of ICAM-1 and CD146 expression, moreover, only their expression of CD146 was comparable to OMM^{12}+MC^{2} and SPF mice (Figure 21A). OMM^{12}+*C. amalonaticus* bacteria were able to slightly induce a stronger ICAM-1 expression than OMM^{12} mice with *E. coli* (Figure 21A). In the absence of OMM^{12} bacteria,

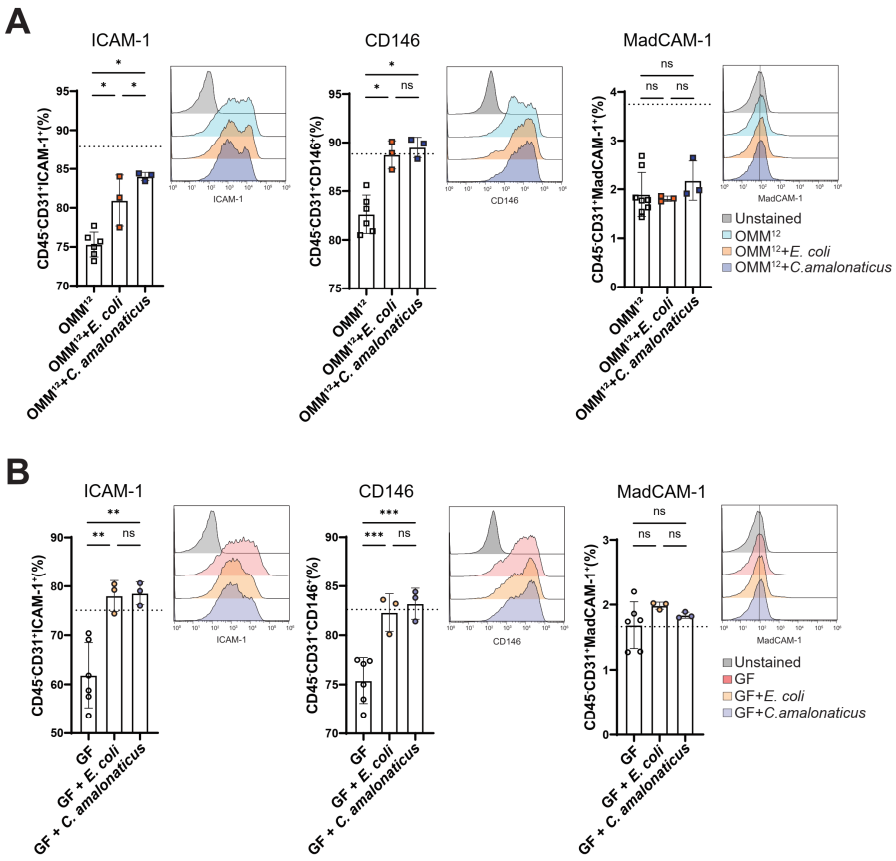

Figure 21: Cell adhesion molecule expression on colonic endothelial cells of gnotobiotic mice.

(**A**, **B**)Expression of ICAM1+, CD146+ and MadCAM1+ on colonic endothelial cells in mice harbouring OMM^{12} (A) GF and monocolonized (B) mice.

Data shown are mean ± SD of 2-3 independent experiments, each symbol represents the value for one mouse. Dotted line represents the reference range for OMM^{12}+MC^{2} mice (A) and OMM^{12} mice (B). One-way ANOVA was used: ****p < 0.0001; ** p ≤ 0.01; * p ≤ 0.05; ns, not significant.

monocolonized mice also showed increased ICAM-1 and CD146 expression, however, only with comparable levels to OMM^{12} mice (Figure 21B). Notably, neither microbial combination was able to induce MadCAM-1 expression as seen previously in OMM^{12}+MC^{2} and SPF mice (Figures 21A and 21B).

To sum up, both *E. coli* and *C. amalonaticus* possess the ability to partially induce endothelial activation in the absence of OMM^{12}. This effect is further enhanced by OMM^{12} bacteria, which probably act as a support system to MC^{2} bacteria.

3.17 *E. coli* or *C. amalonaticus* colonization decrease crypt bifurcations only in GF mice.

OMM^{12} colonization led to a significant reduction of crypt bifurcations, which was further enhanced by the addition of MC^{2} bacteria. In order to find out if this additional reduction of branched crypts was specifically promoted by either *E. coli* or *C. amalonaticus*, whole mount staining was done in the absence or presence of OMM^{12} bacteria.

Unexpectedly, OMM^{12}+*E. coli* and OMM^{12}+*C .amalonaticus* mice showed similar cryptal bifurcations as OMM^{12}mice (Figure 22A). The relative abundance of endothelial cells was also unaffected by the addition of *E. coli* or *C. amalonaticus* to the OMM^{12} consortium (Figure 22B). Monocolonized mice, on the other end, showed reduced crypt bifurcations in comparison to GF and slightly more than OMM^{12} mice (Figure 22C). Despite this observation, monocolonization did not increase the relative abundance of colonic endothelial cells (Figure 22D).

The data suggest that MC^{2} bacteria cooperate with one another to enhance the reduction of crypt branching. An increase in the relative abundance might only be achieved if the percentage of bifurcated crypts remains bellow ~5% (Figure 10B).

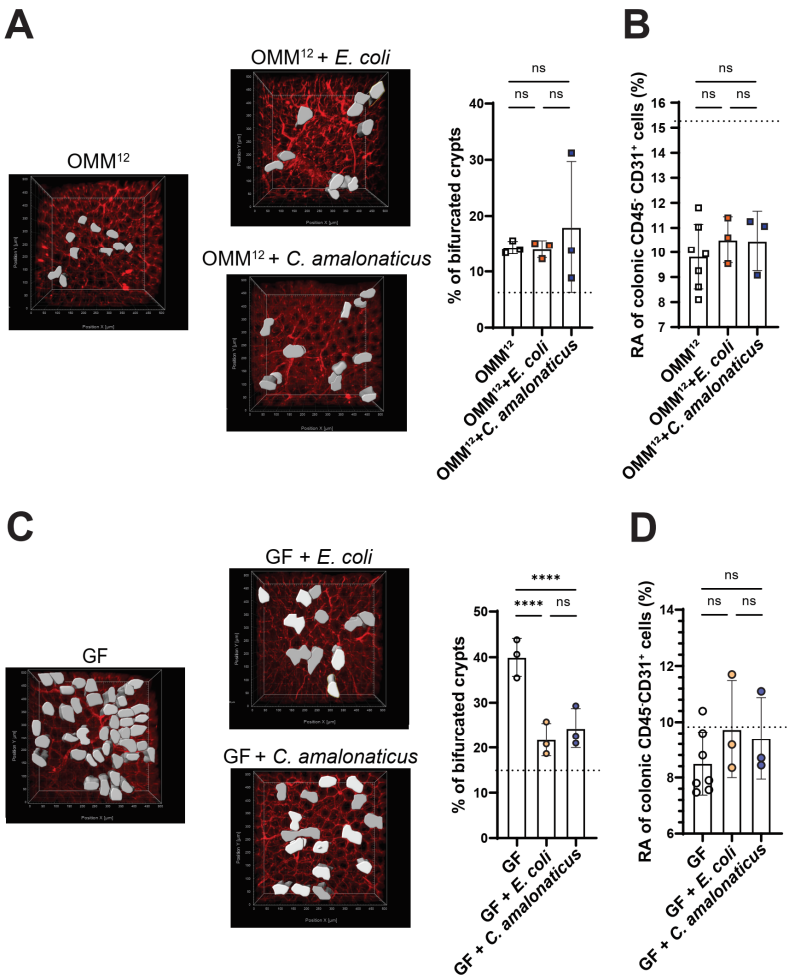

Figure 22: Crypt bifurcations in gnotobiotic mice

(**A**, **C**) Representative images and quantification of whole-mount-staining in mice harbouring OMM[12] (A), GF and monocolonized (C) mice. Partial vascularized crypts were quantified by insertion of contour surface modules (grey areas). (**B**, **D**) Relative abundance (RA) of colonic endothelial cells in the LP of mice harbouring OMM[12] (B), GF and monocolonized (D) mice.

Data shown are mean ± SD of 2-3 independent experiments, each symbol represents the value for one mouse. Dotted line represents the reference range for OMM[12]+MC[2] mice (A, B) and OMM[12] mice (C, D). One-way ANOVA was used: ****p < 0.0001; ** p ≤ 0.01; * p ≤ 0.05; ns, not significant.

3.18 *E. coli* and *C. amalonaticus* strongly induce villus angiogenesis.

In the literature, so far only two bacterial strains have been described to induce small intestinal angiogenesis, namely *B. thetaiotaomicron* and *E. coli* (Stappenbeck et al. 2002; Uchimura et al. 2018).

As expected, both OMM[12]+*E. coli* and *E. coli*-monocolonized mice exhibited an increase in the microvascular density of the villus capillaries (Figures 23A and 23B). Surprisingly, this was also the case for OMM[12]+*C. amalonaticus* and *C. amalonaticus* monocolonized mice (Figures 23A and 23B).

Thus, *C. amalonaticus* is a newly-described commensal bacterium capable of inducing small intestinal angiogenesis

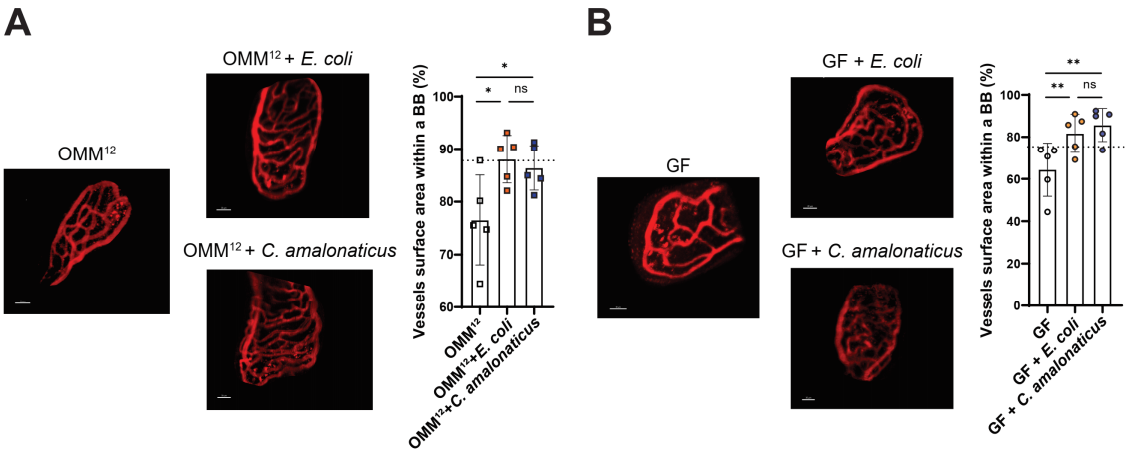

Figure 23: *E. coli* and *C. amalonaticus* increase the microvascular density of the ileal villi.

(**A**, **B**) Intravital, multi-photon microscopy of small intestinal blood capillaries in mice harbouring OMM[12] (A), GF and monocolonized (B) mice after i.v. injection of Qtracker™ 655. Vessel areas were quantified with trace image processing to make morphometric measurements within a bounding box (BB). Results are representative of 4-5 experiments.

Data shown are mean ± SD of 2-3 independent experiments, each symbol represents the value for one mouse. Dotted line represents the reference range for OMM[12]+MC[2] mice (A) and OMM[12] mice (B). One-way ANOVA was used: ****p < 0.0001; ** p ≤ 0.01; * p ≤ 0.05; ns, not significant.

3.19 *E. coli* and *C. amalonaticus*, individually, induce lysozyme producing PC differentiation.

The observed angiogenesis in the SI of OMM[12]+*E. coli* and OMM[12]+*C. amalonaticus* mice, prompted the investigation of PCs. To our surprise, total PC frequencies were unaffected by the addition of *E. coli* or *C. amalonaticus* to OMM[12] mice (Figure 24A). However, both bacteria did induce the differentiation of lysozyme producing PCs (Figure 24B). Hence, the observed angiogenesis might be regulated by antimicrobial signals from granular PCs.

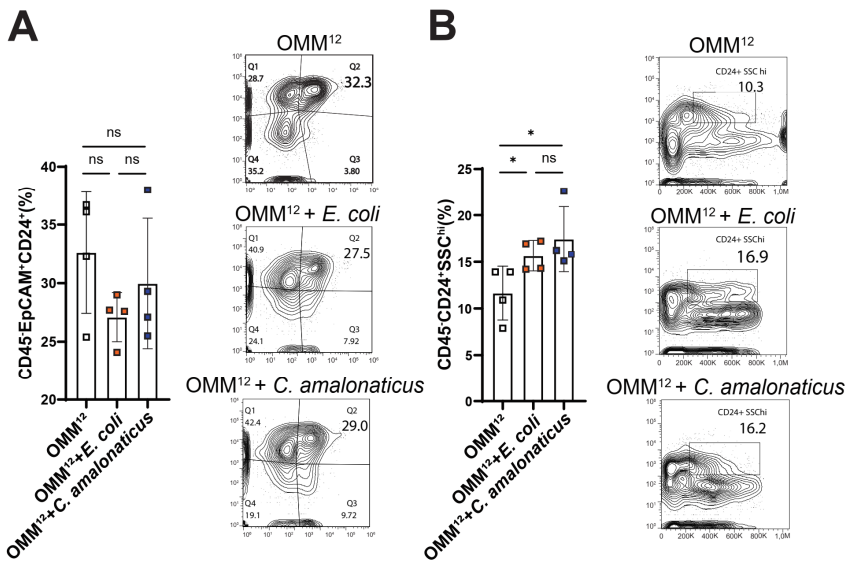

Figure 24: Lyzozyme producing PCs can be specifically activated by *E. coli* and *C. amalonaticus.*

(**A**, **B**) Quantification and representative flow cytometry plots of CD45-EpCAM+CD24+ (A) and CD45-CD24+SSC+ (B) PCs in colonized mice.

Shown are representative data of at least two independent experiments with means ±SD, each symbol represents the individual value for one mouse. One-way ANOVA was used: ****p < 0.0001; ** p ≤ 0.01; * p ≤ 0.05; ns, non-significant.

3.20 The OMM[12]+MC[2] consortium is suitable to treat asymptomatic *C. rodentium* infections.

Asymptomatic carriers pose a great threat to society, since they can spread the disease unknowingly (Chisholm et al. 2018). Treatment of certain persistent enteric infections involved the use of FMTs (Czepiel et al. 2019).

In order to check if OMM[12]+MC[2] could provide pathogen eradication once *C. rodentium* has permanently established itself in the intestine of GF mice, asymptomatic *C. rodentium*-carrier GF mice were given the bacterial consortium

as a treatment. To this end, on day 22 p.i. the mice were cohoused with naïve OMM[12] mice (Figure 25A). While GF mice showed a rapid reduction in the *C. rodentium* titer (Figure 25A), OMM[12] mice were quickly infected as seen by the rapid increase in pathogen burden in these mice (Figure 25A). Ten days after cohousing, all mice received MC[2] bacteria, which led to gradual reduction of *C. rodentium* load resulting in the complete elimination of the pathogen (Figure 25A). Even though no more *C. rodentium* CFUs were found in the shed feces of the mice (Figure 25B, left), the facultative commensals were still present long after pathogen elimination (Figure 25B, right).

Thus, OMM[12]+MC[2] bacteria also provide colonization resistance after *C. rodentium* infection has been established in the gut of GF mice. Furthermore, bacterial strains with similar properties could be useful as a potential therapy against other enteric infections such as EPEC/ EHEC or *Salmonella* infection in humans.

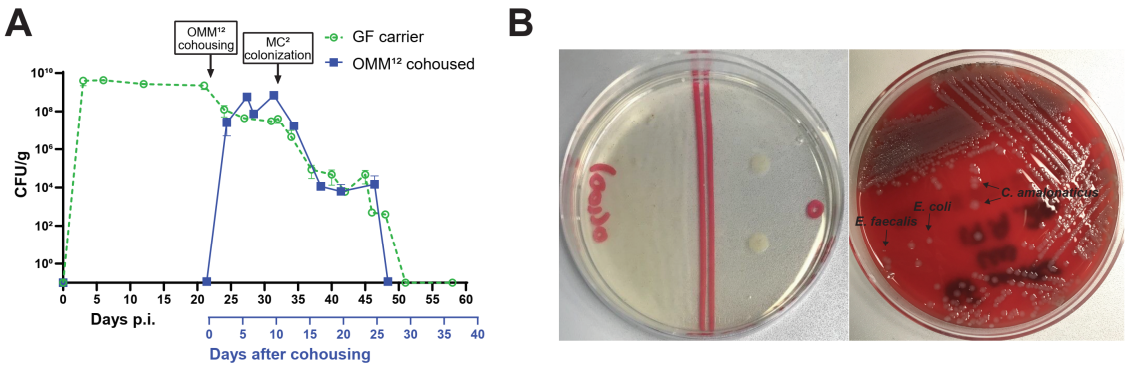

Figure 25: Therapeutic properties of OMM[12]+MC[2] bacteria against *C. rodentium* asymptomatic infections.

(**A**) *C. rodentium*-carriers were cohoused with OMM[12] on day 22 p.i. All mice were gavaged 10 days later with MC[2] bacteria. CFUs of *C. rodentium* were determined in feces. (**B, left**) Representative Nalidixic acid-*C. rodentium* selective agar plate, showing no colonies in 1:100 dilution (left) and 1:10 dilution (right) of the fecal samples from experiment (A). (**B, right**) Representative Columbia blood agar universal plate of feces from experiment (A) mice after pathogen elimination, showing colonies for *E. feacalis* (from OMM[12]), *E. coli* and *C. amalonaticus*.

For *C. rodentium* infection: animals were orally infected with (10^9 CFUs/ ml) *C. rodentium*. Shown are representative data of at least two independent experiments with means ±SD.

4 Discussion

4.1 *C. rodentium*-carrier versus responder mice.

Asymptomatic carriers of different pathogenic infections are a great enigma in the scientific community. For enteric infections, several intestinal bacteria and parasitic pathogens have been described in healthy individuals (Umo and Okon, 2017). Perhaps the most famous case was Mary Mallon, also known as Typhoid Mary, a cook believed to have infected around 50 people with *S. Typhimurium* (Marr, 1999). While in chronic carriers of *Salmonella* the gallbladder has been singled out as an important organ reservoir for the pathogen, for other enteric pathogens such as EPEC and EHEC, more research is needed (Gunn et al. 2014). Unlike *Salmonella*, a natural reservoir has been described for EPEC and EHEC bacteria, namely cattle and other ruminants (Gunn et al. 2014; Stein and Katz, 2017). It is believed that ruminants lack receptors that prevent EPEC and EHEC intestinal and vascular lesions and thus, these animals generally remain asymptomatic (Stein and Katz, 2017; Pruimboom-Brees et al. 2000). Similarly, it has been proposed that asymptomatic EPEC carriers have a deficiency in certain binding receptors that impair EPEC pathogenic colonization as well (Hu and Torres, 2015). Furthermore, additional nonspecific host factors might also predispose the occurrence of an asymptomatic carrier state; for instance, the shape of the intestinal barriers, such as the epithelium, the mucus and, of course, the intestinal microbiota (Levine and Robins-Browne, 2012). Due to the immense variability of complex microbiomes and the fact that asymptomatic carriers of enteric pathogens are usually unaware of their carrier-status, causality investigations are very challenging as well as limiting in human individuals (Hu and Torres, 2015).

As previously mentioned, GF mice become asymptomatic carriers of EPEC's distant cousin, *C. rodentium*. In the present study, it was revealed that OMM^{12} mice also become carriers of the pathogen. Even though we did not perform quantifications of the virulence gene expression in *C. rodentium*-carrier OMM^{12} mice, it is highly likely that these mice also harbored avirulent pathogenic bacteria and remained asymptomatic as seen in GF mice, due to the way *C. rodentium* behaves during the infection. In contrast to commensal bacteria, *C.*

rodentium is a murine pathogen that colonizes by attacking its host. This "attack" is modulated by the formation of dynamic microcolonies on epithelial cells that create A/E lesions (Buschor et al. 2017). While epithelial cells increase their turnover and are shed into the lumen to get rid of the pathogen, the immune system is activated and innate immune cells, in particular neutrophils, gather to phagocytize IgG-opsonized virulent *C. rodentium* intimately attached to the epithelium (Collins et al. 2014; Kamada et al. 2015). In best case scenario, the virulent bacteria is neutralized and eliminated by the immune system and avirulent bacteria are outcompeted by the intestinal microbiota (Kamada et al. 2015; Kamada et al. 2012).

In GF mice, the infection course occurs to a great extent differently. As GF mice lack the intestinal microbiota, *C. rodentium* can colonize the intestine much easier and quicker than in SPF mice. This can be confirmed in the high bacterial burden ($\geq 10^9$ CFUs/g) seen in GF mice already on the next day p.i.; conversely, a similar pathogen load is usually seen in later time-points in SPF mice (days 6-8 p.i.). Due to the rapid colonization in GF mice, the activation of the immune system also occurs faster. In accordance, GF mice show a poor neutrophil migration that peaks on day 8 p.i., 2 days earlier than SPF mice (Zarzycka, 2017). The question then arises as to how GF mice do not succumb to the infection but remain healthy with a high pathogen burden even when neutrophil infiltration is significantly impaired. This is where the quorum sensing system in *C. rodentium* might come into play. *C. rodentium* possesses an N-acylhomoserine lactone (AHL) quorum sensing system by which its population cell density can be detected, and the virulence genes adjusted accordantly (Coulthurst et al. 2007). High bacterial burden leads to downregulation of virulence genes probably in order to prevent overpopulation and the death of the host (Coulthurst et al. 2007). Thus, in GF mice, *C. rodentium* senses a stable colonization and decides to remain in the mice as an "avirulent commensal".

OMM^{12} mice, on the other hand, showed a strong neutrophilic migration almost comparable to OMM^{12}+MC^2 and SPF mice. Moreover, OMM^{12} bacteria showed a partial colonization resistance, with a 200-fold less pathogen burden reduction, in comparison to GF mice. Therefore, it is to be expected that the immune activation would be slightly delayed to that of GF mice, and indeed, the peak of neutrophil migration in OMM^{12} mice is spread between days 8 and 10 p.i.

Hence, OMM^{12} mice eliminate virulent attaching bacteria, but the 12 bacterial strains fail to provide out-competition of avirulent luminal *C. rodentium*. Judging by the mice body weight and the non-existent colonic inflammation at the end of the experiment (day 40 p.i.), one can assume that similar to GF mice, *C. rodentium* was avirulent in OMM^{12} mice at later time-points. This is due to the fact that *C. rodentium* was able to stably colonize the mice, as seen in the high bacterial titer, while not having to share niche space and nutrients with similar competing commensals.

Despite the fairly similar pathogen clearance dynamics between OMM^{12}+MC^{2} and SPF mice, one has to bear in mind that, on the one hand, OMM^{12}+MC^{2} mice harbor only 12 bacterial strains and, on the other, SPF mice possess a complex microbiota. This difference becomes especially clear at the initial time points of the infection, where SPF mice show a much stronger colonization resistance than OMM^{12}+MC^{2} mice. Concordantly, OMM^{12}+MC^{2} mice show a peak in the neutrophil migration on days 8 and 10 p.i. as also seen in OMM^{12} mice. In contrast, in SPF mice, infiltrating neutrophils peak on day 10 p.i. and to a lesser extent on day 12 p.i. into the colon (Zarzycka, 2017). Both mice, however, exhibited a normal infection course, with virulent *C. rodentium* elimination by the immune system and avirulent *C. rodentium* outcompeted by the commensal microbiota.

Next, we further investigated in depth the individual role of MC^{2} bacteria in the presence or absence of OMM^{12} bacteria. OMM^{12}+*E. coli* mice presented less bacterial CFUs than OMM^{12} later in the infection and, similarly, these mice were unable to eliminate the pathogen. As the OMM^{12} consortium already promotes a strong, and probably sufficient, neutrophil migration into the intestine, *E. coli* needed to directly compete against *C. rodentium* to ensure pathogen elimination. *In-vitro* bacterial competition assays revealed that *E. coli* scarcely inhibited the growth of *C. rodentium*. Yet, *in-vivo*, *E. coli* provided a stronger but still insufficient competition as seen in the pathogen titers of monocolonized and OMM^{12}+*E. coli* mice. Thus, *E. coli* probably does not occupy crucial niche space which is then exploited by *C. rodentium* to remain in the animals. Conversely, OMM^{12}+*C. amalonaticus* mice eliminated the pathogen in around 6 weeks after initial infection. This finding correlated with the observed strong growth inhibition of *C. rodentium* provided by *C. amalonaticus in-vitro.* Looking back at

the infection course in OMM^{12}+*C. amalonaticus* mice, there was a strong colonization resistance at the beginning of the infection and pathogen burden reduction appeared to happen slowly and unevenly at later time points. This observation points to an active battlefield between *C. rodentium* and *C. amalonaticus* to determine which bacterium gets to stably seize the gut. Ultimately, the battle was won by *C. amalonaticus*, nevertheless, even though all mice survived the infection, we noticed an increased weight loss in OMM^{12}+*C. amalonaticus* mice than in the other groups (data not shown). Therefore, despite OMM^{12}+*C. amalonaticus* bacteria's success in eliminating the pathogen, the OMM^{12}+MC^{2} consortium was chosen as a better candidate to base this study on. Monocolonized mice with *C. amalonaticus*, interestingly, showed similar *C. rodentium* pathogen burden as *E. coli* monocolonized mice. MC^{2} bicolonized mice showed less pathogen burden than monocolonized mice, but no pathogen clearance either. These findings highlight the role of OMM^{12} bacteria in providing a foundation and support for MC^{2} bacteria to eliminate enteric pathogens.

Lastly, additional bacterial combinations were tested. OMM^{12}+MC^{3} (outlined in Figure 3) mice showed a similar bacterial burden as OMM^{12} mice and were unable to eliminate *C. rodentium*, most likely due to the lack of competing bacteria. One combination involving SFB further emphasized the role of OMM^{12} bacteria in providing pathogen clearance. As previously mentioned, SFB bacteria cannot colonize OMM^{12} mice (Bolsega et al. 2019). Therefore, SFB monocolonized mice were given OMM^{12}+MC^{2} bacteria and subsequently challenged to a *C. rodentium* infection. Surprisingly, SFB+OMM^{12}+MC^{2} mice harboured an almost undetectable *C. rodentium* burden ($\leq 10^{2}$ CFUs/g), but did not completely eliminate the pathogen (data not shown). Thus, unknown specific members from the OMM^{12} consortium that are outcompeted by SFB seem to play a crucial role in providing *C. rodentium* efficient elimination.

In conclusion, responder *C. rodentium* animals possess specific members of the gut microbiota that regulate the migration and activation of crucial lymphocytes to efficiently orchestrate the immune response against *C. rodentium*. Furthermore, these bacterial members can be narrowed down to 14 strains that additionally provide colonization resistance and outcompetition of the pathogen.

4.2 Gut microbes, the intestinal vascular system and leukocyte transmigration

The gut microbiota is constantly linked to the activation and development of the intestinal and peripheral immune system (O'Hara and Shanahan, 2006), however, its role in shaping the intestinal vascular system is beginning to receive more recognition (Stappenbeck et al. 2002; Spadoni et al. 2015). Here, we used the murine pathogen *C. rodentium* to investigate the role of the microbiota in inducing effective leukocyte transendothelial migration during an enteric infection.

GF mice displayed an impaired neutrophil recruitment to the intestinal iEL compartment, but neutrophil numbers and percentages were normal in the blood and the colonic LP in the absence of the commensal microbiota. However, it has been reported that GF animals have a suboptimal BM granulopoiesis as well as decreased amounts of circulating neutrophils under physiological conditions (Balmer et al. 2014; Ohkubo et al. 1990). Our data suggest that a compartmentalized enteric pathogen is able to systemically induce neutrophil production in the BM of GF mice in order to achieve normally circulating neutrophils similar to conventional mice during the infection. Furthermore, blood neutrophils managed to reach the inflamed colonic LP of GF mice, but failed to extravasate into the iEL compartment, a crucial step for the elimination of *C. rodentium* (Kamada et al. 2015). As neutrophil expression of LFA-1 was confirmed to be normal in GF mice, we moved on to its binding partner, ICAM-1 on endothelial cells. Intestinal endothelial cells were examined during infection or under steady state conditions. During the infection, we observed, as expected, a strong increase in ICAM-1, CD146 and MadCAM-1 expression on endothelial cells from GF and OMM^{12} mice (data not shown). Interestingly, a proper analysis of cell adhesion molecule expression on endothelial cells from OMM^{12}+MC^{2} and SPF mice could not be performed due to contaminating mononuclear lymphocytes firmly attached to the endothelial cells (data not shown). This compromised purity was only observed in isolated endothelial cells from OMM^{12}+MC^{2} and SPF mice and could indicate that endothelial cells from these animals are more permissive to leukocyte attachment and transmigration than the ones from GF and OMM^{12} mice during *C. rodentium* infection. FACS analysis of endothelial cells in steady state conditions revealed a decreased ICAM-1,

CD146 and MadCAM-1 expression in GF mice. OMM^{12} colonization was able to marginally increase ICAM-1 and CD146 expression, but only once OMM^{12} mice were given MC^{2} bacteria, the expression levels of all three cell adhesion molecules were comparable to SPF mice. This strong endothelial activation in OMM^{12}+MC^{2} and SPF mice under steady state conditions most likely ensures a better immune response against enteric pathogens by allowing a quicker establishment of first responder leukocytes for the secretion of cytokines and chemokines (Fine et al. 2020). The effects of microbial colonization on endothelial cells were further confirmed by transcriptome analysis. To our knowledge, colonic endothelial cells have not been analysed and compared between GF, gnotobiotic and SPF mice. While microbial colonization upregulated the gene expression of cell adhesion molecules, only OMM^{12}+MC^{2} bacteria and SPF microbiota induced genes involved in angiogenesis.

A central question remains: How do gut microbes modulate endothelial cell function? Despite not providing a mechanistic explanation, we performed several extensive analyses to understand how the host's intestine reacts to microbial introduction as well as how microbes behave in the host. Normal microbial colonization takes place at the postnatal stage (Tlaskalova-Hogenova et al. 2015). During weaning, the *weaning reaction* induces a strong immune response that activates the differentiation of specialized Tregs that later in life lower the susceptibility to pathological inflammations (Al Nabhani et al. 2019). The authors emphasized that this immune response can only occur during a specific timeframe during the postnatal stage and cannot be reproduced in adulthood (Al Nabhani et al. 2019). However, stepwise colonization of GF mice with OMM^{12} bacteria followed by MC^{2} bacteria also led to a strong immune response. Since we did not quantify the intestinal T-cell populations in the mice after the introduction of the bacteria, we cannot corroborate that colonization with OMM^{12}+MC^{2} recreated the weaning reaction. Nevertheless, the observed immune response might explain the activation of the endothelium. Several cytokine families were upregulated in the colon after OMM^{12} and MC^{2} bacteria colonization, such as IL-6, IL-1, TNF, and IL-17, all of which are known to activate endothelial cells (Ley, 2008). Moreover, the increased expression of chemokines correlated with a possible innate-, T- and B-cell recruitment, which requires the participation of an activated endothelium (Nourshargh and Alon, 2014).

Importantly, neither GF nor SPF mice showed gene networks for immune activation, which indicates that only once mice are newly introduced to commensals does this immune response takes place and not under *other* physiological conditions. Considering that the intestine has specialized cells that sense the microbiota (Miron and Cristea, 2012), the immune response and the resulting endothelial activation could simply be triggered by the presence of the bacteria in the intestinal lumen. However, MAMPs and bacterial-derived metabolites are known to exert several immunomodulatory effects. For this reason, we first investigated the production of SCFAs in the caecum. OMM^{12} and OMM^{12}+MC^{2} bacteria produced high levels of acetate and marginal levels of butyrate and propionate, which were all completely absent in GF mice. Butyrate has been linked to the induction of ICAM-1 in human umbilical vein endothelial cells (HUVECs) (Li et al. 2018), thus, SCFAs may also be indirectly responsible for the activation of the endothelium. Similarly, the addition of MC^{2} bacteria, two gram-negative bacteria, surely increased the levels of LPS reaching endothelial cells which is known to induce cell adhesion molecules (Ley, 2008). However, endothelial cells from MyD88- and TLR2/4 KO SPF mice showed normal expression of ICAM-1, CD146 and MAdCAM-1 (data not shown). Lastly, cell adhesion molecule expression on endothelial cells from the SI was not affected by the intestinal microbiota, which stands in contrast to previous studies that showed decreased ICAM-1 expression in the ileum of GF mice (Komatsu et al. 2000). Since endothelial cells from the whole SI, and not from the different compartments, were analysed, we cannot exclude that ICAM-1, CD146 and MadCAM-1 expression in the ileum might indeed be regulated by the intestinal microbiota. This would be a logical conclusion, since, in term of the microbiota, the ileum is far more densely colonized than the duodenum or the jejunum (Saavedra and Moore, 2005).

Activation of the endothelium in colonized mice was also accompanied by intestinal angiogenesis. In accordance to previous studies, the villi of GF mice had a decreased microvascular density (Stappenbeck et al. 2002; Uchimura et al. 2018), which was partially restored by OMM^{12} bacteria and completely restored by OMM^{12}+MC^{2} colonization. Taking into consideration that PCs have a crucial role in regulating angiogenesis in the SI (Stappenbeck et al. 2002; Hassan et al. 2020), the observed new capillary formation might have also been triggered by

the PC differentiation after OMM^{12}+MC^{2} colonization. Notably, PC frequencies were only elevated in OMM^{12}+MC^{2} mice, even though there was a light increase in the microvascular density of OMM^{12} mice in comparison to GF. It needs to be noted though that the observed villus capillary increment in OMM^{12} mice might be modulated by a PC-independent mechanism. PC frequencies were similar in GF, OMM^{12} and, unexpectedly, SPF mice. These contradictory results led us to investigate PC differentiation in young SPF mice, as these animals, similar to OMM^{12}+MC^{2} mice, were recently introduced to the microbiota. Young SPF mice showed elevated percentages of PCs in the SI, thus, PC differentiation potentially occurs as a direct result of the intestinal introduction of specific bacteria (Lueschow and McElroy, 2020). PCs have an average lifespan of 20 days, afterwards, they are phagocytized by neighbouring iEL lymphocytes (Porter et al. 2002). PC dysfunction has been associated with different IBDs (Wehkamp and Stange, 2020), so their activation needs to be carefully regulated. Thus, PCs in SPF mice are probably differentiated during the postnatal stage and at later time points their numbers and their production of antimicrobial proteins are reduced in order to maintain intestinal homeostasis under physiological conditions (Lueschow and McElroy, 2020). Importantly, PCs from OMM^{12}+MC^{2} mice were isolated approximately 2 weeks after MC^{2} colonization, hence, analysis of PCs at later time points might deliver similar results as in SPF mice. These findings also point to the initial PC differentiation as a stimulus that induces intestinal angiogenesis. However, villus capillaries have been shown to constantly need microbial signals to maintain a high vascularization. These microbial signals are sensed by PCs to produce angiogenic factors (Hassan et al. 2020). In SPF mice, differentiated PCs might produce these factors continuously, while in GF and OMM^{12}, immature PCs might not. In accordance, ABX-treatment of SPF mice for 4 weeks led to a significant reduction of villus capillaries (Suh et al. 2019), but transient *E. coli* colonization showed high SI vascularization 2 weeks after the mice returned to the GF status (Uchimura et al. 2018). As PC renewal happens every 20 days (Porter et al. 2002), these studies could indicate that microbial-sensitized PCs maintain vascularization, while newcomer PCs need microbial signals to ensure the production of angiogenic factors. In addition to the pronounced SI angiogenesis in OMM^{12}+MC^{2} and SPF, there was an increased production of VEGFa. Whether VEGFa was directly produced by small intestinal

PCs or by villus macrophages (Suh et al. 2019), remains to be elucidated. Interestingly, OMM^{12}+MC^{2} bacteria produced the metabolite 3-indoxyl sulfate, which might regulate endothelial cell function and angiogenesis (Pei et al. 2019).

Next, we investigated the vascularization of the colon using whole-mount staining, which led to the finding that GF mice have an aberrant number of bifurcated crypts in the medial colon, in accordance to previous reports on GF rats (McCullough et al. 1998). Crypt bifurcations correlated with a decreased vascularization, as colonic vessels usually have a honeycomb appearance (Araki et al. 1996), which was disrupted in branched crypts. OMM^{12} colonization significantly reduced cryptal bifurcations, however, these animals displayed neither an increase in the relative abundance of endothelial cells nor gene networks for angiogenesis in transcriptomics of isolated endothelial cells or the colonic tissue. MC^{2} addition to the OMM^{12} consortium further reduced the crypt bifurcations similar to SPF mice. Moreover, OMM^{12}+MC^{2} mice had a higher relative abundance of colonic endothelial cells and displayed upregulation of angiogenesis genes both in endothelial cells and the whole colon transcriptomics. For this reason, we propose that reduction of cryptal bifurcations correlates with colonic angiogenesis only once ~5% of crypts are bifurcated in the medial colon. Similar as in the SI, we expected that Paneth-like cells in the colon might regulate colon angiogenesis. To our surprise, the frequencies of Paneth-like cells and Ki67-positive enterocytes were similar in all the groups. Bearing in mind that the colon has a much higher density of microbial microorganisms and needs to maintain a more careful immunological tolerance towards microbes than the SI (Miron and Cristea, 2012), Paneth-like cells might not react as strongly as PCs in the SI. However, since OMM^{12} and OMM^{12}+MC^{2} bacteria induced gene networks for antimicrobial peptides in the colonic RNA sequencing, maybe other markers should be used to characterize different types of Paneth-like cells in the colon (Rothenberg et al. 2012; Schmitt et al. 2018). The reduced Ki67 expression on colonic epithelial cells also stands in contrast to the different gene networks for tissue development and epithelial proliferation observed after OMM^{12} and OMM^{12}+MC^{2} colonization. Similar as in PCs, since the gut epithelium renews every 3-7 days, the FACS analyses for Ki67 might have been conducted at a wrong time point. It has to be pointed out that colonic tissue staining as well as

transcriptomics were done on a small piece of the medial colon, while Paneth-like cells and Ki67-positive epithelial cells were isolated from the whole colon.

Lastly, different bacterial community combinations were tested for endothelial activation and intestinal angiogenesis. In the absence of OMM^{12} bacteria, monocolonized mice with *E. coli* or *C. amalonaticus* were able to similarly induce the partial expression of ICAM-1 and CD146 as seen in OMM^{12} mice. Conversely, in the presence of OMM^{12}, endothelial cells from OMM^{12}+*E. coli* and OMM^{12}+*C. amalonaticus* mice showed more ICAM-1 and especially CD146 expression when compared to OMM^{12} mice. These data suggest a supporting role of the OMM^{12} bacteria towards MC^{2} bacteria for regulating endothelial activation. In the colon, OMM^{12} bacteria probably colonize spatial niches that *E. coli* and *C. amalonaticus* cannot, thus, ensuring a homogenous distribution and the activation of endothelial cells from different colonic compartments. However, other factors, such as LPS availability, SCFAs and metabolite production should also be taken into consideration. Interestingly, all bacteria combinations that involved the presence of either *E. coli* or *C. amalonaticus* resulted in strong SI angiogenesis. Concordantly, OMM^{12}+*E. coli* and OMM^{12}+*C. amalonaticus* showed lysozyme producing PCs differentiation, which hints at a PC-mediated mechanism. On the other hand, only monocolonized mice showed a reduction in the crypt bifurcations from 40% to 20%, which did not correlate with an increase in the relative abundance of endothelial cells. These findings indicate that both *E. coli* and *C. amalonaticus* possess the ability to decrease cryptal bifurcations in the absence of OMM^{12}. However, in the presence of OMM^{12}, both bacteria need to cooperate to further reduce the bifurcations.

To sum up, specific commensals shape the intestinal vascular system by activating the endothelium and inducing angiogenesis in physiological conditions. These activated endothelial cells and potentially a highly vascularized intestine favour the recruitment of leukocytes during enteric infections. Despite PCs playing an important role in inducing angiogenesis, their role in other endothelial functions has not yet been described. Therefore, the activation of the intestinal endothelium is most likely induced by the immune response triggered by commensals colonization.

4.3 Better together: OMM^{12} and MC^{2} microbial and host interactions

The symbiotic relationship between the microbiota and its host involves a myriad of complex interactions, many of which are hardly understood or even known (Figueiredo and Kramer, 2020). Here, we could show how different bacterial combinations induce completely different but sometimes also similar effects. For our particular research question, we carefully chose the OMM^{12}+MC^{2} minimal consortium to investigate how these 14 bacteria shape their host while engaging in complex interactions at the microbial level.

OMM^{12}+MC^{2} spatial organization was investigated using FISH. FISH analyses could show that all 14 commensals remain in the intestinal lumen and were not invasive towards the gut epithelium at least in the medial colon. The distribution of OMM^{12} bacteria after MC^{2} association revealed a reduction in the relative abundance of *A. muciniphila* while the relative abundance of *B. caecimuris* was increased. Even though not much is yet known about *B. caecimuris*, a lot of research has been done on *A. muciniphila*. *A. muciniphila* is one of the few commensals that mostly inhabits the mucus layer of the intestine and is equipped with mucus degrading enzymes (Xu et al. 2020). Concordantly, we observed an increased abundance of adherent mucus in OMM^{12}+MC^{2} mice in comparison to OMM^{12} mice. As the RNA sequencing data did not show activation of goblet cells or gene networks for mucus production in OMM^{12}+MC^{2} mice, the augmentation of adherent mucus might be explained by the reduction of mucus-degrading *A. muciniphila*. Moreover, colon transcriptomics showed gene families for smooth muscle activation after OMM^{12}+MC^{2} colonization (data not shown). Thus, mucus transport might work better in OMM^{12}+MC^{2} due to an increase in the intestinal peristalsis (Ge et al. 2017), as indeed, the colons of OMM^{12}+MC^{2} and SPF mice harboured more fecal pellets than the ones from GF or OMM^{12} mice. Further, OMM^{12} mice displayed more colonic adherent mucus than GF, which was the lowest in all groups similar to previous results (Petersson et al. 2011). OMM^{12} colonization did induce a few genes for mucins and sialomucins as seen in the RNA sequencing (data not shown). Thus, bacterial introduction might directly activate goblet cells to increase their mucus production.

At the microbial level, OMM^{12} and OMM^{12}+MC^{2} bacteria showed similar metabolite production profiles that were fairly different to the ones from GF and SPF mice. These results were quite unexpected, since, in many ways, OMM^{12}+MC^{2} mice resemble SPF mice. It must be noted that small-polar metabolome analysis was performed instead of high-throughput metabolomics, which could provide more information on metabolite production. Nevertheless, these data go to show how different the microbial interactions are perceived by the host versus within microbial communities.

4.4 "RePOOPulating" the gut using FMTs or isolated bacterial strains as therapies to eliminate persistent enteric infections.

Currently, FMTs are used as a standard treatment with high success rates against persistent and recurrent *Clostridium difficile* infections (CDI) (Gupta et al. 2016). Nevertheless, some patients show refractory infections and do not respond to FMTs (Gupta et al. 2016). Petrof and colleagues created a "stool substitute" (synthetic bacterial mixture) by isolating and cultivating few bacterial strains from healthy donors to treat patients infected with a hyper virulent and antibiotic-resistant *C. difficile* (Petrof et al. 2013). It was thereby demonstrated that a simplified bacterial community can also be used to cure CDI, a process conveniently named "gut rePOOPulation" (Petrof et al. 2013). In the current study, we used both FMTs and isolated bacterial strains to treat persistent *C. rodentium* infections. While some FMTs were successful in inducing pathogen clearance, some others were not. Interestingly, OMM^{12}+MC^{2} bacteria were able to induce pathogen elimination in asymptomatic carrier mice.

The main goal of this study was to find a new minimal consortium that on its own or together with OMM^{12} bacteria could eradicate *C. rodentium* in carrier mice. In order to isolate MC^{2} bacteria, facultative anaerobic bacteria were mined from the microbiota of SPF mice by cultivating cecal and colon feces overnight under aerobic conditions. The bacterial suspension (aerobic-FMT) was given orally and only once to asymptomatic long-time *C. rodentium*-carrier GF mice. The mice then exhibited a rapid and uniform pathogen reduction for around 10 days and until the pathogen was no longer detectable. Then, unexpectedly, there was a pathogen surge that lasted about 7 days, afterwards, the pathogen was

successfully eliminated as no more *C. rodentium*'s CFUs were spotted throughout a month (data not shown). The rapid pathogen reduction was probably due to avirulent luminal *C. rodentium* being quickly outcompeted by the introduction of the aerobic-FMT, while the sudden pathogen surge could indicate the reactivation of *C. rodentium* virulence genes in an effort to try and recolonize the intestine. Interestingly, through the isolation of bacterial strains present in the aerobic-FMT, we identified some bacterial strains that were no longer found in the recovered mice (e.g., *Staphylococcus aureus*, *Lactobacillus johnsonii*) (data not shown). This finding indicates that not all bacteria from the aerobic-FMT managed to successfully colonize the mice. Moreover, bacterial isolation from stool samples from recovered mice revealed that despite the aerobic incubation of the FMT, around six strict-anaerobic bacteria were present in addition to the five facultative anaerobes (MC^5). Of note, colonization of GF mice with a bacterial cocktail consisting of MC^5 and the six strict-anaerobia did not lead to pathogen elimination (data not shown).

Considering that the aerobic-FMT was a successful treatment against persistent *C. rodentium* infections, we wondered if the microbiota that colonized and remained in recovered mice could also induce similar effects. Thus, a stool suspension from the shed feces of recovered mice (recovered-FMT) was administered to *C. rodentium*-infected GF mice at different time points during the infection (outlined in Figure 26), which led to conflicting results. *C. rodentium*-infected GF mice that received recovered-FMT on day 3 p.i. were able to completely eliminate the infection (data not shown). However, oral administration of recovered-FMT to long *C. rodentitum*-carrier GF mice (day 22 p.i.) did not lead to pathogen elimination (data not shown). Several different factors could be used to explain this observation, however, I will discuss only two. The first one is of course the FMT microbial composition. Stool samples for the aerobic-FMT were taken by sacrificing the mice and removing the cecal and colon fecal contents. In contrast, for the recovered-FMT only shed feces were gathered. Since each intestinal compartment has a particular microbial composition (Dehmer et al. 2011), the microbiota present in the aerobic-FMT probably had a richer diversity than the one present in the recovered-FMT. The recovered-FMT induced clearance only when administered in early stages of the infection possibly since the immune system was beginning to be activated and *C. rodentium* had

not yet stably established itself in the gut. Moreover, the richer microbial diversity in aerobic-FMT could have contained bacteria that specifically colonized spatial niches that were used by persistent *C. rodentium* for hiding. Furthermore, as mentioned above, not all bacteria present in the aerobic-FMT stably colonized the mice, but these non-colonizing bacteria may have played an important role in aiding in pathogen eradication. The second factor could be the treatment of the samples prior to transfer. Stool samples were incubated aerobically overnight to create the aerobic-FMT, while stool samples for the recovered-FMT were quickly homogenized in PBS. The aerobic incubation may have actually protected cultivable and uncultivable strict-anaerobic bacteria, since the facultative anaerobes might have consumed the oxygen (Friedman et al. 2018), thus, maintaining the medium more oxygen-depleted than the PBS solution and ensuring more microbial diversity. These potential problems can be surpassed by switching to the administration of simplified bacterial communities, instead of using FMTs. Here, we described 14 bacteria that could induce pathogen elimination in *C. rodentium*-carrier GF mice. Bearing in mind that different FMTs also provide persistent pathogen elimination, we believe that a different minimal consortium can surely achieve similar results.

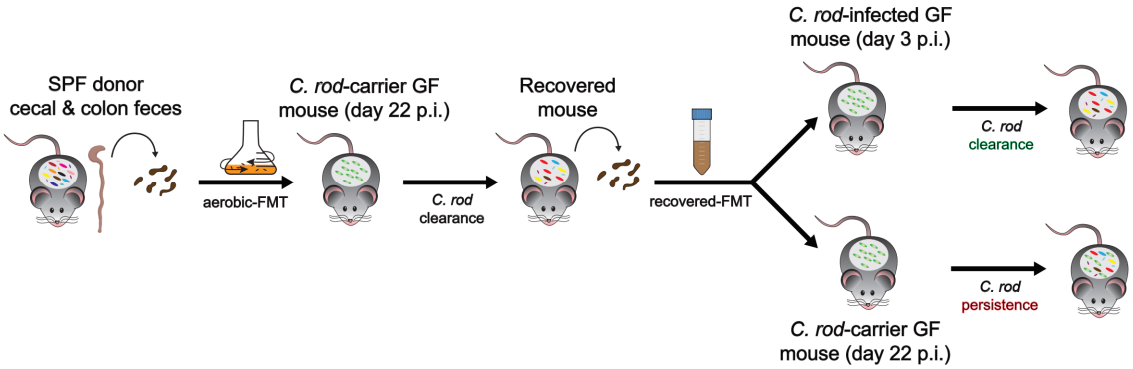

Figure 26: Different FMTs used to treat *C. rodentium*-carrier and *C. rodentium*-infected GF mice.

Image abbreviations. SPF: specific pathogen free, FMT: fecal microbiota transplant, *C. rod*: *Citrobacter rodentium*, GF: germ-free, p.i.: post-infection.

To conclude, these findings demonstrate the ability of specific bacterial strains to revert asymptomatic carriers to a normal bowel microbial pattern. Furthermore, identification, isolation, and administration of specific bacterial strains from healthy donors whose stool samples provided strong colonization against specific enteric infections to patients with persistent or antibiotic

resistant infections, might be a more suitable treatment than FMTs. Thus, different synthetic bacterial mixtures to treat either EPEC, EHEC, *Salmonella* or *C. difficile* infections might become a reality in the foreseeable future.

5 Summary

The intestinal microbiota constitutes one of the most important symbiotic relationships between animals and microbes. The host provides nutrients and protection while gut microbes shape animal physiology and evolution. Gnotobiology research has expanded our knowledge on microbial-host interactions by allowing the identification and cultivation of isolated members of the gut microbiota to administrate into gnotobiotic animals. In the current study, we identified a minimal bacterial consortium consisting of 14 isolated commensals (OMM^{12}+MC^{2}) that restored immunocompetence in germ-free mice to eliminate *Citrobacter rodentium* infections. While germ-free animals exhibited an impaired neutrophil migration into the colon during infection, the addition of OMM^{12}+MC^{2} bacteria promoted intestinal endothelial activation and angiogenesis to ensure a proper leukocyte migration and pathogen elimination. Moreover, in a proof-of-concept approach, OMM^{12}+MC^{2} bacteria also showed potential therapeutic properties by promoting *C. rodentium* elimination in asymptomatic carrier mice. This study contributes to the understanding of how gut microbes modulate the maturation of the intestinal vascular system to favor the elimination of an enteric pathogen and provides evidence that selected commensals can potentially be used to treat persistent enteric infections.

6 Zusammenfassung

Die Darmmikrobiota stellt eine der wichtigsten symbiotischen Beziehungen zwischen Tieren und Mikroben dar. Der Wirt bietet Nährstoffe und Schutz, während Darmmikroben die Tierphysiologie und Evolution prägen. Die gnotobiologische Forschung hat unser Wissen über mikrobielle Wirtsinteraktionen erweitert, indem sie die Identifizierung und Kultivierung isolierter Mitglieder der Darmmikrobiota ermöglicht hat, sowie deren Verabreichung an gnotobiotische Tiere. In der aktuellen Studie haben wir ein minimales Bakterienkonsortium aus 14 isolierten Kommensalen (OMM^{12}+MC^{2}) identifiziert, das die Immunkompetenz bei keimfreien Mäusen wiederherstellt, um eine *Citrobacter rodentium*-Infektion zu beseitigen. Während keimfreie Tiere während der Infektion eine beeinträchtigte Neutrophilenmigration in den Dickdarm zeigten, förderte die Zugabe von OMM^{12}+MC^{2}-Bakterien die intestinale Endothelaktivierung und Angiogenese, um eine ordnungsgemäße Leukozytenmigration und Pathogenelimination sicherzustellen. Darüber hinaus zeigten OMM^{12}+MC^{2}-Bakterien in einem Proof-of-Concept-Ansatz potenzielle therapeutische Eigenschaften, indem sie die Elimination von *C. rodentium* bei asymptomatischen Trägermäusen förderten. Diese Studie trägt zum Verständnis davon bei, wie Darmmikroben die Reifung des intestinalen Gefäßsystems modulieren, um die Eliminierung eines enterischen Pathogens zu begünstigen, und liefert Hinweise darauf, dass ausgewählte Kommensale potenziell zur Behandlung persistierender enterischer Infektionen verwendet werden können.

7 References

Abe, H., Tatsuno, I., Tobe, T., Okutani, A., & Sasakawa, C. (2002). Bicarbonate ion stimulates the expression of locus of enterocyte effacement-encoded genes in enterohemorrhagic Escherichia coli O157:H7. *Infection and immunity*, 70(7), 3500–3509. https://doi.org/10.1128/IAI.70.7.3500-3509.2002

Abt, M. C., Osborne, L. C., Monticelli, L. A., Doering, T. A., Alenghat, T., Sonnenberg, G. F., Paley, M. A., Antenus, M., Williams, K. L., Erikson, J., Wherry, E. J., & Artis, D. (2012). Commensal bacteria calibrate the activation threshold of innate antiviral immunity. *Immunity*, 37(1), 158–170. https://doi.org/10.1016/j.immuni.2012.04.011

Amann, R. I., Binder, B. J., Olson, R. J., Chisholm, S. W., Devereux, R., & Stahl, D. A. (1990). Combination of 16S rRNA-targeted oligonucleotide probes with flow cytometry for analyzing mixed microbial populations. *Applied and environmental microbiology*, 56(6), 1919–1925. https://doi.org/10.1128/aem.56.6.1919-1925.1990

An, J., Zhao, X., Wang, Y., Noriega, J., Gewirtz, A. T., & Zou, J. (2021). Western-style diet impedes colonization and clearance of Citrobacter rodentium. *PLoS pathogens*, 17(4), e1009497. https://doi.org/10.1371/journal.ppat.1009497

Al Nabhani, Z., Dulauroy, S., Marques, R., Cousu, C., Al Bounny, S., Déjardin, F., Sparwasser, T., Bérard, M., Cerf-Bensussan, N., & Eberl, G. (2019). A Weaning Reaction to Microbiota Is Required for Resistance to Immunopathologies in the Adult. *Immunity*, 50(5), 1276–1288.e5. https://doi.org/10.1016/j.immuni.2019.02.014

Al Nabhani, Z., & Eberl, G. (2020). Imprinting of the immune system by the microbiota early in life. *Mucosal immunology*, 13(2), 183–189. https://doi.org/10.1038/s41385-020-0257-y

Alberts B, Johnson A, Lewis J, et al. (2002). Blood Vessels and Endothelial Cells. *Molecular Biology of the Cell*. 4th edition. New York: Garland Science. Available from: https://www.ncbi.nlm.nih.gov/books/NBK26848/

References

Al-Soudi, A., Kaaij, M. H., & Tas, S. W. (2017). Endothelial cells: From innocent bystanders to active participants in immune responses. *Autoimmunity reviews*, 16(9), 951–962. https://doi.org/10.1016/j.autrev.2017.07.008

Araki, K., Furuya, Y., Kobayashi, M., Matsuura, K., Ogata, T., & Isozaki, H. (1996). Comparison of Mucosal Microvasculature between the Proximal and Distal Human Colon. *Journal of Electron Microscopy*, 45(3), 202–206. https://doi.org/10.1093/oxfordjournals.jmicro.a023433

Atarashi, K., Tanoue, T., Ando, M., Kamada, N., Nagano, Y., Narushima, S., Suda, W., Imaoka, A., Setoyama, H., Nagamori, T., Ishikawa, E., Shima, T., Hara, T., Kado, S., Jinnohara, T., Ohno, H., Kondo, T., Toyooka, K., Watanabe, E., Yokoyama, S., ... Honda, K. (2015). Th17 Cell Induction by Adhesion of Microbes to Intestinal Epithelial Cells. *Cell*, 163(2), 367–380. https://doi.org/10.1016/j.cell.2015.08.058

Baker D. G. (1998). Natural pathogens of laboratory mice, rats, and rabbits and their effects on research. *Clinical microbiology reviews*, 11(2), 231–266. https://doi.org/10.1128/CMR.11.2.231

Balmer, M. L., Schürch, C. M., Saito, Y., Geuking, M. B., Li, H., Cuenca, M., Kovtonyuk, L. V., McCoy, K. D., Hapfelmeier, S., Ochsenbein, A. F., Manz, M. G., Slack, E., & Macpherson, A. J. (2014). Microbiota-derived compounds drive steady-state granulopoiesis via MyD88/TICAM signaling. *Journal of immunology* (Baltimore, Md. : 1950), 193(10), 5273–5283. https://doi.org/10.4049/jimmunol.1400762

Barthold, S. W., Coleman, G. L., Jacoby, R. O., Livestone, E. M., & Jonas, A. M. (1978). Transmissible murine colonic hyperplasia. *Veterinary pathology*, 15(2), 223–236. https://doi.org/10.1177/030098587801500209

Barthold S. W. (1980). The microbiology of transmissible murine colonic hyperplasia. *Laboratory animal science*, 30(2 Pt 1), 167–173.

Berer, K., Mues, M., Koutrolos, M., Rasbi, Z. A., Boziki, M., Johner, C., Wekerle, H., & Krishnamoorthy, G. (2011). Commensal microbiota and myelin autoantigen cooperate to trigger autoimmune demyelination. *Nature*, 479(7374), 538–541. https://doi.org/10.1038/nature10554

Bernier-Latmani, J., Cisarovsky, C., Demir, C. S., Bruand, M., Jaquet, M., Davanture, S., Ragusa, S., Siegert, S., Dormond, O., Benedito, R., Radtke, F., Luther, S. A., & Petrova, T. V. (2015). DLL4 promotes continuous adult intestinal lacteal regeneration and dietary fat transport. *The Journal of clinical investigation*, 125(12), 4572–4586. https://doi.org/10.1172/JCI82045

Bernier-Latmani, J., & Petrova, T. V. (2017). Intestinal lymphatic vasculature: structure, mechanisms and functions. *Nature reviews*. Gastroenterology & hepatology, 14(9), 510–526. https://doi.org/10.1038/nrgastro.2017.79

Bolsega, S., Basic, M., Smoczek, A., Buettner, M., Eberl, C., Ahrens, D., Odum, K. A., Stecher, B., & Bleich, A. (2019). Composition of the Intestinal Microbiota Determines the Outcome of Virus-Triggered Colitis in Mice. *Frontiers in immunology*, 10, 1708. https://doi.org/10.3389/fimmu.2019.01708

Bouladoux, N., Harrison, O. J., & Belkaid, Y. (2017). The Mouse Model of Infection with Citrobacter rodentium. *Current protocols in immunology*, 119, 19.15.1–19.15.25. https://doi.org/10.1002/cpim.34

Brinkmann, V., Reichard, U., Goosmann, C., Fauler, B., Uhlemann, Y., Weiss, D. S., Weinrauch, Y., & Zychlinsky, A. (2004). Neutrophil extracellular traps kill bacteria. *Science* (New York, N.Y.), 303(5663), 1532–1535. https://doi.org/10.1126/science.1092385

Britannica, T. Editors of Encyclopaedia (2020, February 7). Cecum. *Encyclopedia Britannica*. https://www.britannica.com/science/cecum

Brown, K., Abbott, D. W., Uwiera, R., & Inglis, G. D. (2018). Removal of the cecum affects intestinal fermentation, enteric bacterial community structure, and acute colitis in mice. *Gut microbes*, 9(3), 218–235. https://doi.org/10.1080/19490976.2017.1408763

Bruens, L., Ellenbroek, S., van Rheenen, J., & Snippert, H. J. (2017). In Vivo Imaging Reveals Existence of Crypt Fission and Fusion in Adult Mouse Intestine. *Gastroenterology*, 153(3), 674–677.e3. https://doi.org/10.1053/j.gastro.2017.05.019

Brugiroux, S., Beutler, M., Pfann, C., Garzetti, D., Ruscheweyh, H. J., Ring, D., Diehl, M., Herp, S., Lötscher, Y., Hussain, S., Bunk, B., Pukall, R., Huson, D. H., Münch, P. C., McHardy, A. C., McCoy, K. D., Macpherson, A. J., Loy, A., Clavel, T., Berry, D., ... Stecher, B. (2016). Genome-guided design of a defined mouse microbiota that confers colonization resistance against Salmonella enterica serovar Typhimurium. *Nature microbiology*, 2, 16215. https://doi.org/10.1038/nmicrobiol.2016.215

Buettner, M., & Lochner, M. (2016). Development and Function of Secondary and Tertiary Lymphoid Organs in the Small Intestine and the Colon. *Frontiers in immunology*, 7, 342. https://doi.org/10.3389/fimmu.2016.00342

Castillo-Álvarez, F., & Marzo-Sola, M. E. (2017). Role of intestinal microbiota in the development of multiple sclerosis. Papel de la microbiota intestinal en el desarrollo de la esclerosis múltiple. *Neurologia* (Barcelona, Spain), 32(3), 175–184. https://doi.org/10.1016/j.nrl.2015.07.005

Chen, J., Luo, Y., Hui, H., Cai, T., Huang, H., Yang, F., Feng, J., Zhang, J., & Yan, X. (2017). CD146 coordinates brain endothelial cell-pericyte communication for blood-brain barrier development. *Proceedings of the National Academy of Sciences of the United States of America*, 114(36), E7622–E7631. https://doi.org/10.1073/pnas.1710848114

Chisholm, R. H., Campbell, P. T., Wu, Y., Tong, S., McVernon, J., & Geard, N. (2018). Implications of asymptomatic carriers for infectious disease transmission and control. *Royal Society open science*, 5(2), 172341. https://doi.org/10.1098/rsos.172341

Clahsen, T., Pabst, O., Tenbrock, K., Schippers, A., & Wagner, N. (2015). Localization of dendritic cells in the gut epithelium requires MAdCAM-1. *Clinical immunology* (Orlando, Fla.), 156(1), 74–84. https://doi.org/10.1016/j.clim.2014.11.005

Clarke, T. B., Davis, K. M., Lysenko, E. S., Zhou, A. Y., Yu, Y., & Weiser, J. N. (2010). Recognition of peptidoglycan from the microbiota by Nod1 enhances systemic innate immunity. *Nature medicine*, 16(2), 228–231. https://doi.org/10.1038/nm.2087

Collins, F. M., & Carter, P. B. (1978). Growth of salmonellae in orally infected germfree mice. *Infection and immunity*, 21(1), 41–47. https://doi.org/10.1128/iai.21.1.41-47.1978

Collins, J. W., Keeney, K. M., Crepin, V. F., Rathinam, V. A., Fitzgerald, K. A., Finlay, B. B., & Frankel, G. (2014). Citrobacter rodentium: infection, inflammation and the microbiota. *Nature reviews. Microbiology*, 12(9), 612–623. https://doi.org/10.1038/nrmicro3315

Cornelis G. R. (2006). The type III secretion injectisome. *Nature reviews*. Microbiology, 4(11), 811–825. https://doi.org/10.1038/nrmicro1526

Coulthurst, S. J., Clare, S., Evans, T. J., Foulds, I. J., Roberts, K. J., Welch, M., Dougan, G., & Salmond, G. P. (2007). Quorum sensing has an unexpected role in virulence in the model pathogen Citrobacter rodentium. *EMBO reports*, 8(7), 698–703. https://doi.org/10.1038/sj.embor.7400984

Crepin, V. F., Collins, J. W., Habibzay, M., & Frankel, G. (2016). Citrobacter rodentium mouse model of bacterial infection. *Nature protocols*, 11(10), 1851–1876. https://doi.org/10.1038/nprot.2016.100

Czepiel, J., Dróżdż, M., Pituch, H., Kuijper, E. J., Perucki, W., Mielimonka, A., Goldman, S., Wultańska, D., Garlicki, A., & Biesiada, G. (2019). Clostridium difficile infection: review. *European journal of clinical microbiology & infectious diseases*: official publication of the European Society of Clinical Microbiology, 38(7), 1211–1221. https://doi.org/10.1007/s10096-019-03539-6

de Oliveira, S., Rosowski, E. E., & Huttenlocher, A. (2016). Neutrophil migration in infection and wound repair: going forward in reverse. *Nature reviews*. Immunology, 16(6), 378–391. https://doi.org/10.1038/nri.2016.49

Dehmer, J. J., Garrison, A. P., Speck, K. E., Dekaney, C. M., Van Landeghem, L., Sun, X., Henning, S. J., & Helmrath, M. A. (2011). Expansion of intestinal epithelial stem cells during murine development. *PloS one*, 6(11), e27070. https://doi.org/10.1371/journal.pone.0027070

Dejana E. (2004). Endothelial cell-cell junctions: happy together. *Nature reviews*. Molecular cell biology, 5(4), 261–270. https://doi.org/10.1038/nrm1357

Deshmukh, H. S., Liu, Y., Menkiti, O. R., Mei, J., Dai, N., O'Leary, C. E., Oliver, P. M., Kolls, J. K., Weiser, J. N., & Worthen, G. S. (2014). The microbiota regulates neutrophil homeostasis and host resistance to Escherichia coli K1 sepsis in neonatal mice. *Nature medicine*, 20(5), 524–530. https://doi.org/10.1038/nm.3542

Dominguez-Bello, M. G., Costello, E. K., Contreras, M., Magris, M., Hidalgo, G., Fierer, N., & Knight, R. (2010). Delivery mode shapes the acquisition and structure of the initial microbiota across multiple body habitats in newborns. *Proceedings of the National Academy of Sciences of the United States of America*, 107(26), 11971–11975. https://doi.org/10.1073/pnas.1002601107

Donohoe, D. R., Wali, A., Brylawski, B. P., & Bultman, S. J. (2012). Microbial regulation of glucose metabolism and cell-cycle progression in mammalian colonocytes. *PloS one*, 7(9), e46589. https://doi.org/10.1371/journal.pone.0046589

Espevik, T., Latz, E., Lien, E., Monks, B., & Golenbock, D. T. (2003). Cell distributions and functions of Toll-like receptor 4 studied by fluorescent gene constructs. *Scandinavian journal of infectious diseases*, 35(9), 660–664. https://doi.org/10.1080/00365540310016493

Fagundes, C. T., Amaral, F. A., Vieira, A. T., Soares, A. C., Pinho, V., Nicoli, J. R., Vieira, L. Q., Teixeira, M. M., & Souza, D. G. (2012). Transient TLR activation restores inflammatory response and ability to control pulmonary bacterial infection in germfree mice. *Journal of immunology* (Baltimore, Md.: 1950), 188(3), 1411–1420. https://doi.org/10.4049/jimmunol.1101682

Falk, P. G., Hooper, L. V., Midtvedt, T., & Gordon, J. I. (1998). Creating and maintaining the gastrointestinal ecosystem: what we know and need to know from gnotobiology. *Microbiology and molecular biology reviews*:

MMBR, 62(4), 1157–1170. https://doi.org/10.1128/MMBR.62.4.1157-1170.1998

Faria, A., Reis, B. S., & Mucida, D. (2017). Tissue adaptation: Implications for gut immunity and tolerance. *The Journal of experimental medicine*, 214(5), 1211–1226. https://doi.org/10.1084/jem.20162014

Figueiredo ART and Kramer J (2020) Cooperation and Conflict Within the Microbiota and Their Effects On Animal Hosts. *Frontiers in Ecology and Evolution*. 8:132. https://doi.org/10.3389/fevo.2020.00132

Filippi M. D. (2019). Neutrophil transendothelial migration: updates and new perspectives. *Blood*, 133(20), 2149–2158. https://doi.org/10.1182/blood-2018-12-844605

Fine, N., Tasevski, N., McCulloch, C. A., Tenenbaum, H. C., & Glogauer, M. (2020). The Neutrophil: Constant Defender and First Responder. *Frontiers in immunology*, 11, 571085. https://doi.org/10.3389/fimmu.2020.571085

Fischer, F., Romero, R., Hellhund, A., Linne, U., Bertrams, W., Pinkenburg, O., Eldin, H. S., Binder, K., Jacob, R., Walker, A., Stecher, B., Basic, M., Luu, M., Mahdavi, R., Heintz-Buschart, A., Visekruna, A., & Steinhoff, U. (2020). Dietary cellulose induces anti-inflammatory immunity and transcriptional programs via maturation of the intestinal microbiota. *Gut microbes*, 12(1), 1–17. https://doi.org/10.1080/19490976.2020.1829962

Fischetti, F., & Tedesco, F. (2006). Cross-talk between the complement system and endothelial cells in physiologic conditions and in vascular diseases. *Autoimmunity*, 39(5), 417–428. https://doi.org/10.1080/08916930600739712

Formes, H., & Reinhardt, C. (2019). The gut microbiota - a modulator of endothelial cell function and a contributing environmental factor to arterial thrombosis. *Expert review of hematology*, 12(7), 541–549. https://doi.org/10.1080/17474086.2019.1627191

Friedman, E. S., Bittinger, K., Esipova, T. V., Hou, L., Chau, L., Jiang, J., Mesaros, C., Lund, P. J., Liang, X., FitzGerald, G. A., Goulian, M., Lee, D., Garcia, B.

A., Blair, I. A., Vinogradov, S. A., & Wu, G. D. (2018). Microbes vs. chemistry in the origin of the anaerobic gut lumen. *Proceedings of the National Academy of Sciences of the United States of America*, 115(16), 4170–4175. https://doi.org/10.1073/pnas.1718635115

Ganesh, B. P., Klopfleisch, R., Loh, G., & Blaut, M. (2013). Commensal Akkermansia muciniphila exacerbates gut inflammation in Salmonella Typhimurium-infected gnotobiotic mice. *PloS one*, 8(9), e74963. https://doi.org/10.1371/journal.pone.0074963

Gantois, I., Ducatelle, R., Pasmans, F., Haesebrouck, F., Hautefort, I., Thompson, A., Hinton, J. C., & Van Immerseel, F. (2006). Butyrate specifically down-regulates salmonella pathogenicity island 1 gene expression. *Applied and environmental microbiology*, 72(1), 946–949. https://doi.org/10.1128/AEM.72.1.946-949.2006

Gasbarrini, G., Montalto, M., Santoro, L., Curigliano, V., D'Onofrio, F., Gallo, A., Visca, D., & Gasbarrini, A. (2008). Intestine: organ or apparatus?. *Digestive diseases* (Basel, Switzerland), 26(2), 92–95. https://doi.org/10.1159/000116765

Gassler N. (2017). Paneth cells in intestinal physiology and pathophysiology. *World journal of gastrointestinal pathophysiology*, 8(4), 150–160. https://doi.org/10.4291/wjgp.v8.i4.150

Ge, X., Zhao, W., Ding, C., Tian, H., Xu, L., Wang, H., Ni, L., Jiang, J., Gong, J., Zhu, W., Zhu, M., & Li, N. (2017). Potential role of fecal microbiota from patients with slow transit constipation in the regulation of gastrointestinal motility. *Scientific reports*, 7(1), 441. https://doi.org/10.1038/s41598-017-00612-y

Geboes, K., Geboes, K. P., & Maleux, G. (2001). Vascular anatomy of the gastrointestinal tract. *Best Practice & Research Clinical Gastroenterology*, 15(1), 1–14. https://doi.org/10.1053/bega.2000.0152

Gentile, M. E., & King, I. L. (2018). Blood and guts: The intestinal vasculature during health and helminth infection. *PLoS pathogens*, 14(7), e1007045. https://doi.org/10.1371/journal.ppat.1007045

Gomez de Agüero, M., Ganal-Vonarburg, S. C., Fuhrer, T., Rupp, S., Uchimura, Y., Li, H., Steinert, A., Heikenwalder, M., Hapfelmeier, S., Sauer, U., McCoy, K. D., & Macpherson, A. J. (2016). The maternal microbiota drives early postnatal innate immune development. *Science* (New York, N.Y.), 351(6279), 1296–1302. https://doi.org/10.1126/science.aad2571

Granger, D. N., Senchenkova, E. (2010). Chapter 7, Leukocyte–Endothelial Cell Adhesion. Inflammation and the Microcirculation. San Rafael (CA): Morgan & Claypool Life Sciences. Available from: https://www.ncbi.nlm.nih.gov/books/NBK53380/

Granger, D. N., Holm, L., & Kvietys, P. (2015). The Gastrointestinal Circulation: Physiology and Pathophysiology. *Comprehensive Physiology*, 5(3), 1541–1583. https://doi.org/10.1002/cphy.c150007

Gunn, J. S., Marshall, J. M., Baker, S., Dongol, S., Charles, R. C., & Ryan, E. T. (2014). Salmonella chronic carriage: epidemiology, diagnosis, and gallbladder persistence. *Trends in microbiology*, 22(11), 648–655. https://doi.org/10.1016/j.tim.2014.06.007

Gupta, S., Allen-Vercoe, E., & Petrof, E. O. (2016). Fecal microbiota transplantation: in perspective. *Therapeutic advances in gastroenterology*, 9(2), 229–239. https://doi.org/10.1177/1756283X15607414

Hakkim, A., Fürnrohr, B. G., Amann, K., Laube, B., Abed, U. A., Brinkmann, V., Herrmann, M., Voll, R. E., & Zychlinsky, A. (2010). Impairment of neutrophil extracellular trap degradation is associated with lupus nephritis. *Proceedings of the National Academy of Sciences of the United States of America*, 107(21), 9813–9818. https://doi.org/10.1073/pnas.0909927107

Hassan, M., Moghadamrad, S., Sorribas, M., Muntet, S. G., Kellmann, P., Trentesaux, C., Fraudeau, M., Nanni, P., Wolski, W., Keller, I., Hapfelmeier, S., Shroyer, N. F., Wiest, R., Romagnolo, B., & De Gottardi, A. (2020). Paneth cells promote angiogenesis and regulate portal hypertension in response to microbial signals. *Journal of hepatology*, 73(3), 628–639. https://doi.org/10.1016/j.jhep.2020.03.019

Hedblom, G. A., Reiland, H. A., Sylte, M. J., Johnson, T. J., & Baumler, D. J. (2018). Segmented Filamentous Bacteria - Metabolism Meets Immunity. *Frontiers in microbiology*, 9, 1991. https://doi.org/10.3389/fmicb.2018.01991

Helander, H. F., & Fändriks, L. (2014). Surface area of the digestive tract - revisited. *Scandinavian journal of gastroenterology*, 49(6), 681–689. https://doi.org/10.3109/00365521.2014.898326

Herath, M., Hosie, S., Bornstein, J. C., Franks, A. E., & Hill-Yardin, E. L. (2020). The Role of the Gastrointestinal Mucus System in Intestinal Homeostasis: Implications for Neurological Disorders. *Frontiers in cellular and infection microbiology*, 10, 248. https://doi.org/10.3389/fcimb.2020.00248

Hidalgo, A., Chilvers, E. R., Summers, C., & Koenderman, L. (2019). The Neutrophil Life Cycle. *Trends in immunology*, 40(7), 584–597. https://doi.org/10.1016/j.it.2019.04.013

Hill, R. R., & Cowley, H. M. (1990). The influence of colonizing micro-organisms on development of crypt architecture in the neonatal mouse colon. *Acta anatomica*, 137(2), 137–140. https://doi.org/10.1159/000146873

Hoffmann, T. W., Pham, H. P., Bridonneau, C., Aubry, C., Lamas, B., Martin-Gallausiaux, C., Moroldo, M., Rainteau, D., Lapaque, N., Six, A., Richard, M. L., Fargier, E., Le Guern, M. E., Langella, P., & Sokol, H. (2016). Microorganisms linked to inflammatory bowel disease-associated dysbiosis differentially impact host physiology in gnotobiotic mice. *The ISME journal*, 10(2), 460–477. https://doi.org/10.1038/ismej.2015.127

Holmes, R., & Lobley, R. W. (1989). Intestinal brush border revisited. *Gut*, 30(12), 1667–1678. https://doi.org/10.1136/gut.30.12.1667

Hu, J., & Torres, A. G. (2015). Enteropathogenic Escherichia coli: foe or innocent bystander?. *Clinical microbiology and infection: the official publication of the European Society of Clinical Microbiology and Infectious Diseases*, 21(8), 729–734. https://doi.org/10.1016/j.cmi.2015.01.015

Hugenholtz, F., & de Vos, W. M. (2018). Mouse models for human intestinal microbiota research: a critical evaluation. Cellular and molecular life sciences: CMLS, 75(1), 149–160. https://doi.org/10.1007/s00018-017-2693-8

Humphries, A., & Wright, N. A. (2008). Colonic crypt organization and tumorigenesis. *Nature reviews. Cancer*, 8(6), 415–424. https://doi.org/10.1038/nrc2392

Jochum, L., & Stecher, B. (2020). Label or Concept - What Is a Pathobiont?. *Trends in microbiology*, 28(10), 789–792. https://doi.org/10.1016/j.tim.2020.04.011

Kagnoff M. F. (1993). Immunology of the intestinal tract. *Gastroenterology*, 105(5), 1275–1280. https://doi.org/10.1016/0016-5085(93)90128-y

Kahai, P., Mandiga, P., Wehrle, C. J., & Lobo, S. (2020). Anatomy, Abdomen and Pelvis, Large Intestine. *In StatPearls*. StatPearls Publishing.

Kamada, N., Kim, Y. G., Sham, H. P., Vallance, B. A., Puente, J. L., Martens, E. C., & Núñez, G. (2012). Regulated virulence controls the ability of a pathogen to compete with the gut microbiota. *Science* (New York, N.Y.), 336(6086), 1325–1329. https://doi.org/10.1126/science.1222195

Kamada, N., Sakamoto, K., Seo, S. U., Zeng, M. Y., Kim, Y. G., Cascalho, M., Vallance, B. A., Puente, J. L., & Núñez, G. (2015). Humoral Immunity in the Gut Selectively Targets Phenotypically Virulent Attaching-and-Effacing Bacteria for Intraluminal Elimination. *Cell host & microbe*, 17(5), 617–627. https://doi.org/10.1016/j.chom.2015.04.001

Kamba, T., Tam, B. Y., Hashizume, H., Haskell, A., Sennino, B., Mancuso, M. R., Norberg, S. M., O'Brien, S. M., Davis, R. B., Gowen, L. C., Anderson, K. D., Thurston, G., Joho, S., Springer, M. L., Kuo, C. J., & McDonald, D. M. (2006). VEGF-dependent plasticity of fenestrated capillaries in the normal adult microvasculature. *American journal of physiology. Heart and circulatory physiology*, 290(2), H560–H576. https://doi.org/10.1152/ajpheart.00133.2005

Karbach, S. H., Schönfelder, T., Brandão, I., Wilms, E., Hörmann, N., Jäckel, S., Schüler, R., Finger, S., Knorr, M., Lagrange, J., Brandt, M., Waisman, A., Kossmann, S., Schäfer, K., Münzel, T., Reinhardt, C., & Wenzel, P. (2016). Gut Microbiota Promote Angiotensin II-Induced Arterial Hypertension and Vascular Dysfunction. *Journal of the American Heart Association*, 5(9), e003698. https://doi.org/10.1161/JAHA.116.003698

Karmarkar, D., & Rock, K. L. (2013). Microbiota signalling through MyD88 is necessary for a systemic neutrophilic inflammatory response. *Immunology*, 140(4), 483–492. https://doi.org/10.1111/imm.12159

Kespohl, M., Vachharajani, N., Luu, M., Harb, H., Pautz, S., Wolff, S., Sillner, N., Walker, A., Schmitt-Kopplin, P., Boettger, T., Renz, H., Offermanns, S., Steinhoff, U., & Visekruna, A. (2017). The Microbial Metabolite Butyrate Induces Expression of Th1-Associated Factors in CD4+ T Cells. *Frontiers in immunology*, 8, 1036. https://doi.org/10.3389/fimmu.2017.01036

Kim, Y. G., Sakamoto, K., Seo, S. U., Pickard, J. M., Gillilland, M. G., 3rd, Pudlo, N. A., Hoostal, M., Li, X., Wang, T. D., Feehley, T., Stefka, A. T., Schmidt, T. M., Martens, E. C., Fukuda, S., Inohara, N., Nagler, C. R., & Núñez, G. (2017). Neonatal acquisition of Clostridia species protects against colonization by bacterial pathogens. *Science* (New York, N.Y.), 356(6335), 315–319. https://doi.org/10.1126/science.aag2029

Kimura, I., Miyamoto, J., Ohue-Kitano, R., Watanabe, K., Yamada, T., Onuki, M., Aoki, R., Isobe, Y., Kashihara, D., Inoue, D., Inaba, A., Takamura, Y., Taira, S., Kumaki, S., Watanabe, M., Ito, M., Nakagawa, F., Irie, J., Kakuta, H., Shinohara, M., ... Hase, K. (2020). Maternal gut microbiota in pregnancy influences offspring metabolic phenotype in mice. *Science* (New York, N.Y.), 367(6481), eaaw8429. https://doi.org/10.1126/science.aaw8429

Knight, J et al (2019). Gastrointestinal tract 6: the effects of gut microbiota on human health. *Nursing Times* [online]; 115: 11, 46-50.

Kokrashvili, Z., Rodriguez, D., Yevshayeva, V., Zhou, H., Margolskee, R. F., & Mosinger, B. (2009). Release of endogenous opioids from duodenal enteroendocrine cells requires Trpm5. *Gastroenterology*, 137(2), 598–606.e6062. https://doi.org/10.1053/j.gastro.2009.02.070

Komatsu, S., Berg, R. D., Russell, J. M., Nimura, Y., & Granger, D. N. (2000). Enteric microflora contribute to constitutive ICAM-1 expression on vascular endothelial cells. *American journal of physiology. Gastrointestinal and liver physiology*, 279(1), G186–G191. https://doi.org/10.1152/ajpgi.2000.279.1.G186

Koopman, J. P., Kennis, H. M., Mullink, J. W., Prins, R. A., Stadhouders, A. M., De Boer, H., & Hectors, M. P. (1984). 'Normalization' of germfree mice with anaerobically cultured caecal flora of 'normal' mice. *Laboratory animals*, 18(2), 188–194. https://doi.org/10.1258/002367784780891253

Kruger, P., Saffarzadeh, M., Weber, A. N., Rieber, N., Radsak, M., von Bernuth, H., Benarafa, C., Roos, D., Skokowa, J., & Hartl, D. (2015). Neutrophils: Between host defence, immune modulation, and tissue injury. *PLoS pathogens*, 11(3), e1004651. https://doi.org/10.1371/journal.ppat.1004651

Krüger-Genge, A., Blocki, A., Franke, R. P., & Jung, F. (2019). Vascular Endothelial Cell Biology: An Update. *International journal of molecular sciences*, 20(18), 4411. https://doi.org/10.3390/ijms20184411

Kvietys, P. R. (2014). Physiology of the Gastrointestinal Microcirculation. *PanVascular Medicine*, 1–38. https://doi.org/10.1007/978-3-642-37393-0_141-1

Langlands, A. J., Almet, A. A., Appleton, P. L., Newton, I. P., Osborne, J. M., & Näthke, I. S. (2016). Paneth Cell-Rich Regions Separated by a Cluster of Lgr5+ Cells Initiate Crypt Fission in the Intestinal Stem Cell Niche. *PLoS biology*, 14(6), e1002491. https://doi.org/10.1371/journal.pbio.1002491

Leroyer, A. S., Blin, M. G., Bachelier, R., Bardin, N., Blot-Chabaud, M., & Dignat-George, F. (2019). CD146 (Cluster of Differentiation 146). *Arteriosclerosis, thrombosis, and vascular biology*, 39(6), 1026–1033. https://doi.org/10.1161/ATVBAHA.119.312653

Levine, M. M., & Robins-Browne, R. M. (2012). Factors that explain excretion of enteric pathogens by persons without diarrhea. *Clinical infectious diseases: an official publication of the Infectious Diseases Society of*

America, 55 Suppl 4 (Suppl 4), S303–S311. https://doi.org/10.1093/cid/cis789

Ley, K. (2008). The Microcirculation in Inflammation. *Microcirculation*, 403–408. https://doi.org/10.1016/B978-0-12-374530-9.00011-5

Li, M., van Esch, B., Wagenaar, G., Garssen, J., Folkerts, G., & Henricks, P. (2018). Pro- and anti-inflammatory effects of short chain fatty acids on immune and endothelial cells. *European journal of pharmacology*, 831, 52–59. https://doi.org/10.1016/j.ejphar.2018.05.003

Life without germs. (1949, September 26). *Life*, 107-113. https://books.google.de/books?id=IkkEAAAAMBAJ&lpg=PA107&hl=EN&pg=PA107&redir_esc=y#v=onepage&q&f=false

Lueschow, S. R., & McElroy, S. J. (2020). The Paneth Cell: The Curator and Defender of the Immature Small Intestine. *Frontiers in immunology*, 11, 587. https://doi.org/10.3389/fimmu.2020.00587

Luperchio, S. A., & Schauer, D. B. (2001). Molecular pathogenesis of Citrobacter rodentium and transmissible murine colonic hyperplasia. *Microbes and infection*, 3(4), 333–340. https://doi.org/10.1016/s1286-4579(01)01387-9

Lupp, C., Robertson, M. L., Wickham, M. E., Sekirov, I., Champion, O. L., Gaynor, E. C., & Finlay, B. B. (2007). Host-mediated inflammation disrupts the intestinal microbiota and promotes the overgrowth of Enterobacteriaceae. *Cell host & microbe*, 2(2), 119–129. https://doi.org/10.1016/j.chom.2007.06.010

Luu, M., Pautz, S., Kohl, V., Singh, R., Romero, R., Lucas, S., Hofmann, J., Raifer, H., Vachharajani, N., Carrascosa, L. C., Lamp, B., Nist, A., Stiewe, T., Shaul, Y., Adhikary, T., Zaiss, M. M., Lauth, M., Steinhoff, U., & Visekruna, A. (2019). The short-chain fatty acid pentanoate suppresses autoimmunity by modulating the metabolic-epigenetic crosstalk in lymphocytes. *Nature communications*, 10(1), 760. https://doi.org/10.1038/s41467-019-08711-2

Luu, M., Romero, R., Bazant, J., Abass, E., Hartmann, S., Leister, H., Fischer, F., Mahdavi, R., Plaza-Sirvent, C., Schmitz, I., Steinhoff, U., & Visekruna, A. (2020). The NF-κB transcription factor c-Rel controls host defense against Citrobacter rodentium. *European journal of immunology*, 50(2), 292–294. https://doi.org/10.1002/eji.201948314

Maaser, C., Housley, M. P., Iimura, M., Smith, J. R., Vallance, B. A., Finlay, B. B., Schreiber, J. R., Varki, N. M., Kagnoff, M. F., & Eckmann, L. (2004). Clearance of Citrobacter rodentium requires B cells but not secretory immunoglobulin A (IgA) or IgM antibodies. *Infection and immunity*, 72(6), 3315–3324. https://doi.org/10.1128/IAI.72.6.3315-3324.2004

Mallapaty, S. Gnotobiotics: getting a grip on the microbiome boom. *Lab Anim* 46, 373–377 (2017). https://doi.org/10.1038/laban.1344

Marr J. S. (1999). Typhoid Mary. *Lancet* (London, England), 353(9165), 1714. https://doi.org/10.1016/S0140-6736(05)77031-8

Maslowski, K. M., Vieira, A. T., Ng, A., Kranich, J., Sierro, F., Yu, D., Schilter, H. C., Rolph, M. S., Mackay, F., Artis, D., Xavier, R. J., Teixeira, M. M., & Mackay, C. R. (2009). Regulation of inflammatory responses by gut microbiota and chemoattractant receptor GPR43. *Nature*, 461(7268), 1282–1286. https://doi.org/10.1038/nature08530

McCullogh, J. S., Ratcliffe, B., Mandir, N., Carr, K. E., & Goodlad, R. A. (1998). Dietary fibre and intestinal microflora: effects on intestinal morphometry and crypt branching. *Gut*, 42(6), 799–806. https://doi.org/10.1136/gut.42.6.799

Miller, S. J., Zaloga, G. P., Hoggatt, A. M., Labarrere, C., & Faulk, W. P. (2005). Short-chain fatty acids modulate gene expression for vascular endothelial cell adhesion molecules. *Nutrition* (Burbank, Los Angeles County, Calif.), 21(6), 740–748. https://doi.org/10.1016/j.nut.2004.11.011

Miron, N., & Cristea, V. (2012). Enterocytes: active cells in tolerance to food and microbial antigens in the gut. Clinical and experimental immunology, 167(3), 405–412. https://doi.org/10.1111/j.1365-2249.2011.04523.x

Mizoguchi, A., Mizoguchi, E., Chiba, C., & Bhan, A. K. (1996). Role of appendix in the development of inflammatory bowel disease in TCR-alpha mutant mice. *The Journal of experimental medicine*, 184(2), 707–715. https://doi.org/10.1084/jem.184.2.707

Mörbe, U. M., Jørgensen, P. B., Fenton, T. M., von Burg, N., Riis, L. B., Spencer, J., & Agace, W. W. (2021). Human gut-associated lymphoid tissues (GALT); diversity, structure, and function. *Mucosal immunology*, 14(4), 793–802. https://doi.org/10.1038/s41385-021-00389-4

Mullineaux-Sanders, C., Collins, J. W., Ruano-Gallego, D., Levy, M., Pevsner-Fischer, M., Glegola-Madejska, I. T., Sågfors, A. M., Wong, J., Elinav, E., Crepin, V. F., & Frankel, G. (2017). Citrobacter rodentium Relies on Commensals for Colonization of the Colonic Mucosa. *Cell reports*, 21(12), 3381–3389. https://doi.org/10.1016/j.celrep.2017.11.086

Mundy, R., MacDonald, T. T., Dougan, G., Frankel, G., & Wiles, S. (2005). Citrobacter rodentium of mice and man. *Cellular microbiology*, 7(12), 1697–1706. https://doi.org/10.1111/j.1462-5822.2005.00625.x

Nataro, J. P., & Kaper, J. B. (1998). Diarrheagenic Escherichia coli. *Clinical microbiology reviews*, 11(1), 142–201. https://doi.org/10.1128/CMR.11.1.142

Nigam Y et al (2019). Gastrointestinal tract 4: anatomy and role of the jejunum and ileum. *Nursing Times* [online]; 115: 9, 43-46.

Noah, T. K., Donahue, B., & Shroyer, N. F. (2011). Intestinal development and differentiation. *Experimental cell research*, 317(19), 2702–2710. https://doi.org/10.1016/j.yexcr.2011.09.006

Nourshargh, S., Hordijk, P. L., & Sixt, M. (2010). Breaching multiple barriers: leukocyte motility through venular walls and the interstitium. *Nature reviews. Molecular cell biology*, 11(5), 366–378. https://doi.org/10.1038/nrm2889

Nourshargh, S., & Alon, R. (2014). Leukocyte migration into inflamed tissues. *Immunity*, 41(5), 694–707. https://doi.org/10.1016/j.immuni.2014.10.008

O'Hara, A. M., & Shanahan, F. (2006). The gut flora as a forgotten organ. *EMBO reports*, 7(7), 688–693. https://doi.org/10.1038/sj.embor.7400731

Ohkubo, T., Tsuda, M., Tamura, M., & Yamamura, M. (1990). Impaired superoxide production in peripheral blood neutrophils of germ-free rats. *Scandinavian journal of immunology*, 32(6), 727–729. https://doi.org/10.1111/j.1365-3083.1990.tb03216.x

Olins, A. L., Zwerger, M., Herrmann, H., Zentgraf, H., Simon, A. J., Monestier, M., & Olins, D. E. (2008). The human granulocyte nucleus: Unusual nuclear envelope and heterochromatin composition. *European journal of cell biology*, 87(5), 279–290. https://doi.org/10.1016/j.ejcb.2008.02.007

Osbelt, L., Thiemann, S., Smit, N., Lesker, T. R., Schröter, M., Gálvez, E., Schmidt-Hohagen, K., Pils, M. C., Mühlen, S., Dersch, P., Hiller, K., Schlüter, D., Neumann-Schaal, M., & Strowig, T. (2020). Variations in microbiota composition of laboratory mice influence Citrobacter rodentium infection via variable short-chain fatty acid production. *PLoS pathogens*, 16(3), e1008448. https://doi.org/10.1371/journal.ppat.1008448

Palm, N. W., de Zoete, M. R., & Flavell, R. A. (2015). Immune-microbiota interactions in health and disease. *Clinical immunology* (Orlando, Fla.), 159(2), 122–127. https://doi.org/10.1016/j.clim.2015.05.014

Panda, S. K., & Colonna, M. (2019). Innate Lymphoid Cells in Mucosal Immunity. *Frontiers in immunology*, 10, 861. https://doi.org/10.3389/fimmu.2019.00861

Papapietro, O., Teatero, S., Thanabalasuriar, A., Yuki, K. E., Diez, E., Zhu, L., Kang, E., Dhillon, S., Muise, A. M., Durocher, Y., Marcinkiewicz, M. M., Malo, D., & Gruenheid, S. (2013). R-spondin 2 signalling mediates susceptibility to fatal infectious diarrhoea. *Nature communications*, 4, 1898. https://doi.org/10.1038/ncomms2816

Parada Venegas, D., De la Fuente, M. K., Landskron, G., González, M. J., Quera, R., Dijkstra, G., Harmsen, H., Faber, K. N., & Hermoso, M. A. (2019). Short Chain Fatty Acids (SCFAs)-Mediated Gut Epithelial and Immune

Regulation and Its Relevance for Inflammatory Bowel Diseases. *Frontiers in immunology*, 10, 277. https://doi.org/10.3389/fimmu.2019.00277

Pei, J., Juni, R., Harakalova, M., Duncker, D. J., Asselbergs, F. W., Koolwijk, P., Hinsbergh, V. V., Verhaar, M. C., Mokry, M., & Cheng, C. (2019). Indoxyl Sulfate Stimulates Angiogenesis by Regulating Reactive Oxygen Species Production via CYP1B1. *Toxins*, 11(8), 454. https://doi.org/10.3390/toxins11080454

Petersson, J., Schreiber, O., Hansson, G. C., Gendler, S. J., Velcich, A., Lundberg, J. O., Roos, S., Holm, L., & Phillipson, M. (2011). Importance and regulation of the colonic mucus barrier in a mouse model of colitis. *American journal of physiology*. *Gastrointestinal and liver physiology*, 300(2), G327–G333. https://doi.org/10.1152/ajpgi.00422.2010

Petty, N. K., Bulgin, R., Crepin, V. F., Cerdeño-Tárraga, A. M., Schroeder, G. N., Quail, M. A., Lennard, N., Corton, C., Barron, A., Clark, L., Toribio, A. L., Parkhill, J., Dougan, G., Frankel, G., & Thomson, N. R. (2010). The Citrobacter rodentium genome sequence reveals convergent evolution with human pathogenic Escherichia coli. *Journal of bacteriology*, 192(2), 525–538. https://doi.org/10.1128/JB.01144-09

Petrof, E. O., Gloor, G. B., Vanner, S. J., Weese, S. J., Carter, D., Daigneault, M. C., Brown, E. M., Schroeter, K., & Allen-Vercoe, E. (2013). Stool substitute transplant therapy for the eradication of Clostridium difficile infection: 'RePOOPulating' the gut. *Microbiome*, 1(1), 3. https://doi.org/10.1186/2049-2618-1-3

Porter, E. M., Bevins, C. L., Ghosh, D., & Ganz, T. (2002). The multifaceted Paneth cell. *Cellular and molecular life sciences*: CMLS, 59(1), 156–170. https://doi.org/10.1007/s00018-002-8412-z

Privratsky, J. R., & Newman, P. J. (2014). PECAM-1: regulator of endothelial junctional integrity. *Cell and tissue research*, 355(3), 607–619. https://doi.org/10.1007/s00441-013-1779-3

Pruimboom-Brees, I. M., Morgan, T. W., Ackermann, M. R., Nystrom, E. D., Samuel, J. E., Cornick, N. A., & Moon, H. W. (2000). Cattle lack vascular receptors for Escherichia coli O157:H7 Shiga toxins. *Proceedings of the*

National Academy of Sciences of the United States of America, 97(19), 10325–10329. https://doi.org/10.1073/pnas.190329997

Rothenberg, M. E., Nusse, Y., Kalisky, T., Lee, J. J., Dalerba, P., Scheeren, F., Lobo, N., Kulkarni, S., Sim, S., Qian, D., Beachy, P. A., Pasricha, P. J., Quake, S. R., & Clarke, M. F. (2012). Identification of a cKit(+) colonic crypt base secretory cell that supports Lgr5(+) stem cells in mice. *Gastroenterology*, 142(5), 1195–1205.e6. https://doi.org/10.1053/j.gastro.2012.02.006

Round, J. L., & Mazmanian, S. K. (2009). The gut microbiota shapes intestinal immune responses during health and disease. *Nature reviews*. Immunology, 9(5), 313–323. https://doi.org/10.1038/nri2515

Saavedra, J. M., & Moore, N. (2005). MICROBIOTA OF THE INTESTINE | Prebiotics. *Encyclopedia of Human Nutrition*, 237–244. doi:10.1016/b0-12-226694-3/02190-6

Sansonetti P. J. (2004). War and peace at mucosal surfaces. Nature reviews. Immunology, 4(12), 953–964. https://doi.org/10.1038/nri1499

Sato, T., van Es, J. H., Snippert, H. J., Stange, D. E., Vries, R. G., van den Born, M., Barker, N., Shroyer, N. F., van de Wetering, M., & Clevers, H. (2011). Paneth cells constitute the niche for Lgr5 stem cells in intestinal crypts. *Nature*, 469(7330), 415–418. https://doi.org/10.1038/nature09637

Satoh-Takayama, N., Vosshenrich, C. A., Lesjean-Pottier, S., Sawa, S., Lochner, M., Rattis, F., Mention, J. J., Thiam, K., Cerf-Bensussan, N., Mandelboim, O., Eberl, G., & Di Santo, J. P. (2008). Microbial flora drives interleukin 22 production in intestinal NKp46+ cells that provide innate mucosal immune defense. *Immunity*, 29(6), 958–970. https://doi.org/10.1016/j.immuni.2008.11.001

Schaedler, R. W., R. Dubos, and R. Costello. 1965. Association of germfree mice with bacteria isolated from normal mice. *The Journal of experimental medicine*, 122(1), 77–82. https://doi.org/10.1084/jem.122.1.77

Schauer, D. B., & Falkow, S. (1993). Attaching and effacing locus of a Citrobacter freundii biotype that causes transmissible murine colonic hyperplasia.

Infection and immunity, 61(6), 2486–2492. https://doi.org/10.1128/iai.61.6.2486-2492.1993

Scher, J.U., Abramson, S. B., Pillinger, M. H. (2013). 11 - Neutrophils, *Kelley's Textbook of Rheumatology (Ninth Edition)*, W.B. Saunders, Pages 152-169, ISBN 9781437717389, https://doi.org/10.1016/B978-1-4377-1738-9.00011-6.

Schippers, A., Leuker, C., Pabst, O., Kochut, A., Prochnow, B., Gruber, A. D., Leung, E., Krissansen, G. W., Wagner, N., & Müller, W. (2009). Mucosal addressin cell-adhesion molecule-1 controls plasma-cell migration and function in the small intestine of mice. *Gastroenterology*, 137(3), 924–933. https://doi.org/10.1053/j.gastro.2009.05.039

Schmitt, M., Schewe, M., Sacchetti, A., Feijtel, D., van de Geer, W. S., Teeuwssen, M., Sleddens, H. F., Joosten, R., van Royen, M. E., van de Werken, H., van Es, J., Clevers, H., & Fodde, R. (2018). Paneth Cells Respond to Inflammation and Contribute to Tissue Regeneration by Acquiring Stem-like Features through SCF/c-Kit Signaling. *Cell reports*, 24(9), 2312–2328.e7. https://doi.org/10.1016/j.celrep.2018.07.085

Schoenborn, A. A., von Furstenberg, R. J., Valsaraj, S., Hussain, F. S., Stein, M., Shanahan, M. T., Henning, S. J., & Gulati, A. S. (2019). The enteric microbiota regulates jejunal Paneth cell number and function without impacting intestinal stem cells. *Gut microbes*, 10(1), 45–58. https://doi.org/10.1080/19490976.2018.1474321

Schreiber, H. A., Loschko, J., Karssemeijer, R. A., Escolano, A., Meredith, M. M., Mucida, D., Guermonprez, P., & Nussenzweig, M. C. (2013). Intestinal monocytes and macrophages are required for T cell polarization in response to Citrobacter rodentium. *The Journal of experimental medicine*, 210(10), 2025–2039. https://doi.org/10.1084/jem.20130903

Schwarzer, M., Hermanova, P., Srutkova, D., Golias, J., Hudcovic, T., Zwicker, C., Sinkora, M., Akgün, J., Wiedermann, U., Tuckova, L., Kozakova, H., & Schabussova, I. (2019). Germ-Free Mice Exhibit Mast Cells With Impaired Functionality and Gut Homing and Do Not Develop Food Allergy.

Frontiers in immunology, 10, 205. https://doi.org/10.3389/fimmu.2019.00205

Shanahan F. (2002). The host-microbe interface within the gut. *Best practice & research. Clinical gastroenterology*, 16(6), 915–931. https://doi.org/10.1053/bega.2002.0342

Shin, J., Noh, J. R., Chang, D. H., Kim, Y. H., Kim, M. H., Lee, E. S., Cho, S., Ku, B. J., Rhee, M. S., Kim, B. C., Lee, C. H., & Cho, B. K. (2019). Elucidation of Akkermansia muciniphila Probiotic Traits Driven by Mucin Depletion. *Frontiers in microbiology*, 10, 1137. https://doi.org/10.3389/fmicb.2019.01137

Spadoni, I., Zagato, E., Bertocchi, A., Paolinelli, R., Hot, E., Di Sabatino, A., Caprioli, F., Bottiglieri, L., Oldani, A., Viale, G., Penna, G., Dejana, E., & Rescigno, M. (2015). A gut-vascular barrier controls the systemic dissemination of bacteria. *Science* (New York, N.Y.), 350(6262), 830–834. https://doi.org/10.1126/science.aad0135

Spees, A. M., Lopez, C. A., Kingsbury, D. D., Winter, S. E., & Bäumler, A. J. (2013). Colonization resistance: battle of the bugs or Ménage à Trois with the host?. *PLoS pathogens*, 9(11), e1003730. https://doi.org/10.1371/journal.ppat.1003730

Spehlmann, M. E., Dann, S. M., Hruz, P., Hanson, E., McCole, D. F., & Eckmann, L. (2009). CXCR2-dependent mucosal neutrophil influx protects against colitis-associated diarrhea caused by an attaching/effacing lesion-forming bacterial pathogen. *Journal of immunology* (Baltimore, Md.: 1950), 183(5), 3332–3343. https://doi.org/10.4049/jimmunol.0900600

Stappenbeck, T. S., Hooper, L. V., & Gordon, J. I. (2002). Developmental regulation of intestinal angiogenesis by indigenous microbes via Paneth cells. *Proceedings of the National Academy of Sciences of the United States of America*, 99(24), 15451–15455. https://doi.org/10.1073/pnas.202604299

Stecher B. (2021). Establishing causality in Salmonella-microbiota-host interaction: The use of gnotobiotic mouse models and synthetic microbial

communities. *International journal of medical microbiology: IJMM*, 311(3), 151484. https://doi.org/10.1016/j.ijmm.2021.151484

Stein, R. A., & Katz, D. E. (2017). Escherichia coli, cattle and the propagation of disease. *FEMS microbiology letters*, 364(6), fnx050. https://doi.org/10.1093/femsle/fnx050

Suh, S. H., Choe, K., Hong, S. P., Jeong, S. H., Mäkinen, T., Kim, K. S., Alitalo, K., Surh, C. D., Koh, G. Y., & Song, J. H. (2019). Gut microbiota regulates lacteal integrity by inducing VEGF-C in intestinal villus macrophages. *EMBO reports*, 20(4), e46927. https://doi.org/10.15252/embr.201846927

Summers, C., Rankin, S. M., Condliffe, A. M., Singh, N., Peters, A. M., & Chilvers, E. R. (2010). Neutrophil kinetics in health and disease. *Trends in immunology*, 31(8), 318–324. https://doi.org/10.1016/j.it.2010.05.006

Sun, Q. H., DeLisser, H. M., Zukowski, M. M., Paddock, C., Albelda, S. M., & Newman, P. J. (1996). Individually distinct Ig homology domains in PECAM-1 regulate homophilic binding and modulate receptor affinity. *The Journal of biological chemistry*, 271(19), 11090–11098. https://doi.org/10.1074/jbc.271.19.11090

Sun, C., Feng, S. B., Cao, Z. W., Bei, J. J., Chen, Q., Zhao, W. B., Xu, X. J., Zhou, Z., Yu, Z. P., & Hu, H. Y. (2017). Up-Regulated Expression of Matrix Metalloproteinases in Endothelial Cells Mediates Platelet Microvesicle-Induced Angiogenesis. *Cellular physiology and biochemistry: international journal of experimental cellular physiology, biochemistry, and pharmacology*, 41(6), 2319–2332. https://doi.org/10.1159/000475651

Tanaka, M., & Nakayama, J. (2017). Development of the gut microbiota in infancy and its impact on health in later life. *Allergology international: official journal of the Japanese Society of Allergology*, 66(4), 515–522. https://doi.org/10.1016/j.alit.2017.07.010

Thomas H. (2016). Intestinal tract: Gut endothelial cells--another line of defence. *Nature reviews. Gastroenterology & hepatology*, 13(1), 4. https://doi.org/10.1038/nrgastro.2015.205

Tlaskalova-Hogenova H., Kverka M., Verdu E. F., Wells J. M. (2015). “Chapter 8-gnotobiology and the study of complex interactions between the intestinal microbiota, probiotics, and the host” in Mucosal immunology. eds. Mestecky J., Strober W., Lambrecht B. N. (Massachusetts, USA: Academic Press;), 109–133.

Treuting P. M., Dintzis S. M. (2012). Lower Gastrointestinal Tract, In Comparative Anatomy and Histology – a Mouse and Human Atlas, 1st edn (ed. Dintzis S. M., Frevert C. W., Liggitt H. D., Montine K. S., Treuting P. M.), Chapter 12. Amsterdam: Elsevier Inc.

Uchimura, Y., Fuhrer, T., Li, H., Lawson, M. A., Zimmermann, M., Yilmaz, B., Zindel, J., Ronchi, F., Sorribas, M., Hapfelmeier, S., Ganal-Vonarburg, S. C., Gomez de Agüero, M., McCoy, K. D., Sauer, U., & Macpherson, A. J. (2018). Antibodies Set Boundaries Limiting Microbial Metabolite Penetration and the Resultant Mammalian Host Response. *Immunity*, 49(3), 545–559.e5. https://doi.org/10.1016/j.immuni.2018.08.004

Umo, A. N., & Okon, A. O. (2017). Asymptomatic Carriers of Enteric Pathogens and the Risk Factors among Food Handlers in a Rural Setting in Nigeria. *Journal of Advances in Microbiology*, 4(3), 1-6. https://doi.org/10.9734/JAMB/2017/34060

van Ogtrop, M. L., Guiot, H. F., Mattie, H., & van Furth, R. (1991). Modulation of the intestinal flora of mice by parenteral treatment with broad-spectrum cephalosporins. *Antimicrobial agents and chemotherapy*, 35(5), 976–982. https://doi.org/10.1128/AAC.35.5.976

Wang J. (2018). Neutrophils in tissue injury and repair. *Cell and tissue research*, 371(3), 531–539. https://doi.org/10.1007/s00441-017-2785-7

Wehkamp, J., & Stange, E. F. (2020). An Update Review on the Paneth Cell as Key to Ileal Crohn's Disease. *Frontiers in immunology*, 11, 646. https://doi.org/10.3389/fimmu.2020.00646

Wiles, S., Clare, S., Harker, J., Huett, A., Young, D., Dougan, G., & Frankel, G. (2004). Organ specificity, colonization and clearance dynamics in vivo following oral challenges with the murine pathogen Citrobacter

rodentium. *Cellular microbiology*, 6(10), 963–972. https://doi.org/10.1111/j.1462-5822.2004.00414.x

Wlodarska, M., Willing, B., Keeney, K. M., Menendez, A., Bergstrom, K. S., Gill, N., Russell, S. L., Vallance, B. A., & Finlay, B. B. (2011). Antibiotic treatment alters the colonic mucus layer and predisposes the host to exacerbated Citrobacter rodentium-induced colitis. *Infection and immunity*, 79(4), 1536–1545. https://doi.org/10.1128/IAI.01104-10

Woodfin, A., Voisin, M. B., & Nourshargh, S. (2007). PECAM-1: a multi-functional molecule in inflammation and vascular biology. *Arteriosclerosis, thrombosis, and vascular biology*, 27(12), 2514–2523. https://doi.org/10.1161/ATVBAHA.107.151456

Wu, H. J., Ivanov, I. I., Darce, J., Hattori, K., Shima, T., Umesaki, Y., Littman, D. R., Benoist, C., & Mathis, D. (2010). Gut-residing segmented filamentous bacteria drive autoimmune arthritis via T helper 17 cells. *Immunity*, 32(6), 815–827. https://doi.org/10.1016/j.immuni.2010.06.001

Wymore Brand, M., Wannemuehler, M. J., Phillips, G. J., Proctor, A., Overstreet, A. M., Jergens, A. E., Orcutt, R. P., & Fox, J. G. (2015). The Altered Schaedler Flora: Continued Applications of a Defined Murine Microbial Community. *ILAR journal*, 56(2), 169–178. https://doi.org/10.1093/ilar/ilv012

Xiao, L., Feng, Q., Liang, S., Sonne, S. B., Xia, Z., Qiu, X., Li, X., Long, H., Zhang, J., Zhang, D., Liu, C., Fang, Z., Chou, J., Glanville, J., Hao, Q., Kotowska, D., Colding, C., Licht, T. R., Wu, D., Yu, J., ... Kristiansen, K. (2015). A catalog of the mouse gut metagenome. *Nature biotechnology*, 33(10), 1103–1108. https://doi.org/10.1038/nbt.3353

Xu, Y., Wang, N., Tan, H. Y., Li, S., Zhang, C., & Feng, Y. (2020). Function of Akkermansia muciniphila in Obesity: Interactions With Lipid Metabolism, Immune Response and Gut Systems. *Frontiers in microbiology*, 11, 219. https://doi.org/10.3389/fmicb.2020.00219

Yang, J., Hart, E., Tauschek, M., Price, G. D., Hartland, E. L., Strugnell, R. A., & Robins-Browne, R. M. (2008). Bicarbonate-mediated transcriptional activation of divergent operons by the virulence regulatory protein, RegA,

from Citrobacter rodentium. *Molecular microbiology*, 68(2), 314–327. https://doi.org/10.1111/j.1365-2958.2008.06171.x

Yang, J., Tauschek, M., Hart, E., Hartland, E. L., & Robins-Browne, R. M. (2010). Virulence regulation in Citrobacter rodentium: the art of timing. *Microbial biotechnology*, 3(3), 259–268. https://doi.org/10.1111/j.1751-7915.2009.00114.x

Yang, Y., Zhang, Y., Cao, Z., Ji, H., Yang, X., Iwamoto, H., Wahlberg, E., Länne, T., Sun, B., & Cao, Y. (2013). Anti-VEGF- and anti-VEGF receptor-induced vascular alteration in mouse healthy tissues. *Proceedings of the National Academy of Sciences of the United States of America*, 110(29), 12018–12023. https://doi.org/10.1073/pnas.1301331110

Yatsunenko, T., Rey, F. E., Manary, M. J., Trehan, I., Dominguez-Bello, M. G., Contreras, M., Magris, M., Hidalgo, G., Baldassano, R. N., Anokhin, A. P., Heath, A. C., Warner, B., Reeder, J., Kuczynski, J., Caporaso, J. G., Lozupone, C. A., Lauber, C., Clemente, J. C., Knights, D., Knight, R., … Gordon, J. I. (2012). Human gut microbiome viewed across age and geography. *Nature*, 486(7402), 222–227. https://doi.org/10.1038/nature11053

Yipp, B. G., Petri, B., Salina, D., Jenne, C. N., Scott, B. N., Zbytnuik, L. D., Pittman, K., Asaduzzaman, M., Wu, K., Meijndert, H. C., Malawista, S. E., de Boisfleury Chevance, A., Zhang, K., Conly, J., & Kubes, P. (2012). Infection-induced NETosis is a dynamic process involving neutrophil multitasking in vivo. *Nature medicine*, 18(9), 1386–1393. https://doi.org/10.1038/nm.2847

Zarzycka, A. (2017). *Gut microbiota mediates clearance of C. rodentium by phagocytes* (Unpublished doctoral dissertation). Philipps Universität Marburg, Marburg, Germany. https://archiv.ub.uni-marburg.de/diss/z2017/0293/pdf/daez.pdf

Zhang, L., Du, J., Yano, N., Wang, H., Zhao, Y. T., Dubielecka, P. M., Zhuang, S., Chin, Y. E., Qin, G., & Zhao, T. C. (2017). Sodium Butyrate Protects - Against High Fat Diet-Induced Cardiac Dysfunction and Metabolic

Disorders in Type II Diabetic Mice. *Journal of cellular biochemistry*, 118(8), 2395–2408. https://doi.org/10.1002/jcb.25902

Zheng, Y., Valdez, P. A., Danilenko, D. M., Hu, Y., Sa, S. M., Gong, Q., Abbas, A. R., Modrusan, Z., Ghilardi, N., de Sauvage, F. J., & Ouyang, W. (2008). Interleukin-22 mediates early host defense against attaching and effacing bacterial pathogens. *Nature medicine*, 14(3), 282–289. https://doi.org/10.1038/nm1720

8 Attachments

8.1 Curriculum vitae

8.2 List of academic teachers

Following ladies and gentlemen taught me during my academic education in Marburg:

Prof. Dr. S. Bauer	Prof. Dr. H-D. Klenk
Prof. Dr. U-M. Bauer	Prof. Dr. R. Lill
Prof. Dr. S. Becker	Prof. Dr. M. Lohoff
Dr. Dominique Brandt	Prof. Dr. A. Maisner
Prof. Dr. A. Brehm	Prof. Dr. U. Mühlenhoff
Prof. Dr. A. del Rey	Prof. Dr. B. Schmeck
Dr. M. Eickmann	Prof. Dr. M. Schnare
Prof. Dr. H-P. Elsässer	Prof. Dr. U. Steinhoff
Dr. B. Feuser	Prof. Dr. G. Suske
Prof. Dr. E. Friebertshäuser	Prof. apl. Dr. A. Visekruna
Prof. Dr. H. Garn	Prof. Dr. F. Weber
Prof. Dr. M. Huber	PD Dr. R. Westermann
Prof. Dr. R. Jacob	Dr. C. Wrocklage
Dr. A. Kaufmann	Dr. P. Yu

8.3 Acknowledgements

First and foremost, I would like to thank my supervisor Prof. Ulrich Steinhoff for his support not only during my PhD but also throughout my scientific career. Thank you for always having an open door for scientific but also general discussions, for helping me believe in myself and guiding me through the hard PhD-road. I would not be where I am now without your endless support.

Next, I would like to thank Prof. Alexander Visekruna for taking so much of his time to sit down with me to discuss my project, read manuscripts and carefully listen to so many of my presentations. Thank you so much Alex.

A special thanks to the head of the institute Prof. Michael Lohoff and also to Prof. Magdalena Huber for her insightful feedback and always friendly conversations.

To the members of AG Steinhoff/ Visekruna a huge thank you, especially to Anne Hellhund and Florence Fischer, for the scientific and emotional support during these years.

Thank you to all the members of the lab. Thank you Maik, Felix, DG, Allu and Hanna for all the brainstormings and amazing atmosphere.

A huge thank you to Melanie Wolf, Katrin Roth, Hartmann Raifer, Guido Schemken and Hosam Shams Eldin for being a friendly helping hand during my time in the lab.

Quiero agradecer a mis padres y mi familia por todo el esfuerzo y apoyo inmesurable que pesar de la distancia y los años sigue muy vigente. En especial quiero agradecer a mi madre Nubia Pérez por ser mi mayor ejemplo de lucha.

I want to thank my friends here in Germany for becoming my newfound family and supporting me throughout all these years.

Last but not least, I want to thank Johannes for being my rock, for proof-reading everything I write and for being my partner in crime.

8.4 Ehrenwörtliche Erklärung

„Ich erkläre ehrenwörtlich, dass ich die dem Fachbereich Medizin Marburg zur Promotionsprüfung eingereichte Arbeit mit dem Titel „A defined bacterial community restores immunity in germ-free mice via maturation of the intestinal vascular system.“ im Institut für medizinische Mikrobiologie und Krankenhaushygiene unter Leitung von Prof. Ulrich Steinhoff mit Unterstützung durch die Jürgen Manchot Stiftung und die Von Behring-Röntgen Stiftung ohne sonstige Hilfe selbst durchgeführt und bei der Abfassung der Arbeit keine anderen als die in der Dissertation aufgeführten Hilfsmittel benutzt habe. Ich habe bisher an keinem in- oder ausländischen Medizinischen Fachbereich ein Gesuch um Zulassung zur Promotion eingereicht, noch die vorliegende oder eine andere Arbeit als Dissertation vorgelegt.

Ich versichere, dass ich sämtliche wörtlichen oder sinngemäßen Übernahmen und Zitate kenntlich gemacht habe.

Mit dem Einsatz von Software zur Erkennung von Plagiaten bin ich einverstanden.

Ort, Datum, Unterschrift Doktorandin/Doktorand

„Die Hinweise zur Erkennung von Plagiaten habe ich zur Kenntnis genommen.“

Ort, Datum, Unterschrift Referentin/Referent
